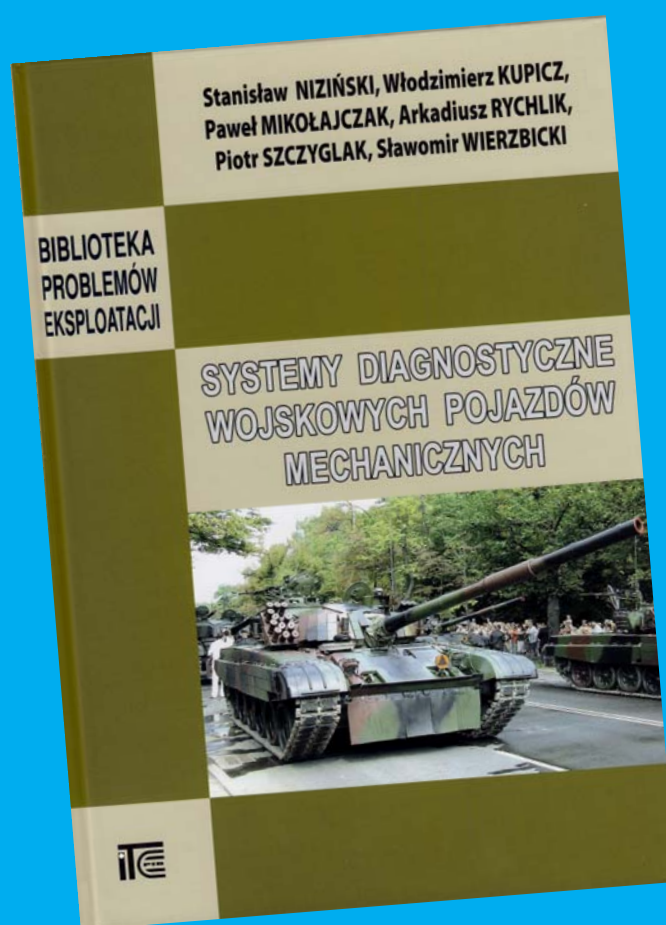


Diagnostyka

Diagnosics and Structural Health Monitoring

Rok założenia 1990

ISSN 1641-6414



Nr 2(58)/2011

RADA PROGRAMOWA / PROGRAM COUNCIL

PRZEWODNICZĄCY / CHAIRMAN:

prof. dr hab. dr h.c. mult. **Czesław CEMPEL** *Politechnika Poznańska*

REDAKTOR NACZELNY / CHIEF EDITOR:

prof. dr hab. inż. **Ryszard MICHAŁSKI** *UWM w Olsztynie*

CZŁONKOWIE / MEMBERS:

prof. dr hab. inż. **Jan ADAMCZYK**

AGH w Krakowie

prof. **Francesco AYMERICH**

University of Cagliari – Italy

prof. **Jérôme ANTONI**

University of Technology of Compiègne – France

prof. dr. **Ioannis ANTONIADIS**

National Technical University Of Athens – Greece

dr inż. **Roman BARCZEWSKI**

Politechnika Poznańska

prof. dr hab. inż. **Walter BARTELMUS**

Politechnika Wroclawska

prof. dr hab. inż. **Wojciech BATKO**

AGH w Krakowie

prof. dr hab. inż. **Adam CHARCHALIS**

Akademia Morska w Gdyni

prof. **Li CHENG**

The Hong Kong Polytechnic University – China

prof. dr hab. inż. **Wojciech CHOLEWA**

Politechnika Śląska

prof. dr hab. inż. **Zbigniew DĄBROWSKI**

Politechnika Warszawska

Prof. **Charles FARRAR**

Los Alamos National Laboratory – USA

prof. **Wiktor FRID**

Royal Institute of Technology in Stockholm – Sweden

dr inż. **Tomasz GAŁKA**

Instytut Energetyki w Warszawie

prof. **Len GELMAN**

Cranfield University – England

prof. **Mohamed HADDAR**

National School of Engineers of Sfax – Tunisia

prof. dr hab. inż. **Jan KICIŃSKI**

IMP w Gdańsku

prof. dr hab. inż. **Jerzy KISIŁOWSKI**

Politechnika Warszawska

prof. dr hab. inż. **Daniel KUJAWSKI**

Western Michigan University – USA

prof. **Graeme MANSON**

University of Sheffield – UK

prof. dr hab. **Wojciech MOCZULSKI**

Politechnika Śląska

prof. dr hab. inż. **Stanisław NIZIŃSKI**

UWM w Olsztynie

prof. dr hab. inż. **Stanisław RADKOWSKI**

Politechnika Warszawska

prof. **Bob RANDALL**

University of South Wales – Australia

prof. dr **Raj B. K. N. RAO**

President COMADEM International – England

prof. **Massimo RUZZENE**

Georgia Institute of Technology – USA

prof. **Vasily S. SHEVCHENKO**

BSSR Academy of Sciences Mińsk – Belarus

prof. **Menad SIDAHMED**

University of Technology Compiègne – France

Prof. **Tadeusz STEPINSKI**

Uppsala University - Sweden

prof. **Wiesław TRĄMPCZYŃSKI**

Politechnika Świętokrzyska

prof. dr hab. inż. **Tadeusz UHL**

AGH w Krakowie

prof. **Vitalijus VOLKOVAS**

Kaunas University of Technology – Lithuania

prof. **Keith WORDEN**

University of Sheffield – UK

prof. dr hab. inż. **Andrzej WILK**

Politechnika Śląska

dr **Gajraj Singh YADAVA**

Indian Institute of Technology – India

prof. dr hab. inż. **Bogdan ŻÓŁTOWSKI**

UTP w Bydgoszczy

WYDAWCA:

Polskie Towarzystwo Diagnostyki Technicznej
ul. Narbutta 84
02-524 Warszawa

REDAKTOR NACZELNY:

prof. dr hab. inż. **Ryszard MICHAŁSKI**

SEKRETARZ REDAKCJI:

dr inż. **Sławomir WIERZBICKI**

CZŁONKOWIE KOMITETU REDAKCYJNEGO:

dr inż. **Krzysztof LIGIER**

dr inż. **Paweł MIKOŁAJCZAK**

ADRES REDAKCJI:

Redakcja Diagnostyki
Katedra Budowy, Eksploatacji Pojazdów i Maszyn
UWM w Olsztynie
ul. Oczapowskiego 11, 10-736 Olsztyn, Poland
tel.: 89-523-48-11, fax: 89-523-34-63
www.diagnostyka.net.pl
e-mail: redakcja@diagnostyka.net.pl

KONTO PTD:

Bank PEKAO SA O/Warszawa
nr konta: 33 1240 5963 1111 0000 4796 8376

NAKLAD: 500 egzemplarzy

Spis treści / Contents

Kanji ONO	3
Application of acoustic emission for structure diagnosis	
Janusz ZACHWIEJA – University of Technology and Life Sciences in Bydgoszcz	19
The analysis of the rotor's longitudinal vibrations with large misalignment of shafts and ROTEX type coupling	
<i>Analiza drgań wzdłużnych wirnika przy dużej niewspółosiowości wałów i sprzęgle typu ROTEX</i>	
Marek FIDALI – Silesian University of Technology	25
Identification of machine technical state on the basis of Fourier analysis of infrared images	
<i>Identyfikacja stanu technicznego maszyn na podstawie wyników analizy Fouriera obrazów termowizyjnych</i>	
Aleksandra ZIAJA, Krzysztof MENDROK – AGH University of Science and Technology	31
Mode shapes subtraction and wavelet analysis for damage detection	
<i>Odejmowanie postaci drgań własnych i analiza falkowa do wykrywania uszkodzeń</i>	
Diego GALAR, Aditya PARIDA, Håkan Schunesson – Luleå University of Technology	39
Overall factory average spectrum: Global vibration index for diagnosis and prognosis of large sets of rotating machinery	
Krzysztof KOSAŁA – AGH University of Science and Technology	49
Decorrelation of indices for a single number assessment of the acoustic quality of sacral objects	
<i>Dekorelacja wskaźników w jednolitej ocenie jakości akustycznej obiektów sakralnych</i>	
Anna BZYMEK – Silesian University of Technology.....	53
A concept of defect identification with use of texture analysis methods	
<i>Koncepcja detekcji defektów powierzchni z zastosowaniem metod analizy obrazów</i>	
Łukasz PIECZONKA, Mariusz SZWEDO, Tadeusz UHL – AGH University of Science and Technology	61
Vibrothermography - measurement system development and testing	
<i>Wibrotermografia - rozwój i testowanie systemu pomiarowego</i>	
XVII Krajowa Konferencja Automatyki – KKA'2011	67
Wspomnienie prof. dr hab. inż. Stanisława NIZIŃSKIEGO	69
Warto przeczytać / Worth to read	70

APPLICATION OF ACOUSTIC EMISSION FOR STRUCTURE DIAGNOSIS

Kanji ONO
e-mail: kanjion1@gmail.com

Summary

This article reviewed acoustic emission testing of structures in various applications, concentrating on those of interest to civil engineers. Current status of AE damage assessment is presented. We have vast knowledge on AE and used it successfully in many cases. We have examined recent applications and tried to direct the way for further improvement, since AE diagnosis of structural health has many obstacles still ahead.

Keywords: acoustic emission, structural materials.

1. INTRODUCTION

Acoustic emission (AE) testing of structures has been utilized in various applications from aerospace to welding. Current status of AE technology is reviewed with emphasis on AE damage assessment. We have accumulated vast knowledge on AE and successful cases abound, although details usually are difficult to access. We examine some of recent applications and try to point the way for improved AE diagnosis of structural health and discuss gaps in our understanding of AE and limits of standard AE approach.

When a structure fails, sounds or ultrasounds are generated and these are known as acoustic emission (AE). Mechanical waves propagate from a source where failure occurred to sensors placed usually on the surface of the structure. Such waves are detected and analyzed to evaluate the integrity of the structure. This is used as a method of nondestructive testing because AE is very sensitive and can detect failure at microcracking stage.

Acoustic emission technology is similar to seismology except AE is in the scale of engineering structures. Research on AE started in the 1930s, but its applications began ~50 years ago in the aerospace and geotechnical fields. When AE occurs in geologic structures, it is often referred to as micro-seismic activity or AE/MS. Research and development efforts continued to this day and AE (and AE/MS) applications have expanded to various fields.

Acoustic emission is a **dynamic** technique. AE occurs when a crack propagates, or when crack faces fret against each other. Usually this occurs when the structure is stressed. AE activities rise sharply when local stress approaches the critical failure point. In contrast, it produces no indication when there are only benign defects, such as voids and non-growing cracks. Acoustic emission is also a **global** inspection technique, analyzing the ultrasonic waves coming from a fault detected by multiple sensors; that is, unlike ultrasonic pulse-echo technique or radiography, inspection path is not predefined by applied stimulus and no volumetric scanning is needed. AE can work without knowing defect location beforehand. A single test evaluates an entire structure quickly and

effectively when adequate sensor placements cover it; it can provide *in situ*, continuous monitoring. When a specific area needs attention, AE can also monitor locally, filtering out external noise. Acoustic emission is also a **visual** technique that can identify, locate and display the faults producing AE signals in almost real time. This part owes much to the advances of signal processing technology, which also allows remote monitoring. Methods to locate the AE sources are well established. However, the principles to identify defect types are still being developed and the experiences of experts play important roles for this phase of AE analysis. Other drawbacks of AE are high attenuation of waves in some materials, like concrete and fiber composites, requiring many sensors, and need for adequate stressing of defects to reveal them. In steels, AE waves are attenuated at 0.1-1 dB/m, but in concrete this jumps to 45 to 118 dB/m [B7]; i.e., amplitude decreases by 200 to 1,000,000 times after traveling 1 m. The stressing requirement can pose difficult problems in large structures, but may be of a lesser problem as structurally significant defects are subjected to loading in other cases. In large steel bridges, electrical grounding poses serious issues with noise and lightening. Bibliography (B1 – B9) lists useful references and major reports.

AE/MS inspection of underground mines started from the 1950s and attempted to evaluate rock stability and to predict rock bursts and roof falls. Accurate source location techniques were developed using multi-channel systems, utilizing travel-time differences of the P- and S-wave onsets. Works on rocks and mines have continued and a large body of knowledge has been accumulated. [B4]

In the 1970s, the prediction of geostress became practical and was first applied in the construction of Seikan undersea tunnel in Japan, still the longest tunnel in the world. [1] This method was based on Kaiser effect of rock AE under repeated loading; i.e., AE is irreversible and its activity resumes only when the previous load is exceeded upon reloading. Initially, geostress was estimated assuming directional independence, but currently AE

measurements try to account for multi-axial state of geostress. [2]

In the 1990s, AE work on concrete became more active and AE applications started to include the evaluation of infrastructures like bridges and dams. AE behavior of concrete from laboratory size to full-size beams has been evaluated. Good understanding has been gained in this area. [B6] Health monitoring of infrastructures is much more involved and the progress has been slow. AE monitoring of local areas has worked well, but full-scale monitoring has been limited.

In this report, we give a general overview of AE and introduce a range of advanced AE analysis methods for the evaluation of infrastructures. Selected examples are provided.

2. ACOUSTIC EMISSION BASICS [B3, B4, B6, B9]

Sensors attached on the surfaces of a structure detect elastic waves from active sources, known as AE signals. Mechanical vibration due to AE signals is weak and requires high-sensitivity sensors and electronic amplification before it can be analyzed. Typically, AE signals are short pulses and can be counted electronically. Counts and rates indicate AE activity. A typical single AE pulse (or burst) from a steel sample is shown in Fig. 1a. Such bursts come from cracking, fiber or inclusion fracture, corrosion bubbles, fluid drop noise, etc. When AE activities are high, many waveforms become inseparable as in Fig. 1b; this is known as continuous AE, originating from plastic

deformation at yield, friction, flow noise, fluid or gas leaks, etc. [3] Another indicator is the intensity of AE signals, defined in terms of amplitude and duration. For burst emissions, we can define peak amplitude (“Amplitude”; in dB scale to cover a wide range), signal length in time (“Duration”; time period between threshold crossing), “Rise time” (initial threshold crossing to the peak), and “Energy” (approximated by squared peak value times duration). Counting the number of burst emissions, we define “AE event counts” [AE hit counts may also be used as a single event arrives at multiple sensors]; we also use “AE counts”, referring to all threshold crossing. “RMS voltage” of AE signals is useful to measure the intensity of continuous AE. The frequency contents of AE signals add more parameters of AE sources, but these are strongly affected by the sensors and measurement conditions, requiring careful analysis before valid information can be extracted. For the signal of Fig. 1 [3], we find only the dominant frequency of 125 kHz from the sensor/sample resonance. Because the sensitivity of AE techniques is high, it is useful in discovering otherwise undetectable mechanical events. This feature has been exploited fully in a large variety of structural testing methods. For the same reason, however, clear correlation between AE observation and direct knowledge of the sources of AE is difficult to establish. This is where much research has been conducted, but the interpretation of AE findings still must depend on empirical deduction of experienced engineers.

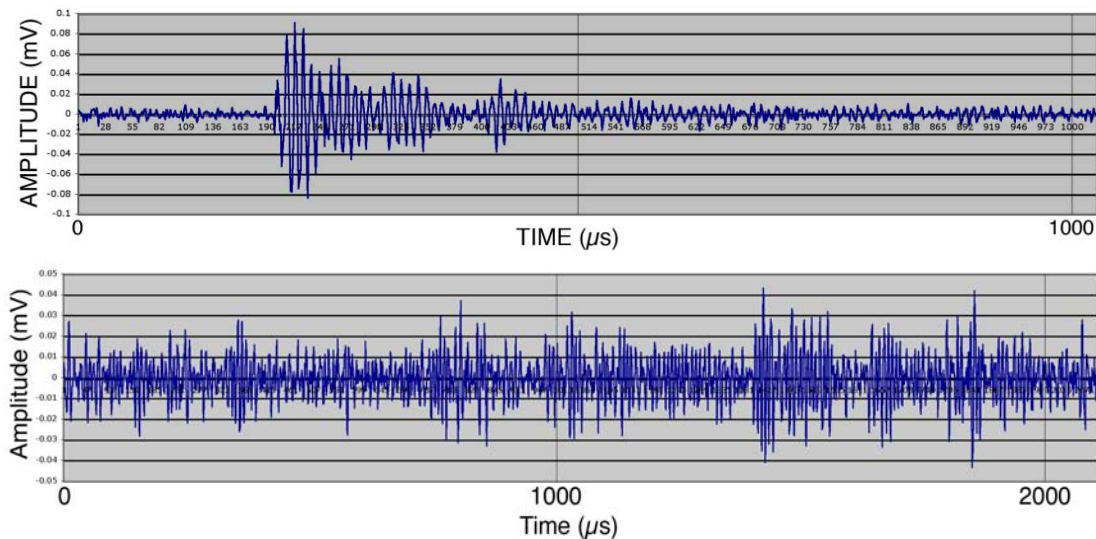


Fig. 1. A typical AE signal from a steel tensile sample (A533B). (a) Burst type. Amplitude: 39 dB (0 dB = 1 μ V at sensor output). Duration: 260 μ s (with the threshold of 20 μ V). Rise time: 19 μ s. (b) Continuous emission from the yielding of the steel. [3]

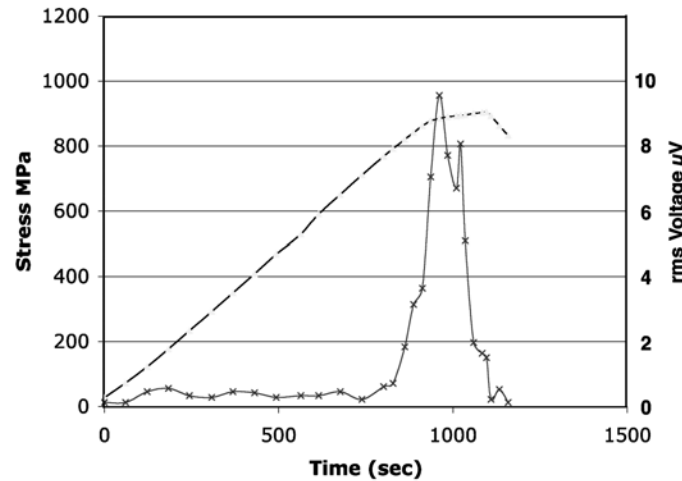


Fig. 2. The stress and rms voltages vs. time curves for a low-alloy steel tensile sample. Rms-voltage values to ~800 s are background noise [3]

3. MATERIALS AND EVALUATION METHODS [B3, B4, B6, B7, B9]

Ductile materials such as steels or aluminum alloys respond to applied stress and plastically deform, progressing to eventual fracture. Figure 2 shows AE intensity (rms voltage) from a steel sample during the initial deformation, also called yielding. [3] No AE arises during elastic straining, although microcracking and other microfracture events may contribute to burst emissions. In most alloys, AE diminishes during work-hardening stage beyond yielding; then burst-type AE signals occur prior to and during fracture. When the materials had been deformed heavily, AE is nearly absent. Some austenitic stainless steels also produce no AE. In many aluminum alloys, micron-sized particles generate AE during the work-hardening stage. The variation in AE reflects the internal constituents of materials and helps in understanding deformation characteristics.

During fracture testing of less ductile materials, AE behavior is similar to that of A470 steel (Fig. 3a) [4], and even fewer AE signals occur in most brittle materials. AE signals are initially produced from micro-fracture when stress level rises. Material fracture results from a main crack formed by the coalescence of microcracks and other internal damage. In A470 steel, quasi-cleavage cracks developed. Such damage develops either gradually or rapidly. While AE cannot detect slow damage formation (like forming voids), rapid damage processes that form cracks are serious defects and can be easily detected by AE. In addition to cracking, both micro and macro, inclusion fracture and its decohesion from the matrix contribute to observed AE substantially. In

composite materials, reinforcement fiber failure and interface separation, as well as matrix failure generate AE.

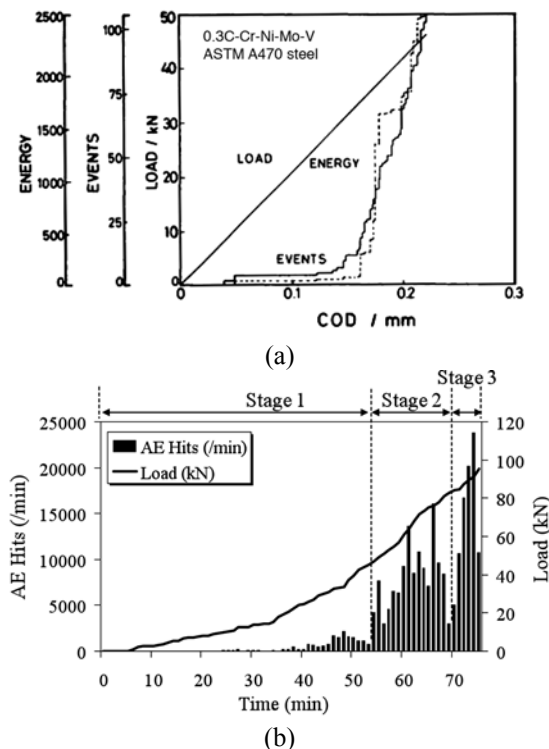


Fig. 3. Load and AE activity. (a) vs. crack opening displacement (COD). A470 steel (1T) compact tension fracture toughness sample. $K_{Ic} = 60$ MPa \sqrt{m} ; $Y_S = 616$ MPa; $T_S = 786$ MPa. [4] (b) vs. loading time. Reinforced concrete (RC) beam (0.15 x 0.25 x 2 m) in bending. 8-channels of PAC R15 sensors; 28-day concrete strength = 29.7 MPa. [5]

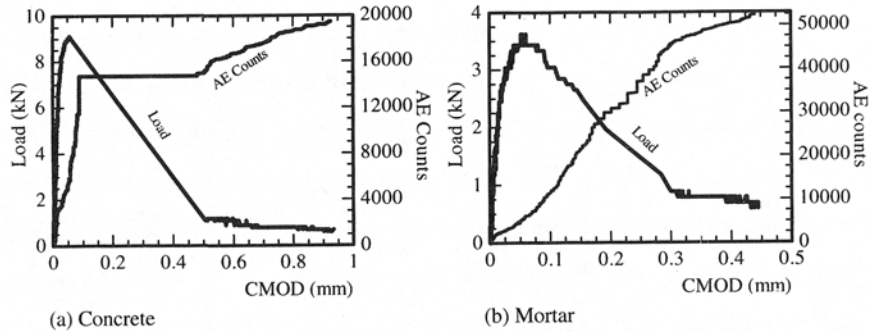


Fig. 4. AE and load vs. CMOD for (a) concrete and (b) mortar notched beam specimens. [6]

A similar trend of rising AE activity with loading is seen in a steel-reinforced concrete beam that failed at 96 MPa in bending (Fig. 3b). [5] This beam started to concentrate AE events in the shear span in Stage II and continued to diagonal shear failure. Another concrete beam test is shown in Fig. 4. [6] This bar has a notch; load and AE counts are plotted against crack mouth opening displacement (CMOD). For concrete, AE counts rapidly increased with loading and into initial unloading part, followed by gradual increase. A mortar sample of the same geometry exhibited 2-3 times more AE continuing through the unloading stage. The maximum load of mortar was $\sim 1/3$ of concrete.

AE behavior of a specific material does depend on a number of variables. While metals and concrete behave within reasonable ranges, AE behavior of natural rocks varies widely with different inclusion structures. As a vast literature has been developed, one can usually find basic concepts governing the AE characteristics of a commonly used material.

Kaiser effect (KE), the absence of AE until the previous maximum load under repeated loading, is the most important AE behavior in structural test applications. [7] Premature AE observation during reloading represents the breakdown of Kaiser effect and is sometimes called Felicity effect (FE). In deformed metals, annealing induces it (recovery of KE), but FE has been substantially linked to crack growth, composite damage, concrete failure and geostress prediction. Of these, AE geostress estimation has been most intensively studied, reflecting its value to geotechnical field. The first successful application by Kanagawa and Nakasa [1] assumed that the normal stress component in each direction can be simply retrieved by uniaxially reloading a specimen oriented in that direction. Later work showed the role of the triaxial state of stress in the stress memory formation must be properly applied for absolute stress measurements by Kaiser effect. [2] Many other influences need consideration as well; AE parameter to use, rock types, stress level, loading rate and duration, time delay, water contents, and so on.

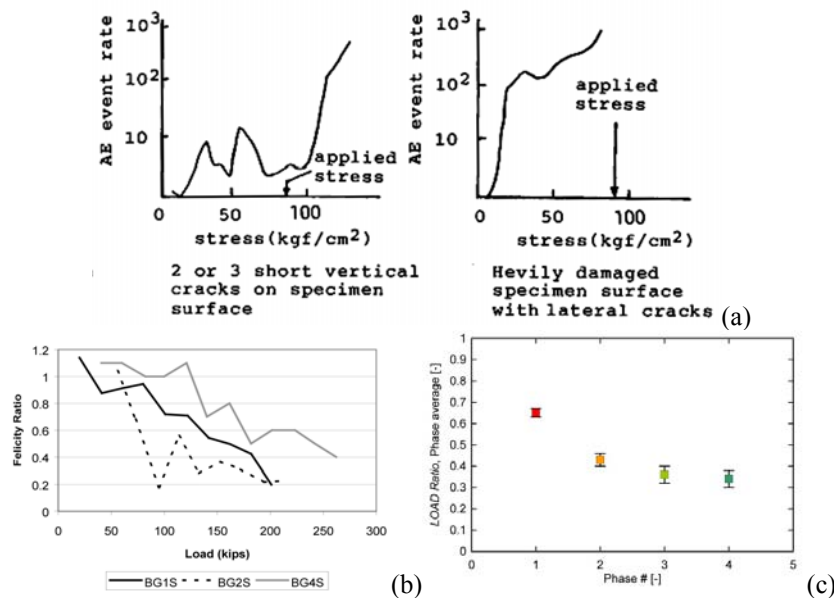


Fig. 5. (a) Relationship between AE event rate and stress in the second loading in concrete cylinders loaded at a high rate. [8] (b) Changes in Felicity ratio in repeatedly loaded full-size box girders. This best indicated distributed damage due to loading. [9] (c) Load ratio (normalized to the ultimate load) vs. applied loading phase, reaching 80% of capacity. [B7]

High stress level relative to the maximum strength affects Felicity effect much, reducing the onset stress (or Felicity ratio (CARP) = Load ratio (JCMS) = onset stress/ previous peak stress). In lightly damaged concrete, Kaiser effect is preserved with loading up to 80% of the maximum strength just as in most rocks, but KE was lost with heavy damage on concrete, giving a low Felicity ratio. See Fig. 5a. [8] In full-scale girders, spatially distributed damage was best correlated to Felicity ratio. Figure 5b shows changes in Felicity ratio on three box girders under shear-dominated test (with repeated loading and unloading). [9] Equivalent Load ratio showed less scatter in Oregon tests of large RC beam. (Fig. 5c) [B6]. Considerable differences in experiences at Texas and Oregon are not explored, but sensor positioning may be at least a contributing factor. In Texas tests, sensor spacing was 1.8 m, while Oregon tests used 0.9 m or less spacing and also concentrated in Array A case. In all cases, as applied load increases closer to the ultimate loading capacity, FE or Load ratio decreased. This demonstrates that these ratios act as indicator of concrete damage.

Amplitude distribution

A widely used analysis method is to examine the peak amplitude distribution. Most common type for burst emissions is a power-law distribution (a form of fractals). With the number of events N having amplitude larger than “ a ”, we have a cumulative amplitude distribution,

$$\log N = (\text{const}) - b \log a,$$

and a differential amplitude distribution,

$$\log n = \log (dN/da) = (\text{const}) - m \log a,$$

where $m = b + 1$ and $N = \int_a^\infty n(a)da$.

The slope of a log-log plot, b , is the parameter of interest. Lower b -values contain more large amplitude events and tend to imply less ductile material behavior. Using modern AE instruments, this is easy to determine. However, b -values sometimes have a large scatter. Notice here that in #

typical plots of AE analysis software, AE amplitude is typically expressed in dB and 20 dB equals a factor of 10; $b = 1$ implies a factor of 10 change in N for 20-dB amplitude variation.

For a steel sample exhibiting quasi-cleavage cracking, the data fits well with the exponent $b = 0.5$, whereas more ductile steels show b values of 1 to 2. [11, 12] For example, a steel showing ductile tear and shear fracture mechanisms generate low level AE signals and $b = 1.8$. AE due to plastic deformation follows an entirely different distribution, but nominal b values are >4 . For various rocks, b -values falls in the range from 0.5 to 1. [13] In concrete, $b = 1$ to 1.2 under uniaxial compression, while it varied from 0.8 to 2.2 under beam bending condition.

In this case, $b = 1.5 - 2.2$ for microcrack dominant (initial stage of bending) segment, while b -values were lowered to unity when macrocracks appeared. In concrete beam loaded in bending, b values decreased with loading, indicative of accumulated damage [14]. This is shown in Fig. 6. [B7] Observed values were less than 0.5 and well below unity.

Because the amplitude distribution is affected by count statistics, Shiotani et al. [15] introduced “improved” b -values or Ib -values, where the range of AE amplitude is determined based on such statistical values as the mean μ and standard deviation σ , where the upper amplitude a_2 and lower a_1 are formulated as $\mu + \alpha_1\sigma$ and $\mu - \alpha_2\sigma$, respectively. Here, α_1 and α_2 are constants. Setting accumulated numbers with amplitude over a_1 and a_2 , as $N(a_1)$ and $N(a_2)$, Ib -value is given by

$$Ib = [\log N(a_1) - \log N(a_2)] / (\alpha_1 + \alpha_2) \sigma$$

where the range of amplitude is $(\alpha_1 + \alpha_2)\sigma$. A note of caution: since Ib -value is calculated on the basis of decibel unit, the Ib value must be multiplied by 20 when comparing with seismic b -value used in conventional AE analysis. The use of Ib decreases the scattering, especially by using sample numbers of more than 50-100.

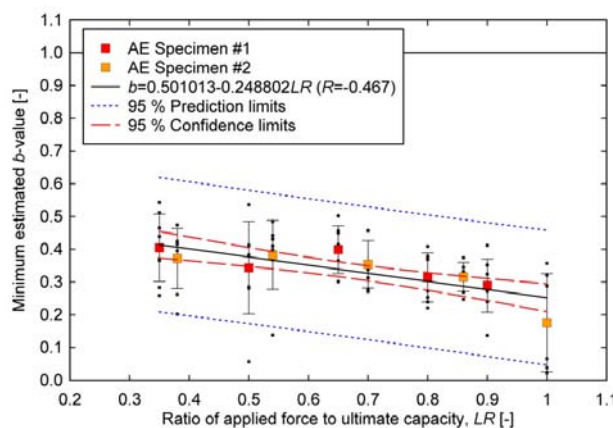


Fig. 6. Minimum b value of two large RC beam tests vs. applied to ultimate load ratio. [B7]

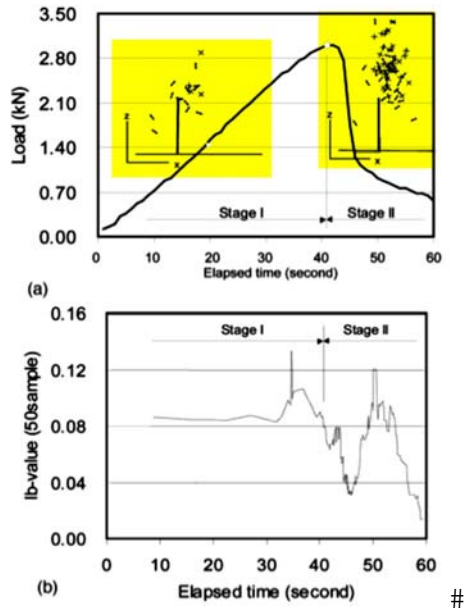


Fig. 7. Results of a center-notched concrete beam; (a) Load vs. t with moment tensor results in inserts. \leftrightarrow and X shows tensile and shear events. (b) Ib -value vs. t . [15]

Figure 7 shows results of the three-point flexure test of a center-notched concrete beam; (a) shows the loading history and (b) shows the Ib -value. The variation in Ib is more consistent than that of conventional b values. Ib decreased steadily during load drop in Stage II, when strong AE events were dominant. Ib below 0.06 (or $b < 1.2$) is considered as the indicator of macro-damage. As moment tensor results show in insert (b), shear events (marked by X) were abundant ahead of the crack tip. Increased Ib values just before the maximum load and during steady load drop toward the end indicate many weak events from frictional sources.

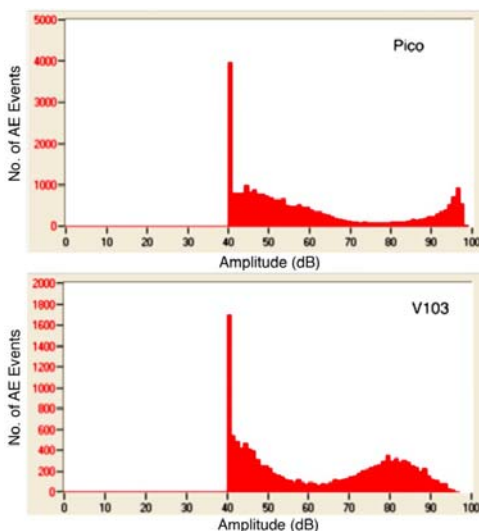


Fig. 8. Differential amplitude distribution of AE from a tensile loading of metal-glass-fiber laminate (GLARE) with boron (B) fibers. [16]

Another type of (differential) peak amplitude distribution is log-normal distribution, which has a peak in probability density distribution. Its cumulative distribution has sigmoidal shape with tails at high and low ends. Quite often, tail parts are ignored and the middle part is represented by a power law. AE analysis based on log-normal distribution has seldom been done, but such distribution has been found on high strength steels and in fiber-composite materials, where single mechanism (e.g., quasi-cleavage, fiber break) can be identified as the origin. Figure 8 gives two examples from a tensile loading of metal-glass-fiber laminate (GLARE) with boron (B) fibers. [16] Using a damped V103 sensor, B-fiber events appear at 60-98 dB, peaking at 82 dB. These AE signals are due to B-fiber fracture since these are absent in plain GLARE. AE due to GLARE with a Pico sensor (about 15 dB more sensitive than V103) appears to show a peak at 45 dB and extends up to 75 dB. Multiple mechanisms are involved with much overlap, making their separation difficult for these lower amplitude events. Low amplitude events below threshold are also hidden. Both factors make many distributions appear as power-law type.

In using amplitude distribution analysis for attenuating media in large scale, like concrete and rock, one must consider source-sensor distance. However, this is often ignored and such results need to be treated with caution.

Other AE Parameters

Many other parameters have been used in AE analysis. It is natural to attempt to utilize the frequency spectra of AE signals. However, this approach is also most difficult to extract valid information. Experimental conditions, including wave propagation modes, sensor responses, structural resonances and frequency dependent attenuation, provide almost insurmountable barriers and no theory predicts identifiable spectra for AE mechanisms except for the presence of upper frequency limit.

A straightforward high-pass (HP) filtering is sometimes an effective method to discriminate between AE signals from defects and frictional noise. Dunegan has been using this concept for some years in DECI instruments. [17] He picked 100 kHz HP as the separation point for valid AE and use intensity ratio of high-frequency and low-frequency components. When this HF/LF ratio is high, AE signals are indicated as, e.g., fatigue crack signals. This method was applied successfully to monitoring of fatigue crack growth in a steel railway bridge at a railroad test facility, on which a 68-car train repeatedly passed at 64 km/hr. In the inspection of a 70+year old concrete bridge, Shiotani et al. [18] used 20 kHz HP filtering to separate critical AE from frictional background. This helped them isolate valid AE information for further analysis with other techniques.

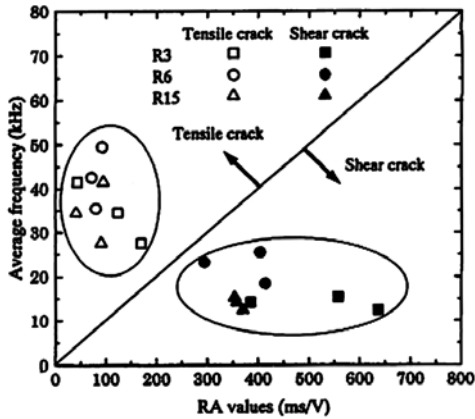


Fig. 9. Distribution of average frequency vs. RA value for AE events obtained in flexural (open symbols) and double-shear (filled) loading experiments. [19]

Some other frequency-related parameters have been used. Average frequency (= AE counts/duration; defined for each AE hit) was used in combination with RA value (= rise time/peak amplitude in mV; the reciprocal of initial signal slope) in a Japanese code for concrete (JCMS-III B5706 2003). The basis for using this correlation is Fig. 9, where a plot of average frequency vs. RA value is given. [19] These two groups of AE events were obtained from flexural and double-shear loading experiments and clearly separated. Here, three different sensors (resonant at 30, 60 and 150 kHz) were used with identical results, indicating possible validity of this approach.

The separation line in Fig. 9 has the slope of 0.1 Hz-s/V. This slope, however, is dependent on various conditions and may reduce the utility of this method. In an RC-beam test (Fig. 3b), this slope was reported as 50 Hz-s/V [5], while another group gives the slope of 8 Hz-s/V in bending and shear tests of concrete [20]. In the latter, the data points for shear cracks are distributed over the entire slope range from low to high with no clear distinction between tensile and shear. The same behavior regardless of crack types was also found in Schumacher report [B7]. Further work is definitely needed.

Fowler et al. [21] developed two parameters of importance in AE evaluation of composite vessels; i.e., historic index and severity. CARP (Comm. on AE from Reinforced Plastics) later adopted the two parameters. Historic index is the ratio of average signal strengths of recent events over all events, while severity is the average signal strengths of ten largest events. Cross plots of these parameters constitute intensity analysis and different “zone intensity” of damage grades are defined from sound (A) to severely damaged (E). For concrete testing, Golaski et al. [22] applied this same procedure to concrete beam tests. Intensity zone shifted from zone A to zone D as the beam was loaded to failure as shown in Fig. 10. In the intensity analysis of a new pre-stressed bridge, all data points lied in the sound zone (or zone A), implying no serious deterioration as expected.

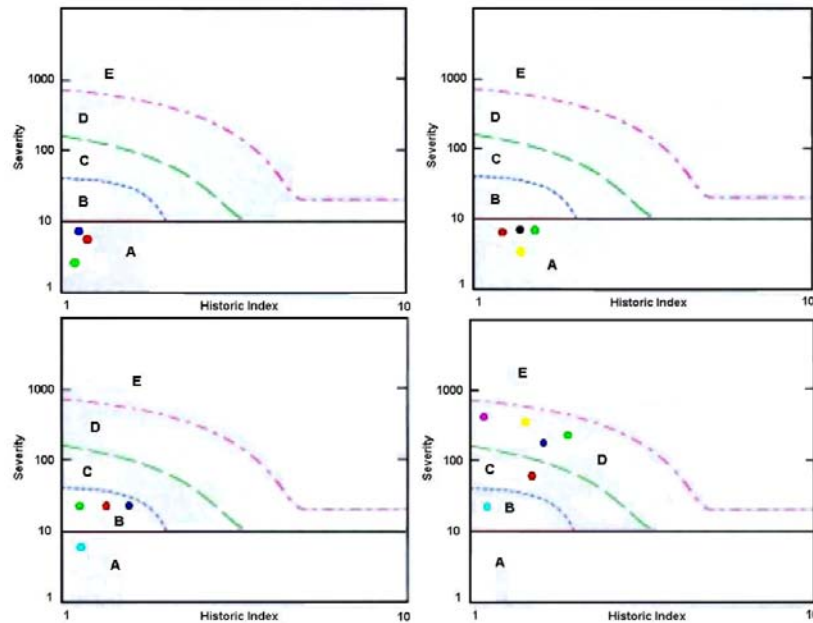


Fig. 10. Intensity plots for different stages of loading: 25% of failure load (upper left), 40% of failure load (upper right), 60% of failure load (lower left), failure load (lower right). Different colored dots indicate different measuring zones or sensor positions

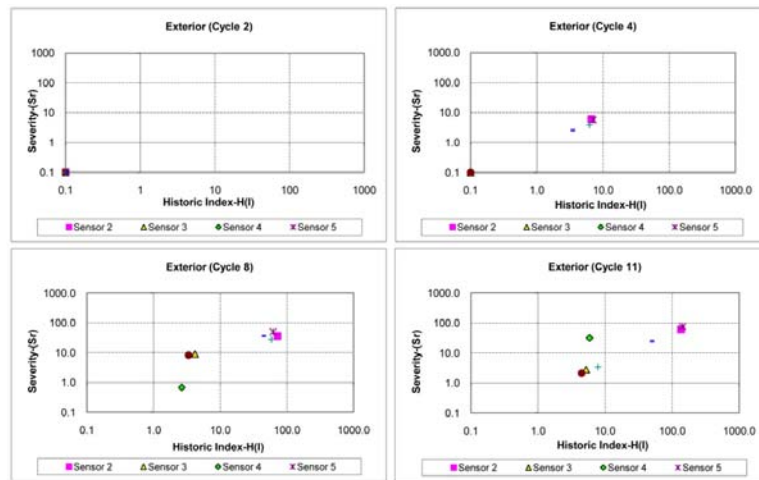


Fig. 11. Intensity analysis, historic index vs. severity, applied to a pre-stressed concrete girder during cyclic loading [23]

Gostautas [23] presented results of intensity analysis applied to a pre-stressed concrete box girder (exterior testing) during cyclic loading, given in Fig. 11. [23] At all sensor locations, indications are moving toward higher historic index and severity or toward upper right. This girder was one of eight deteriorated full-size samples tested and was loaded in 4-point bending to 69 to 327 kN, producing mid-span displacements of 7~239 mm. AE area of coverage was the mid-span section where the majority of cracking was expected to occur. In Fig. 11, results indicate that up to Cycle 4, both indices are under 10 and damage is expected to be insignificant (zone A). In Cycles 8 and 11, some points are in zone E, indicative of severe damage in accordance with severe cracking of the girder. [22]

Fowler's group used another approach involving high (>85 dB) amplitude hits and Felicity ratio for concrete box-girder evaluation. [9] They found distributed damage in a girder was most closely related to the Felicity ratio, and ones with more damage showed more high amplitude hits. Evaluation criteria developed are illustrated in Fig. 12. They also noted the utility of unloading emissions and historic index. However, they noted that intensity analysis method failed to properly account for damage state when one is dealing with distributed heavy damage.

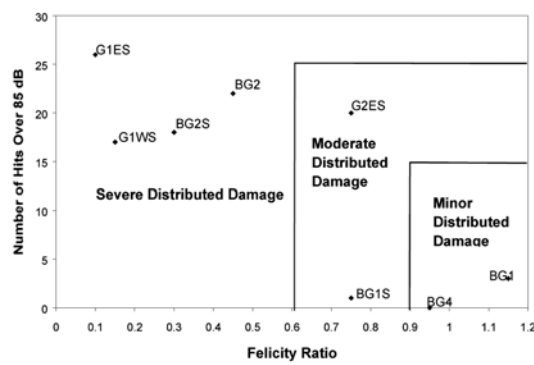


Fig. 12. Evaluation criteria for distributed damage in a girder using AE hit number and Felicity ratio. Results of eight girder tests are shown in the figure [9]

Following Fowler-Golaski approach, Nair and Cai used intensity analysis method on the evaluation of bridges and reported insignificant damage based on low historic index (<5) and low severity (0.1~5). [B8] They noted that the intensity analysis technique assesses cumulative AE data over successive loads and requires a minimum AE events, thus, continuous monitoring can help trace the health of a bridge. Some of their sensors did not record adequate AE data.

Severe cracking in bridges in use is not tolerated, of course, but more testing of damaged bridges will be needed to further confirm this method. One such case of unintentional cracking is known [B9], as will be discussed later.

Ohtsu and coworkers [19] parameterized unloading emissions as Calm ratio. This is defined by dividing the cumulative unload emissions by the total emissions in a loading cycle. Renaming Felicity ratio as Load ratio, they drew a damage classification diagram, shown in Fig. 13. The change of AE activities during cyclic loading was used to evaluate the damage in RC beams of 3.2-m long. Data was classified with the maximum values of CMOD and the beams were loaded in bending or in shear. Three different zones from minor to heavy damage were defined in good agreement with CMOD-based damage assessment.

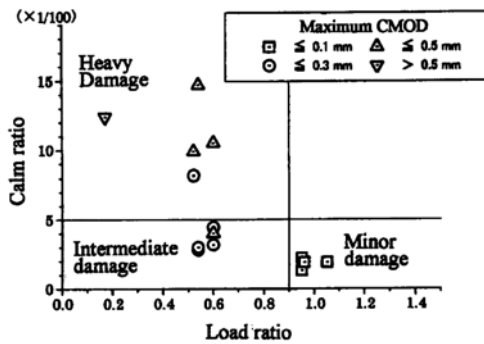


Fig. 13. Classification of AE data by the load and calm ratios [19]

For field testing, a variation of Load ratio, named RTRI ratio, is defined as follow [24]: the onset of AE activity is estimated from any measured parameters of load, deformation, etc. Next, the ratio is obtained as the ratio of the parameter's value corresponding to the onset of the AE activity to the maximum value (or peak value) on the structure during the whole inspection period. This is needed because the maximum stress the structure experienced is not readily available. Shiotani et al. [25] utilized this parameter to characterize an elevated railway bridge pier of ~6m height when they applied lateral displacements of up to 128 mm in cyclic loading. With increasing lateral displacement, RTRI ratio decreased on all sides (Fig. 14a), while Calm ratio increased especially during the last cycle. Damage classification diagram (Fig. 14b) indicates a shift to the heavy damage zone for 32- and 64-mm cycles.

In many AE applications, one is confronted with vast amount of data, from which critical information must be extracted and analyzed to solve problem at hand. One approach to tackle this task is the use of pattern recognition (PR) analysis. [26, 27] In essence, multiple features are identified from measured individual AE signals. These can be based on frequency content (autoregressive coefficients or partial spectral power) [26] and/or AE parameters such as amplitude, duration, rise time, etc. [27] Each signal is then represented as a vector in the multi-dimensional feature space. By grouping the signals in the feature space with suitable separation criteria, each signal gains the identity of a group, which has a unique "pattern". Use of available software like NOESIS and VisualClass vastly simplifies PR analysis and allows the integration of AE data acquisition and PR analysis.

Work at Kielce for concrete beam evaluation is a good example of PR applications. Golaski et al.

[28, 29] conducted a number of laboratory bending tests of RC beams ranging up to 26-m long samples and accumulated a database for AE signals for pattern recognition using NOESIS. This has been successfully used for various evaluations of concrete structures in field.

Moment tensor analysis

Starting from the integral formulation of elastodynamics and dislocation models, Ohtsu and Ono [30, 31] formulated the generalized theory of AE and described the displacement u_k of AE waves as,

$$u_k(\mathbf{x}, t) = G_{kp,q}(\mathbf{x}, \mathbf{y}, t) C_{pqij} n_j l_i \Delta V * S(t) = G_{kp,q}(\mathbf{x}, \mathbf{y}, t) M_{pq} * S(t).$$

Here, \mathbf{u} is measured at \mathbf{x} , a source is at \mathbf{y} , $G_{kp,q}$ is the spatial derivative of Green's function G_{ij} , ΔV is crack volume and M_{pq} is the moment tensor. The moment tensor represents the motion of an AE source (a crack) and characterizes the nature and intensity of AE signals emanating from the source. In isotropic media, terms are simplified and M_{pq} can be separated into crack opening and shear components. $S(t)$ is the time dependence of the AE source and defines the frequency spectrum of an AE signal. The aim of this theory was to specify the crack source from observable surface displacement (or velocity).

Ohtsu developed a simplified procedure to deduce the moment tensor, taking only the initial P-wave arrivals along with the far-field approximation of Green's function. [32, 33] This is known as **Simplified Green's function for Moment tensor Analysis (SiGMA)** procedure. In using SiGMA, a source needs to be surrounded by multiple sensors and initial P-arrivals that are usually weak must be determined for more than six channels. Results yield the location and the nature of an AE source; tensile, shear or mixed and the associated orientation. [34]

Figure 15 shows a sequence of AE locations (see Fig. 3b for load history and staging information), where one finds AE sources located along the eventual crack position (diagonal shear mode). [5] Starting at Stage II, AE cluster concentrated close to the final failure plane. Overall, about a half of the events were shear cracks, indicated as blue dots. Tensile cracks, indicated by purple dots, were located near the tensile surface, while mixed cracks (magenta dots) were distributed along the crack plane (Note colors were reversed from the original).

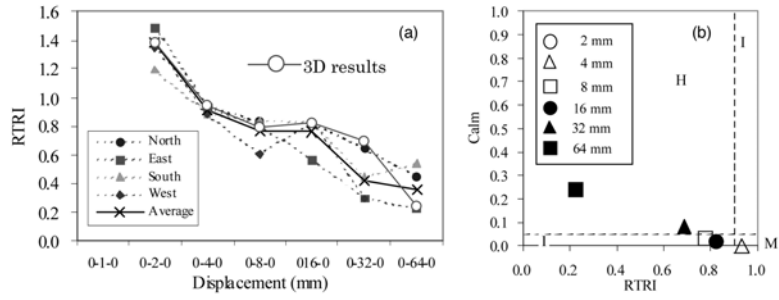


Fig. 14. Railway bridge pillar evaluation. (a) Results of RTRI obtained from AE location analyses. (b) Relations between the Calm ratio and RTRI ratio [25]

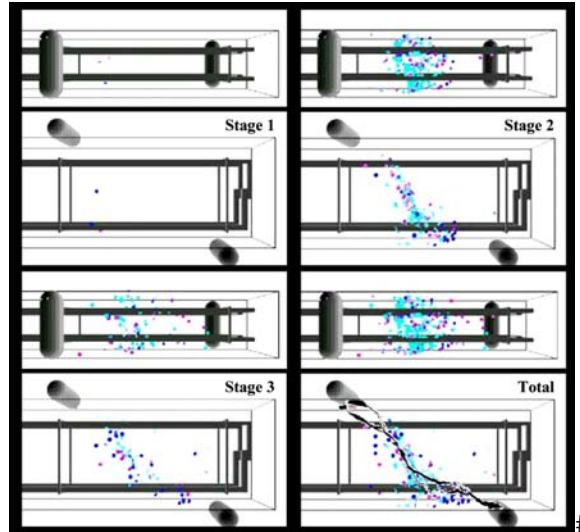


Fig. 15. 3D-visualized results of SiGMA analysis in the bending test of RC beam [5]

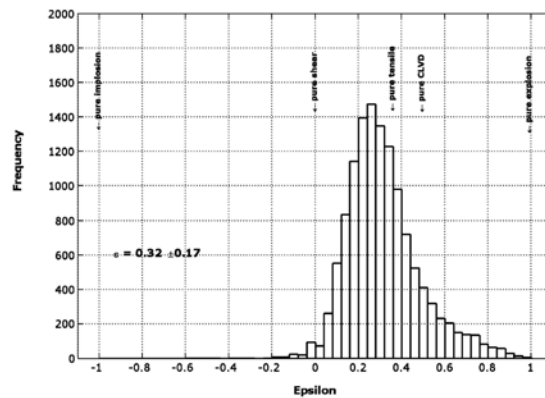


Fig. 16. Histogram of the ϵ values calculated by the eigenvalues of the moment tensor [37]

More elaborate moment tensor analysis (MTA) methods [35, 36] have been applied when larger geologic structures are evaluated. In an MTA method, the source mechanisms are estimated in a least-squares inversion calculation from amplitudes of the first motion as well as from full waveforms of P- and S-waves. MTA requires additional knowledge about the Green's function of the medium and sensor response. The moment tensor of each AE event can be evaluated if the displacements at a sufficiently large number of sensor positions are known. The sensor distorts the displacement signal emitted from the source. So, a well-characterized material and sensor are crucial in evaluating the source mechanisms with MTA

method. Manthei [37] examined rock salt and analyzed 100 k-samples using an automated procedure. Stable moment tensor solutions were obtained for 12.5% of the case using at least ten P-wave arrivals. From the results, he showed $\sim 90\%$ of the events were tensile type, oriented in the expected radial direction. This classification relied on ϵ parameter, which compares eigenvalues of moment tensor with $\epsilon = 0.37$ for pure tension. Figure 16 shows the obtained distribution of observed events. Grosse and Manthei [35, 36] also reviewed other advanced signal analysis methods, especially those that can be used in large geologic structures.

Location analysis methods

It is important to know the positions of AE sources within a structure. Linear location accomplishes this in 1-D by using two sensors and by determining the times of arrival (or onset times) with the knowledge of wave speed. Planar location extends this to 2-D and at least 3 sensors are needed. Triangulation is used to obtain AE source location. The same principle applies to the case of 3-D source location. As geometry of a structure becomes complex, it becomes necessary to define the entire volume in terms of arrival time delay to all the sensors. For most common geometries, commercial AE analysis software can adequately function. It is also customary to break up monitoring areas to simpler geometries to allow for efficient analysis. [38, 39]

In this approach, three aspects need attention. (a) As in other area, wave attenuation poses a serious obstacle especially for large structures. Main countermeasures are the use of lower frequency and reduced sensor spacing. High attenuation zones are indicative of structural damage and the mapping of such zones is a useful addendum in structural monitoring. (b) When materials have low attenuation characteristics, reverberation can be an issue. Suitable choices of signal acquisition timing parameters are used to minimize this interference. (c) Last issue is environmental noise, unavoidable in many field applications. Use of guard sensors is the primary means against this problem.

When waves propagate in heterogeneous materials, like concrete, rocks and soils, wave attenuation becomes severe and the detection frequency must be reduced. In concrete, using frequency above 100 kHz is difficult, while in geotechnical applications, less than 20 kHz is

typical. On the other hand, working on large structures at lower frequency provides certain advantages. One now treats body waves, instead of guided waves in thinner or smaller structures. Large distances from sources separate P- and S-wave components. The frequency response of sensors can be flat. Three-axes sensors can be buried inside the observed medium. Taking advantage of such conditions, despite the difficulty of working with underground geologic state, AE/MS has yielded significant wealth in geotechnical applications. [35-37, 40, 41] Moriya and coworkers [42], for example, pressurized a subsurface formation and then used AE/MS to identify hydraulically activated fracture and fluid flow direction in subsurface reservoir. They used AE multiplets to estimate the critical pore-pressure for shear slip of fractures, as shown in Fig. 17.

An entirely different approach utilizes the zone of monitoring around each sensor in a system. Here, one seeks no explicit location of an AE source. Rather, AE activities of zones are evaluated and active or inactive zones are identified for further evaluation. This approach is taken when the attenuation of wave propagation is high and the number of required sensors becomes too large. An example of zone location is the AE monitoring of a pre-stressed concrete viaduct, where several pre-stressed concrete beams (17.5-m-long) were tested [22]. The examination was performed under the loading from regular traffic. 12 measurement zones, 145-cm long each, were monitored. AE parameters such as "Amplitude", "Duration" and "Energy" were recorded. With the use of comparative evaluation criterion, this beam was found to have one high AE activity zone and three medium zones, as shown in Fig. 18.

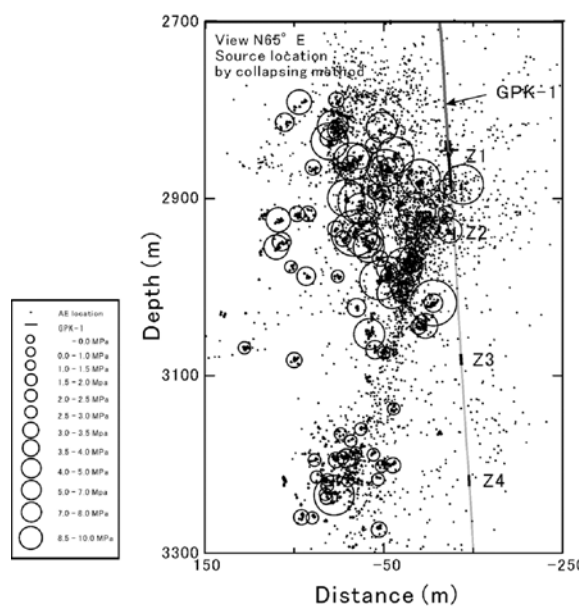


Fig. 17. Distribution of source locations with the calculated critical pore-pressure for each fracture plane. The size of circle represents the value of critical pore-pressure [41]

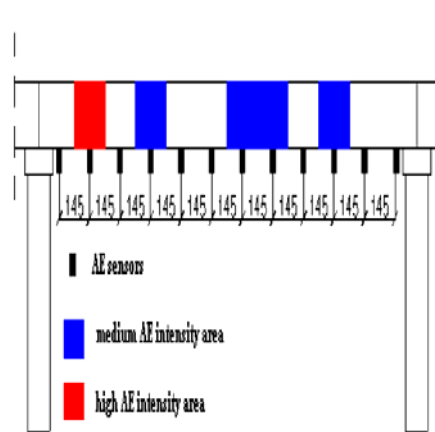


Fig. 18. Results of zone location showing areas of different levels of AE intensity [22]

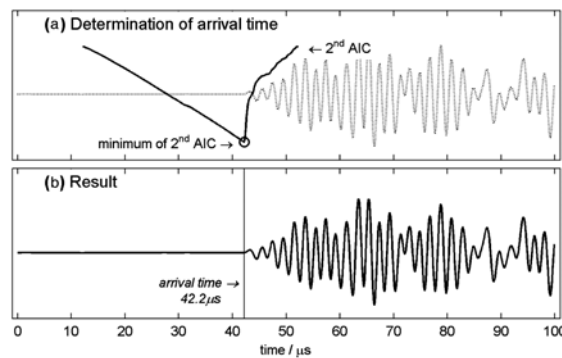


Fig. 19. Visual description of two-step AIC picker. (a) Second AIC vs. time plot, (b) Determination of final arrival time at 42.2 μs [44]

The first refinement of source location strategy involves automatic onset detection. [38] The original method of arrival time determination relied on threshold crossing. However, this often causes large errors. Modeling of a signal as an autoregressive process is an effective approach for arrival time determination. Akaike [43] showed that a signal can be divided into local segments treating each as an autoregressive process; known as Akaike Information Criterion, or abbreviated as AIC. Before the signal onset time is background noise, while AE signal begins at onset. These behave as two different stationary time series and can be separated. A typical signal waveform and AIC value are seen in Fig. 19. [44] When the signal starts, AIC suddenly changes its slope, clearly defining the signal onset. (Note threshold crossing method could put onset time as late as 67 μs for this signal.) This process can be automated and applied to a large number of AE events, leading to much improved source location accuracy.

The second refinement of source location method utilizes wavelet transform. [45] In most metallic and fiber composite structures, section thickness is limited and elastic waves propagate as

guided waves. These are always dispersive; i.e., wave velocity varies with frequency. Consequently, a short pulse at a source is extended in time with slower segments arriving at later onset. Conventional filtering introduces phase delays and is unsuitable for this purpose. The wavelet transform solved this dilemma as shown in the following example: An AE signal from stress corrosion cracking in a brass tube was detected at 20 cm from the source (Fig. 20). [46] The rise time of this signal at the source was less than 0.5 μs , but the duration of this signal at 20 cm is over 150 μs due to dispersive mode-conversion effects. This signal has spread into two main components, L(0,1) and F(2,1) cylindrical waves, as shown in the 190-kHz-wavelet coefficient plot at right. Here, one can choose suitable onset time corresponding to the known wave speed of one of these modes.

This wavelet transform analysis is also useful in understanding the nature of AE signals in steel structures since section thicknesses are generally of the same order of wavelength. Thus, waves propagate as guided waves and wavelet transform analysis allows one to set appropriate wave velocity in source location set-up.

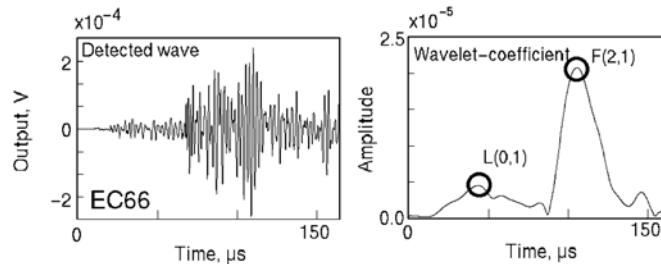


Fig. 20. An AE signal in a brass tube detected at 20 cm from the source (left). Its wavelet coefficient at 190 kHz showing two cylindrical wave modes [46]

4. Structural Monitoring

Steel bridges

AE monitoring of large structures has been conducted for many years, starting from the rocket motorcase monitoring at Aerojet in late 1950s. However, most such works have not been disseminated in general AE literature. For example, Canadian National Railway (CN) has tested hundreds of steel bridges, conducted by TISEC, but we only have limited knowledge through a few papers. [47, 48] Cavaco showed most AE test sites have no indication of fatigue, but a dozen or so test sites had high AE activity in a ten-year period (Fig. 21). [48] He states that AE monitoring is especially useful in providing essential information on the progression and intensity of existing cracks over time and that it can verify whether or not crack activity has initiated much before the actual crack can be visually detected. At CN, AE monitoring has proven to be valuable in providing information that assisted in making decisions involving the replacement, retrofit or the timely maintenance on many bridges. Hay [47] has recently summarized TISEC's work on these CN bridges. In these inspections, AE monitoring is applied to selected locations; not globally to large structures. These include among others: Hanger connections, Link

pin connection, Copes and stringers, Stiffener to weld connection. Loading is supplied by regular rail traffic, since the bridges are normally subject to high loads relative to their design loads. Planar and linear location methods are used in coordination with strain and temperature sensing. The number of repeated loading cycles is used as the primary stimulus input for AE data evaluation per ASTM E569.

Northwestern University group has been active in bridge monitoring for some time. [49] Their most recent report details the monitoring effort of a large Interstate bridge, which found no growing crack. [50] However, spatial/temporal AE cluster analysis did show indications of a defect in the area where AE activity of low amplitude was observed. They used a weatherproof enclosure, installable at the area of interest eliminating long cables and exposure of AE equipment to the elements. This approach also facilitates longer-duration tests, allowing test flexibility and robustness. Prine examined several bridges. [51] On an Oregon bridge #1377, he found crack-induced AE activity on a steel trunnion shaft, which correlated with ultrasonic test result. On another bridge, he confirmed one crack to be active while another was dormant via AE monitoring along with strain gages.

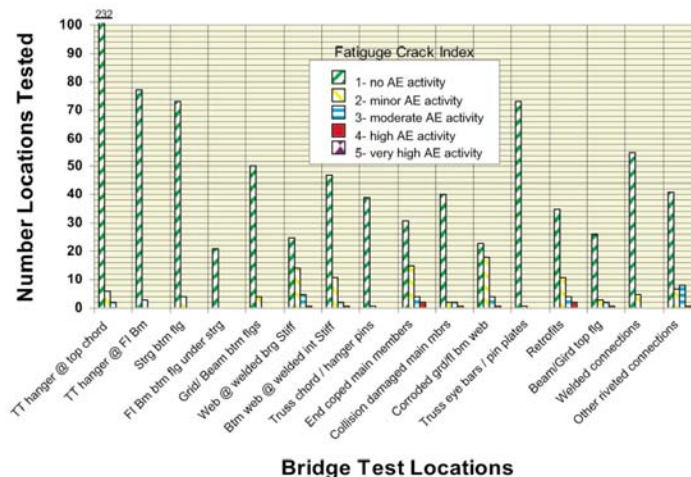


Fig. 21. Categorized summary for number of AE CN bridges tests – 1995 to 2005 [48]

Gostautas [23] summarized PAC's experiences of AE inspection of in-service bridges at AEWG in 2009. He lists the following as the attributes of AE monitoring: detect active damage, its rate and/or frequency; a tool for condition ranking; continuous remote monitoring; locate damage in real-time (e.g. crack, wire rupture); locate hidden/buried defects; inspection in areas that have limited access; combined with external parametrics (e.g. strain, displacement, temperature, pressure, etc.) to assist in identifying environmental effects that may lead to damage. In AE monitoring of a bridge, they inspected 30 sites, ranking each using 2 active and 4 guard sensors, and monitoring any extant crack tip with linear location. An indicative diagram is given in Fig. 22.

Concrete bridges

Published reports of the health monitoring of in-service concrete bridges and their structural elements are limited. Golaski et al. [22] reported testing of five bridges with various stages of damage. Results on one deteriorated bridge were in tabular forms, but one sensor position was active, in particular. The increase of the AE hits recorded under the constant loading indicated the serious damage near the sensor position. No visual damage was found and this emission was suggested to be from sources located in concrete-reinforcement interface. Repair or reinforcement of the bridge was recommended. The same bridge was tested after it was repaired. As expected, the multi-parameter AE analysis of repaired bridge did not indicate any active damage. By 2008, Kielce group has successfully tested more than 50 concrete highway bridges [29], though details are only available in Polish reports.

Nair and Cai [B8] reported AE parameter and intensity analysis of an in-service bridge (prestressed concrete slab-on-girder bridge), but obviously applied loading was limited and it was found to be sound as expected. There were some AE activities related to a known crack, but these were deemed not serious.

A major project was reported by Strategic Targeted Research Project, on "Assessment and Rehabilitation of Central European Highway Structures (ARCHES)". [B9] In its recommendation D08 (Recommendations on the use of results of monitoring on bridge safety assessment and maintenance: Annex C: The Acoustic Emission Method), they report laboratory study of old girders and field studies of two bridges. Their method appears to be similar to Kielce multi-parameter procedures. The first bridge test (Barcza) applied static load up to 92% of bending moment allowed by class B, Polish Code PN-85/S-10030. This generated new cracks detected by AE, though it remained without any significant damage to the girders. This test demonstrated that non-linearity of load-deflection curves cannot be used to assure the prevention of crack introduction. Using AE, the crack initiation can be detected at load 20% below that from visual crack detection. Figure 23 shows signal strength and amplitude including the time when cracking occurred. Signal strength jumped up to ten times and events with amplitude of over 90 dB are shown. In the second example given, they considered frequency spectrum variation of bridge AE signals. This may be worth further evaluation for possible source discrimination. However, care must be exercised as this approach has often produced false hope in the past.

Shigeishi et al. [52] examined feasibility of using AE on concrete bridges and conducted preliminary evaluation. Some valid AE signals were recorded and they concluded this to be promising. Yuyama et al. [53] evaluated fracture of high-strength steel cables in pre-stressed concrete beams and two in-service bridges. Linear source location of the events was performed by three AE sensors placed in the center and both ends of the beams. Reliability was shown to be 82–86% in terms of detectability of the failures. On 24-hr continuous monitoring of the bridges, the detected AE signals showed that meaningful AE events from cable failures are clearly discernable from other sources, such as traffic noise and hammering.

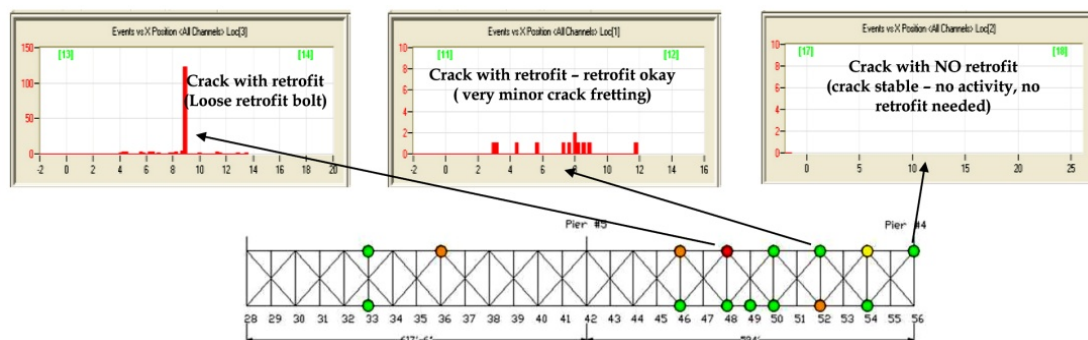


Fig. 22. Condition of 15 sites on two sections of a bridge. AE activity vs. location diagrams shown indicate the status of each site, from high to low

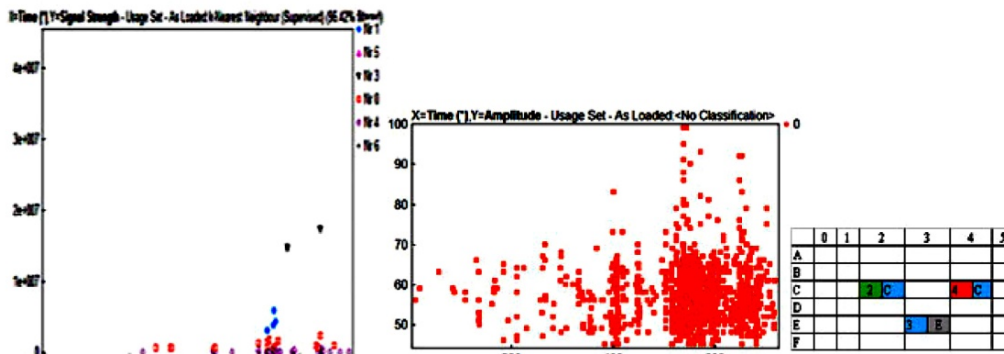


Fig. 23 AE measurements during the last phase at girder midpoint zone. AE condition rating by severity code and extent indicated 2-C (moderate damage/moderate (5-20%) coverage) [B9]

Other structures

Rock and mine stability monitoring have been extensively studied. Hardy's books [B4 and soon to be published vol. 2] and a series of conference proceedings [B5] are valuable for this area. See also [36].

Wind turbine blades are large fiber composite structures and their AE studies have been conducted in Europe and the US. [e.g., 54] While on-board applications need further development, AE has proven its utility in on-ground tests. Beattie [55] recently provided a successful example of AE application during a long-term fatigue study of a 9-m long blade, while other structural health monitoring schemes failed to identify the crack initiation and location.

Offshore oil-drilling rigs are another huge structures with abundant opportunity for AE monitoring. Brief reports of AE applications have existed since the 1970s, but this apparently is the exclusive domain of commercial enterprises. Few technical reports exist in open literature. However, a number of firms boast of successful AE monitoring experiences. For example, Tangent Technology web page [56] states "AET has been used on a North Sea platform since 2004 where chloride stress corrosion cracking was detected by AET in duplex pipework downstream of the wellhead." Discussion of AE potentials can be found in [57]. Monitoring of ships and tankers is in the same category.

Bibliography

B1. Journal of Acoustic Emission, Vol. 1 - (27), 1982 - (2009), editor, Kanji Ono, AE Group, Encino, CA.
 B2. *Progress in Acoustic Emission I - (XIV)**, Proc. of International Acoustic Emission Symposium (IAES 6 to 19; 1982 - 2008), Japan Soc. Nondestructive Inspection, Tokyo. * First five volumes (IAES 1 to 5; 1972-1980) were published under different titles.
 B3. *Acoustic Emission Testing, Nondestructive Testing Handbook, 3rd edition*, Vol. 6, American Society for Nondestructive Testing, Columbus, OH, 2005.

B4. *Acoustic Emission Microseismic Activity*, Vol. 1: Principles, Techniques and Geotechnical Applications, H.R. Hardy Jr, Taylor & Francis, 292 p., 2003.
 B5. *Acoustic Emission/Microseismic Activity in Geologic Structures and Materials: First to Sixth conference proceedings*, edited by H. Reginald Hardy, Jr. and Frederick W. Leighton, Trans Tech Publications; 1977, 1980, 1984, 1989, 1995, 1998.
 B6. C. U. Grosse and M. Ohtsu, eds., *Acoustic Emission Testing, Basics for Research - Applications in Civil Engineering*, Springer, 414 p., 2008.
 B7. T. Schumacher, *AE techniques applied to conventionally reinforced concrete bridge girders*, Oregon DOT Report SPR633, 2008, 199 p.
www.oregon.gov/ODOT/TD/TP_RES/ReportsbyYear.shtml#2008
 B8. A. Nair and C.S. Cai, *Acoustic emission monitoring of bridges: Review and case studies*, Engineering Structures, **32** (2010) 1704-1714.
 B9. Strategic Targeted Research Project, "Assessment and Rehabilitation of Central European Highway Structures (ARCHES)" Report ARCHES-02-DE08-C (http://arches.fehrl.org/?m=7&id_directory=1615)

References

1 T. Kanagawa and H. Nakasa, *Method of Estimating Ground Pressure*, US Patent, No. 4107981, 1978.
 2 A. Lavrov, *The Kaiser effect in rocks: principles and stress estimation techniques*, Int J. Rock Mech. Min. Sci. 40 (2003), 151-171.
 3 K. Ono, H. Cho and M. Takuma, *Journal of Acoustic Emission*, 23, 206-214 (2005).
 4 M. Enoki, T. Kishi and S. Kohara, *Proc. IAES*, vol. 8, p. 766, 1986.
 5 K. Ohno, Y. Sawada, K. Utsunomiya and M. Ohtsu, *Proc. IAES*, vol. 19, p. 351, 2008.

- 6 M.C. Munwam and M. Ohtsu, Proc. 6th Intl Symp. on Acoustic Emission from Composite Materials, ASNT, pp. 153-162 (1998).
- 7 J. Kaiser: Arch. Eisenhüttenwesen 24, 43 (1953); J. Kaiser: Forsch. Ing. Wesen, 38 (1957).
- 8 S. Niiseki, M. Satake, H. Kanemori and Y. Ito, Proc. IAES, vol. 9, p. 324.
- 9 B. V. Tinkey, T. J. Fowler, and R. E. Klingner, *Texas DOT Report*, FHWA/TX-03/1857-2, 2002. 108 p.
- 10 H.B. Teoh and K. Ono, *J. Acoustic Emission*, 6, 1 (1987).
- 11 H. Hatano and K. Ono, Proc. IAES, vol. 3, 476 (1976).
- 12 M.A. Khan, T. Shoji and H. Takahashi, Proc. IAES, vol. 6, 531-541 (1982).
- 13 K. Mogi, Bull. Earthquake Res. Inst., 40, 125-173; 831-853 (1962).
- 14 M. Ohtsu, *Characteristics and Theory of Acoustic Emission*, 2nd ed. Morikita, p. 41, 2005.
- 15 T. Shiotani, S. Yuyama, Z. W. Li and M. Ohtsu, *J. Acoustic Emission*, 19, 118 (2001).
- 16 K. Ono, Proc. IAES, vol. 19, 203 (2008).
- 17 H.L. Dunegan, DECI reports #0005, #9810; www.deci.com/publications.html
- 18 T. Shiotani, Y. Nakanishi, X. Luo and H. Haya, *J. Acoustic Emission*, 22, 39 (2004).
- 19 M. Ohtsu and S. Yuyama, *J. Acoustic Emission*, 19, 184-190 (2001).
- 20 S. Takaya, T. Yamamoto and T. Miyagawa, Proc. IAES, vol. 19, p. 303, (2008).
- 21 T.J. Fowler, J.A. Blessing, P.J. Conlisk and T.L. Swanson, *J. Acoustic Emission*, 8, 1-10 (1989).
- 22 L. Golaski, P. Gebiski and K. Ono, *J. Acoustic Emission*, 20, 83-98 (2002).
- 23 R. Gostautas, presented at Primer, 52nd AEWG Meeting, October 2009.
- 24 X. Luo, H. Haya, T. Inaba, T. Shiotani and Y. Nakanishi, *Proc. Structural Engineering World Congress 2002*, Paper No. T9-1-e-3, 2002.
- 25 T. Shiotani, X. Luo and H. Haya, *J. Acoustic Emission*, 24, 205-214 (2006).
- 26 M. Ohtsu and K. Ono, *J. Acoustic Emission*, 3, 69-80 (1984); 5, 61-72 (1986).
- 27 A. Anastasopoulos, *J. Acoustic Emission*, 23, 318-330 (2005).
- 28 L. Golaski, G. Swit, M. Kalicka and K. Ono, *J. Acoustic Emission*, 24, 187-195 (2006).
- 29 M. Kalicka, *J. Acoustic Emission*, 27, 18-26 (2009).
- 30 M. Ohtsu and K. Ono, *J. Acoustic Emission*, 3, 27-40 (1984).
- 31 M. Ohtsu and K. Ono, *J. Acoustic Emission*, 5, 124-133 (1986).
- 32 M. Ohtsu, *Materials Evaluation*, 45, 1070-1075 (1987).
- 33 M. Ohtsu, *J. Geophysical Res.*, 96(B4), 6211-6221.
- 34 M. Ohtsu, *Acoustic Emission – Beyond the Millenium*, Elsevier, pp. 19-34, (2000); see also Chap. 7 and 8, B6, pp. 149-200.
- 35 C.U. Grosse and L.M. Linzer, Chap. 5 in B6, pp. 53-99.
- 36 G. Manthei and J. Eisenblätter, Chap. 11 in B6, pp. 239-310.
- 37 G. Manthei, Bull. Seismological Soc. Am., 95, 1674-1700 (2005).
- 38 J.H. Kurz, S. Köppel, L.M. Linzer, B. Schechinger and C.U. Grosse, Chap. 6 in B6, pp. 101-147.
- 39 M. Ge, *J. Acoustic Emission*, 21, 14-28, 29-51 (2003).
- 40 H. Niitsuma, *Acoustic Emission – Beyond the Millenium*, (2000), Elsevier, pp. 109-125.
- 41 G. Manthei, J. Eisenblätter, and T. Spies, *Acoustic Emission – Beyond the Millenium*, (2000), Elsevier, pp. 127-143.
- 42 H. Moriya, H. Niitsuma and R. Baria, *J. Acoustic Emission*, 23, 113-118 (2005).
- 43 H. Akaike, *Annals Inst. Statistical Math.*, 26, 363-387 (1974).
- 44 P. Sedlak, Y. Hirose, M. Enoki and J. Sikula, *J. Acoustic Emission*, 26, 182-188 (2008).
- 45 M. Takemoto, H. Nishino and K. Ono, *Acoustic Emission – Beyond the Millenium*, (2000), Elsevier, pp. 35-56.
- 46 F. Uchida, H. Nishino, M. Takemoto and K. Ono, *J. Acoustic Emission*, 19, 75-84 (2001).
- 47 D.R. Hay, J.A. Cavaco and V. Mustafa, *J. Acoustic Emission*, 27, 1-10 (2009).
- 48 J.A. Cavaco, *Bridge Structures*, 3 (1), 51-66 (2007).
- 49 D.E. Kosnik and D.R. Marron, *Civil Structures*, presented at Primer, 52nd AEWG Meeting, October 2009.
- 50 D.E. Kosnik, *J. Acoustic Emission*, 27, 11-17 (2009).
- 51 D.W. Prine, Technical report #6 and #12, Infrastructure Technology Institute, Northwestern University, (1994, 1995).
- 52 M. Shigeishi, S. Colombo, K.J. Broughton, U. H. Rutledge, A.J. Batchelor, M.C. Forde, *Construction and Building Materials*, 15, 35-49, (2001).
- 53 S. Yuyama, K. Yokoyama, K. Niitani, M. Ohtsu, T. Uomoto, *Construction and Building Materials*, 21, 491-500, (2007).
- 54 A.A. Anastasopoulos, D.A. Kouroussis, V.N. Nikolaidis, A. Proust, A.G. Dutton, M. Blanch, L.E. Jones, P. Vionis, D.J. Lekou, D.R.V. van Delft, P.A. Joosse, T. Philippidis, T. Kossivas, G. Fernando, *J. Acoustic Emission*, 20, 229-237, (2002).
- 55 A.G. Beattie in M.A. Rumsey and J.A. Paquette, Proc. of SPIE, vol. 6933, 69330E, (2008).
- 56 www.sovereign-publications.com/tangent-tech.htm
- 57 A. Anastasopoulos, D. Kourousis, S. Botten and G. Wang, *Ships and Offshore Structures*, 4(4), 363-372(2009).

THE ANALYSIS OF THE ROTOR'S LONGITUDINAL VIBRATIONS WITH LARGE MISALIGNMENT OF SHAFTS AND ROTEX TYPE COUPLING

Janusz ZACHWIEJA

Department of Applied Mechanics,
University of Technology and Life Sciences in Bydgoszcz
Prof. Sylwester Kaliski street no 7, 85-791 Bydgoszcz

Summary

It is very difficult to unambiguously define the symptoms of misalignment of rotating elements of machine on the basis of vibration spectrum. With numerous states of inefficiency the picture of amplitude-frequency characteristic which is the basic tool of vibrodiagnostics is similar. Loose coupling or rubbing of the rotor's moving parts against fixed elements cause large vibration velocity amplitudes for the sequence of ultra-harmonics of the rotational frequency, similarly as in the case of drive system misalignment.

The author analyzes the character of the rotor's longitudinal vibrations in which there is a large misalignment of shafts joined by coupling with spring elements in a form of a plastic insert with high hardness. It is also showed how the response of the system to the axial force changes in the case where spring element is damaged.

Keywords: misalignment, vibrations in the direction of the rotor's axis, rotor dynamics, vibration spectrum, rotor modelling, numerical computation.

ANALIZA DRGAŃ WZDŁUŻNYCH WIRNIKA PRZY DUŻEJ NIEWSPÓŁOSIOWOŚCI WAŁÓW I SPRZĘGLE TYPU ROTEX

Streszczenie

Jednoznaczne określenie symptomów występowania niewspółosiowości wirujących elementów maszyny na podstawie widma drgań jest zagadnieniem bardzo trudnym. Przy licznych stanach niesprawności obraz charakterystyki amplitudowo-częstotliwościowej, będącej podstawowym narzędziem wibro-diagnostyki, jest podobny. Luz w łożysku lub ocieranie części ruchomych wirnika o elementy nieruchome są przyczyną dużych wartości amplitud prędkości drgań dla kolejnych ultraharmonicznych częstotliwości obrotowej, analogicznie jak w przypadku niewspółosiowości w układzie napędu.

Autor analizuje charakter drgań wzdłużnych wirnika, w którym występuje duża niewspółosiowość wałów łączonych sprzęgłem z elementem sprężystym w postaci wkładki wykonanej z tworzywa sztucznego o dużej twardości. Pokazano również jak zmienia się odpowiedź układu na wymuszenie siłą osiową w przypadku, gdy element sprężysty ulega uszkodzeniu.

Słowa kluczowe: niewspółosiowość, drgania w kierunku osi wirnika, dynamika wirnika, widmo drgań, modelowanie wirnika, obliczenia numeryczne.

1. INTRODUCTION

The diagnosis of misalignment of shafts joined by coupling based on amplitude-frequency characteristic of a particular parameter of their vibrations is burdened with a high degree of uncertainty. Usually, it is stated that the dominant value in vibration spectrum for frequencies $1x$ and $2x$ constitutes believable symptom of this inefficiency. Rotor's vibration spectrum during resonance and with clearance between coupling and casing has often similar shape. This is understandable because in each case we are dealing with non-linear stiffness of the system.

The machines' rotors very often operate at rotational speeds close to critical velocities. The analysis of the character of the rotor's resonance vibration during misalignment of shafts becomes particularly important. Misalignment of the joined rotating elements, to greater or lesser extent, occurs almost always. That is why properly designed joint should show flexibility in a degree allowing the compensation of the effects connected with it.

The influence of the joint type and contact interaction between stiff and elastic elements on the character of the rotor's vibrations was discussed in the thesis [1]. The identification of main factors which affect transverse vibrations of the rotor was

made by Woodcock [2]. Bloch and Geitner [3] estimated maximum values of misalignment for the joints because of the stress state in a coupling. Grigoriev [4] in theoretical and experimental way determined and then compared amplitude-frequency characteristics of bearing bodies' vibrations for different types of joints of cooperating shafts. Gibbons proved that misalignment causes the forces in a coupling which extort the vibration of the system [5].

Numerous researchers [6-7] have tried to define the symptoms of the system's misalignment by showing on the basis of the character of rotor's vibrations that most often the symptom is a huge value of amplitude for frequencies twice bigger than the rotational frequency of the shafts. Dewell and Mitchel [8] proved that vibration spectrum of the system with misalignment consists of components with broad frequency spectrum, however the components $2x$ and $4x$ of the rotational speed experience the greatest changes when the misalignment rises.

The shafts' misalignment, especially of an angular character, is accompanied by a time-varying axial force which composes a force for rotor's longitudinal displacements. This effect influences the form of amplitude-frequency response of the vibration's velocity. Therefore, an examination of the rotor's longitudinal vibrations character is as much important as analyzing its lateral vibrations.

2. THE ANALYSIS OF THE CHARACTER OF LONGITUDINAL VIBRATIONS OF THE ROTOR WITH MISALIGNMENT IN THE DRIVE SYSTEM.

The object of the research was twin-disk stiff rotor joined with the shaft of the motor by ROTEX type coupling with intermediary element in a form of plastic insert of 92°Sh hardness. The resulting misalignment of the system was superposition of parallel shift of shafts' axis and their relative rotation. The values of parameters describing reciprocal position of axis were depicted for three cases for which the research was conducted. They are presented in table 1.

Table 1. Parameter values of joined shafts misalignment

Surface	Type of misalignment	Parameter value of misalignment		
		state 1	state 2	state 3
horizontal	parallel	0.01mm	0.04mm	0.05mm
	angular	0.083%	0.133%	0.183%
vertical	parallel	0.01mm	0.13mm	0.47mm
	angular	0.017%	0.717%	2.333%

State 1 corresponds with the situation when misalignment of the rotor's and motor's shafts is little. State 3 relates to the case of very big misalignment. This applies mainly to relative angular position of the shaft's axis which amounts to 2.33%. As for the diameter of the coupling equal to

60mm it corresponds with the angle of 1.4° . State 2 defines the intermediate case between states 1 and 3.

Fig. 1 presents the way of measuring deviation of the rotor's and motor's shafts misalignment. On one of them there is an emitter/detector of laser beam reflected by the mirror placed on the second shaft. Measurement error is 0.001mm which affects precision of the shift of the regulated element in both surfaces of 0.01mm. Relative placement of the shafts is determined during their simultaneous rotation by angle the minimum value of which is 60° .

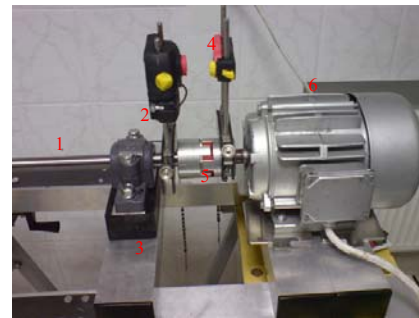


Fig. 1. The way of measuring misalignment of the rotor's and motor's shafts by using laser tool:

1 - rotor's shaft, 2 - bearing with the casing, 3 - rubber pad, 4 - laser tool, 5 - coupling, 6 - motor

Measurements of longitudinal vibration parameters of the motor and rotor's bearing located by the coupling were conducted for the rotational speed of 1200r.p.m, which is equal to frequency of 20Hz. It was also checked by determination of resonance curve of bearings' vibrations that the exploitative rotational speed of the rotor is not in the resonance area.

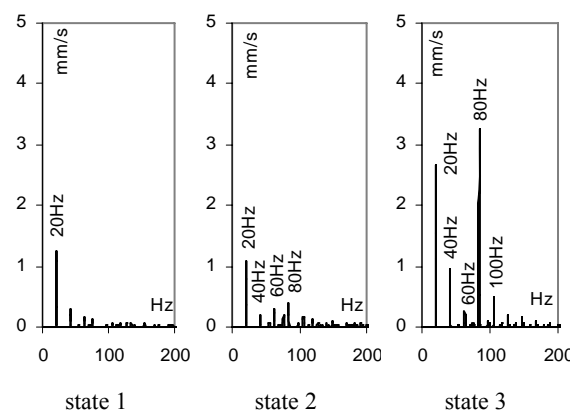


Fig. 2. Longitudinal vibration velocity spectrums of the rotor's bearing by the coupling

Fourier transforms determined on the basis of the time course of displacement speed prove that longitudinal vibrations of the rotor's bearing with bigger misalignment are characterized by the growth

of components' amplitude with frequency of 1x, 2x and in particular 4x (Fig. 2).

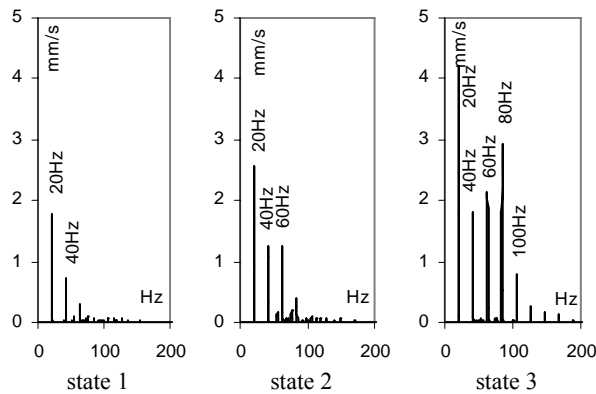


Fig. 3. Longitudinal vibration velocity spectrums of the motor

In the case of longitudinal vibrations of the motor which feet were lowered compared to the rotor's axis of 3.5 mm at the front and 5.83 mm at the back, the growth of the amplitude of components 1x, 2x, 3x, 4x, and even 5x was observed (Fig. 3). The characteristic thing is that high value of vibration amplitude of ultra-harmonic frequencies 1x and 4x occurs for numerous rotational speeds of the rotor (Fig. 4). This conclusion results from the analysis of vibration spectrum of the system of 1.64% misalignment.

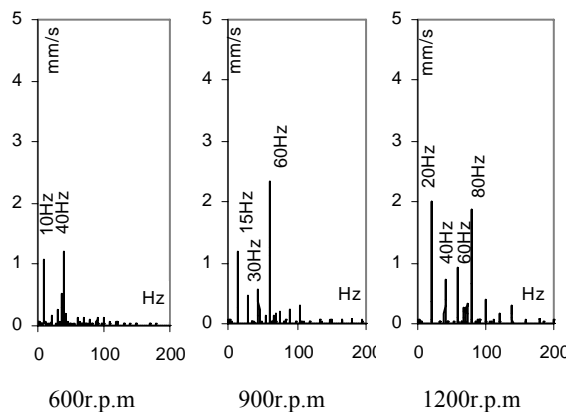


Fig. 4. Longitudinal vibration velocity spectrums of the rotor with angular misalignment of 1.64%

This kind of distribution of amplitude values results from the construction features of coupling. Its each half has four interlocking during the rotation centres. Contact force exerts longitudinal vibrations of frequency which is the product of the amount of pairs of elements and rotational frequency of the rotor. Interesting is the fact that if the geometry of coupling allows temporary contact between one centre and the socket so in fact the occurrence of high amplitude values in longitudinal vibration spectrum should be expected, also with the frequency of 8x. The correctness of this assumption

was verified on the basis of the numerical analysis of the rotor's movement.

3. NUMERICAL ANALYSIS OF LONGITUDINAL VIBRATIONS OF THE ROTOR

The rotor which is a model for calculation is presented in Fig. 5. It can be used for the analysis of transverse vibrations as well as longitudinal vibrations and also torsional vibrations.

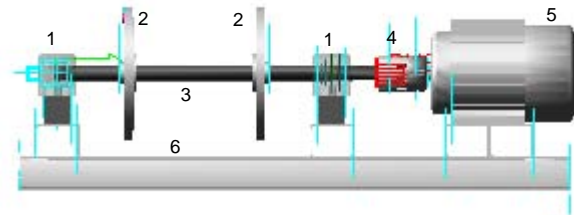


Fig. 5. Numerical model of the rotor: 1 - bearings and casings, 2 - discs, 3 - rotor's shaft, 4 - coupling, 5 - motor, 6 - frame

The model reflects the features of the stand presented in Fig.1 in the field of interial properties (mass and moments) and stiffness and damping of the support. The most crucial, from the point of view of the problem analysis, is the applied ROTEX model coupling. The halves of the coupling are treated as rigid blocks (Fig. 6), while the intermediary insert is a deformable element (Fig. 7a) which was discretized into finite elements in a way showed in Fig. 7b.

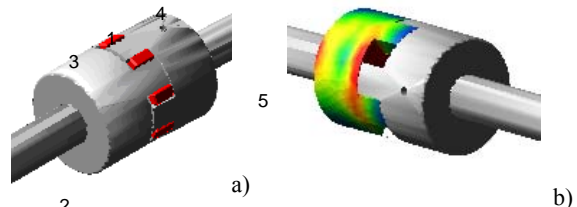


Fig. 6. a) The model of the rotor used for calculations: 1 - intermediary element, 2 - rotor's shaft, 3 - the element of coupling connected with the rotor, 4 - the element of coupling connected with the motor, 5 - motor's shaft
 b) Stress distribution in a half of the coupling from the rotor's side without the elastic insert

Thanks to that it was possible to determine the method of element's deformation during rotation of the rotor as well as stress distribution in its sections.

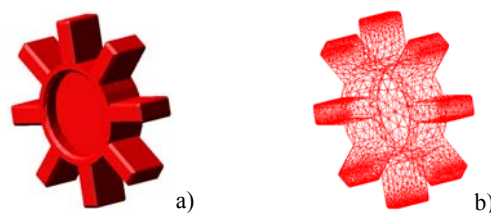


Fig. 7. Intermediary element: a) look, b) the method of finite elements' discretization

Twisting moment by affecting the halves of the coupling causes bending of pads in a shape of cuboid placed symmetrically on the perimeter. The pads act identically as the beam clamped by one end and loaded in a continuous manner. Therefore, the greatest deformation occurs at the ends of elements (Fig. 8a).

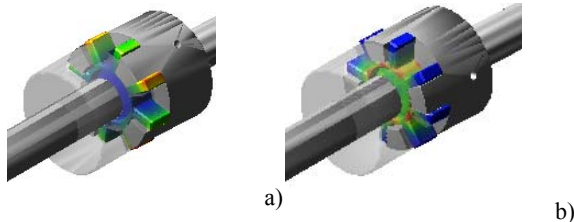


Fig. 8. a) Deformation of intermediary element in the next phase of rotation, b) stress distribution in the element

Maximum value of the stress occurs at the base of the element (Fig. 8b). For the torsion moment transferred by the coupling the coupling's material effort is small and amounts to only a few megapascals. The elastic intermediary element was also used in order to determine its damping properties. Fig. 9 presents longitudinal vibration velocity spectrums of the rotor for different stiffnesses in the contact area of coupling's metal elements separated by the susceptible insert.

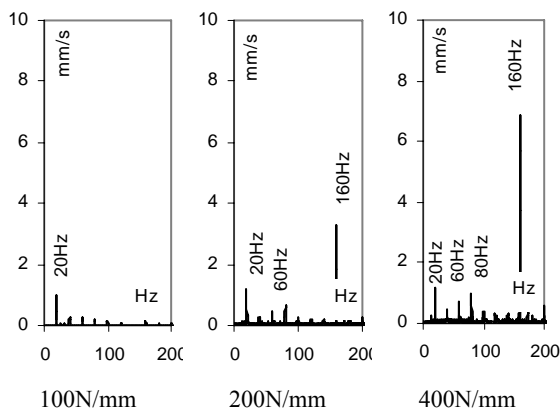


Fig. 9. The character of longitudinal vibration velocity spectrum of the rotor for different stiffnesses in the contact area of coupling's halves with elastic insert – numerical computations results

The analysis of vibration spectrums of the simulated rotor allows to draw a conclusion that along with the growth of stiffness in the contact area the value of vibration amplitude with frequency of $8x$ is growing. Therefore, it can be assumed that the actual stiffness in the contact area of coupling's elements is low and that is why we observe the dominant value of velocity amplitude of vibrations at the frequency of $4x$. The correctness of this assumption can be proved by the picture of velocity spectrum of rotor's vibrations with coupling without the susceptible element (Fig. 10) for the stiffness of

the contact between coupling's elements amounting to 100N/mm . The comparison of Fig. 9 and 10 gives an overview on the role of the insert in damping coupling's vibrations.

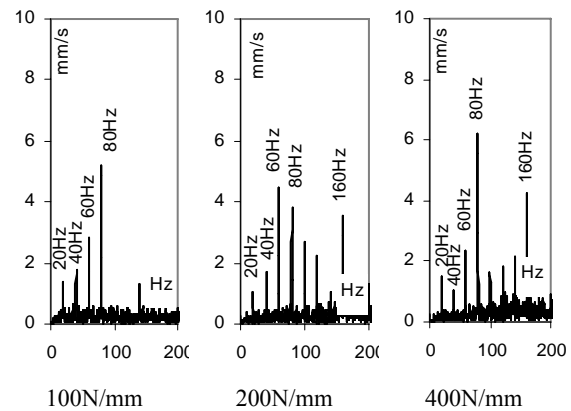


Fig. 10. Longitudinal vibration velocity spectrums of the rotor for different stiffnesses in the contact area of coupling's halves without the elastic insert – numerical computations results

Stress distribution in coupling without the intermediary element is presented in Fig. 6b. This state corresponds with the position where there is no axial play. For greater clarity, the stress map was visualized only in one part of coupling.

4. CONCLUSIONS

The research as well as numerical analysis of the system's vibrations confirmed the thesis presented at the beginning that unambiguous definition of the symptoms of misalignment is almost impossible. The picture of vibration spectrum depends on the size of misalignment, rotational speed of the rotor, construction features of coupling as well as stiffness in the contact area between its elements.

ROTEX type coupling with susceptible elements which was used in the research does not allow to obtain large angular misalignment of the shafts. For the value over 1.5° , as the rotational speed of the rotor was growing, the temperature of the elastic element was growing, and acoustic effects accompanied the work of the system. Durability of the insert in such conditions is rapidly declining. This situation is extremely unfavourable because susceptible element has damping properties and its damage causes the growth of vibration level of the rotor.

REFERENCES

- [1] Mancuso J. R.: *The manufacturers world of coupling potential unbalance*. Proceedings of the Thirteenth Turbomachinery Symposium, 1985, s. 97-103.
- [2] Woodcock J. S.: *The effects of couplings upon the vibration of rotating machinery*. Proceedings of the International Conference on

- Flexible Coupling University of Sussex, Brighton U.K, Farnham U.K. Michael Neale and Associates Ltd., 1977, s. 1-20.
- [3] Bloch H. P., Geitner F. K.: *An Introduction to Machinery Reliability Assessment*. New York, 1990.
- [4] Grigoriev N. V.: *An investigation into the vibration isolation properties of elastic couplings of connected shafts under flexural vibration*. Soviet Engineering Research 2(12), 1976, s. 42-43.
- [5] Gibbons C. B.: *Coupling misalignment forces*. Proceedings of the Fifth Turbomachinery Symposium, Gas Turbine Laboratories, Texas A&M University, College Station, Texas, 1976, s. 111-116.
- [6] Schwerdlin H.: *Reaction forces in elastomeric couplings*. Machine Design 51(16), 1979, s. 76-79.
- [7] Maten S.: Program machine maintenance by measuring vibration velocity. Hydrocarbon Processing, 49(9), 1970, s. 291-296.
- [8] Dewell D. L., Mitchell L. D.: *Detection of a misaligned disk coupling using spectrum analysis*. American Society of Mechanical Engineers Journal of Vibration, Acoustics, Stress and Reliability in Design, 106, 1984, s. 9-15.

Janusz ZACHWIEJA - Phd. eng.
is an assistant professor in the
Department of Applied Mechanics
in University of Technology and
Life Sciences in Bydgoszcz.



IDENTIFICATION OF MACHINE TECHNICAL STATE ON THE BASIS OF FOURIER ANALYSIS OF INFRARED IMAGES

Marek FIDALI

Department of Fundamentals of Machinery Design, Silesian University of Technology
Konarskiego 18a, tel.: 32 237 1063, fax.: 32 237 1360, e-mail: marek.fidali@polsl.pl

Summary

In the article results of analysis of sequence of infrared images with use 1D Fourier transform is presented. Images were analyzed in the same way like this known from branch of active thermography where pulse phase method is applied in order to detect structural defects in the materials. Research was carried out with use of thermovision images recorded during operation of rotating machinery. The amplitude and phase images which described different technical states of observed machines were calculated. In order to generate the most informative images of amplitude and phase a procedure of frequency selection was proposed. Qualitative and quantitative estimation of the amplitude and the phase images shows that presented way of sequence of infrared image analysis provide useful diagnostic data which allow identification changes of machine technical state.

Keywords: diagnostics, thermovision, Fourier analysis, image processing.

IDENTYFIKACJA STANU TECHNICZNEGO MASZYN NA PODSTWIE WYNIKÓW ANALIZY FOURIERA OBRAZÓW TERMOWIZYJNYCH

Streszczenie

W artykule przedstawiono wyniki analizy obrazów termowizyjnych z zastosowaniem jednowymiarowej transformaty Fouriera. Obrazy analizowano w sposób znany z dziedziny termografii aktywnej gdzie dla potrzeb detekcji defektów materiałowych stosowana jest metoda impulsowo fazowa. Badania przeprowadzono na obrazach zarejestrowanych podczas działania maszyny wirnikowej w różnych stanach technicznych. W wyniku analizy zarejestrowanych termogramów wyznaczono amplitudogramy i fazogramy reprezentujące różne stany techniczne maszyny. Jakościowa i ilościowa analiza obrazów amplitudy i fazy wskazują, że prezentowane podejście do analizy sekwencji obrazów termowizyjnych umożliwia identyfikację zmian stanu technicznego maszyny.

Słowa kluczowe: diagnostyka, termowizja, analiza Fouriera, analiza obrazów.

1. INTRODUCTION

Thermographical measurements find a broad application in maintenance and technical state assessment of machinery, apparatus and industrial processes [5]. Continuous thermovision diagnostics of a technical object requires that systematic series of operations consisting in acquiring, processing, analyzing and recognizing infrared images have to be carried out. As a result of image analysis, important diagnostic information coded in thermographic images is extracted.

The research connected with infrared image processing and analyzing for machinery diagnostic has been carried out in Department of Fundamentals of Machinery Design for a few years [2],[3],[4]. During the previous research a formalized method of thermovision data analysis has been proposed. According to the method a sequence of thermograms acquired during a continuous observation of

a machine is treated as a multidimensional thermographic signal $ST(T(x,y),t)$ where $T_i(x,y)$ is thermographic image recorded in given moment of time t_i and x, y describe spatial resolution of the image. Thermographic signal could be analyzed under assumption that real time domain could be partitioned into "micro" (dynamic) and "macro" (operational) time domains [1]. Such approach allows treating short sequence of infrared images as thermographic signal in "micro" time. One could assume that analysis of thermographic signal in "micro" time result one relevant feature value which could be treated as value of diagnostic signal in "macro" time (Fig.1).

Due to large thermal inertia of most mechanical objects, "micro" time should be treated in range of minutes or hours and "macro" time in range of days and weeks.

Example of application of assumed methodology is presented in the article. A results of the research

concern in “micro” time analysis of thermographic signals recorded during operation of investigated machine in different technical states.

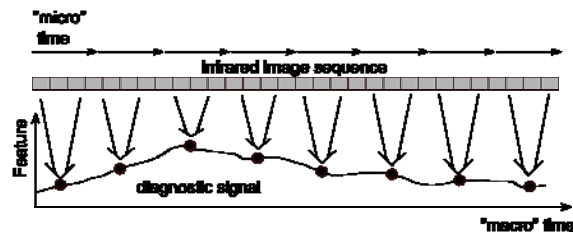


Fig. 1. Idea of analysis of sequence of infrared images in both “micro” and “macro” time

For purposes of analysis of thermovision image sequence approach based on commonly used method in branch of active thermography was applied. The method use 1D Fourier analysis of thermovision image sequence.

2. FOURIER ANALYSIS OF SEQUENCE OF THERMOVISION IMAGES

1D Fourier transform can be applied to the thermographic signal acquired during machine observation in the same way as it is known in the field of active thermography where a pulse phase method is applied in order to detect structural defects in materials [7].

In this method a signal describing temperature evolution over time for a given pixel of each recorded infrared image is transformed to frequency domain with the use of Fourier transform. The results of Fourier transform are represented in a form of real and imaginary parts estimated for given discrete frequency values f_n calculated in the following way [7]:

$$f_n = \frac{n}{Nt_s} \quad (1)$$

where:

N – number of thermal images in the sequence
 t_s – time interval between thermal images ($t_s=30s$)
 $n=0,1,\dots,N/2$.

On the basis of the real and imaginary parts of spectrum calculated for all pixels at given frequency new images of magnitude and phase are formed. As shown in the literature [7], phase and amplitude images have selective, frequency-dependent capability in identification of heating uniformity. The amplitude images are less noisy but are sensitive to non uniform heating what can be referred to low-pass filter behavior. The phase images allow us to probe under the surface of observed an object and are less sensitive to degradation coming from optical and infrared surface features. The phase images can be also considered with respect to the band-pass filter behavior [7].

One can expect that discussed method could be useful to estimation of machine technical states whose manifest in non uniform distribution of temperature on observed surface and produce more heat in short time e.g. during machine run-up or during disturbance of machine operation.

Application of 1D Fourier analysis to sequence of thermovision images generates two series of images both magnitude and phase in frequency domain. The images could be called magnitudegrams and phasegrams. Analysis of these images seems to be time consuming because need to examine and interpret each of them in order to choose relevant one. Selecting of relevant images strongly depend on experience and subjective decision of the researcher. Make of the magnitudegrams and phasegrams suitable for automatic evaluation of machine technical state requires procedure of selecting of representative images for further analysis. Such procedure was proposed and is based on assumption that reference sequence of images described proper and nominal machine technical state is available. On the basis of such reference sequence of infrared images one can find coordinates of such image pixel over which temperature evolution in time have the highest variation. Such pixel could be called as reference one. Function described temperature evolution over reference pixel is transformed to frequency domain in order to obtain reference spectrum for further analysis. On the basis of the reference spectrum one can identify n meaningful frequency components e.g. components with first few highest values. For the frequencies corresponding to chosen spectrum components one can select magnitudegrams and phasegrams for further analysis.

In order to obtain qualitative or quantitative data both amplitude and phase images could be processed and analyzed with use of suitable fitted methods [6].

2.1. Considered data

Usability of application of Fourier analysis of infrared image sequence for the purposes of machinery diagnostics was verified on experimental data acquired during an active diagnostic experiment. The experiment has been performed in the Laboratory of Technical Diagnostics of Department of Fundamentals of Machinery Design. The aim of the experiment has been to acquire thermographic signals during operation in following manually simulated technical (operational) states:

- S0 – machine during heating (run-up) – 120 images
- S1 – machine without faults – 120 images
- S2 – 50% throttling of air pump - 120 images
- S3 – 90% throttling of air pump – 120 images
- S4 - 90% throttling of air pump + clearance of second bearing mounting – 120 images
- S5 – load of disk brake – 120 images
- S6 – faulty bearing no 2– 120 images.

Infrared images have been acquired with use of thermovision system every 30 seconds period. The total number of recorded images has been 840. The machine was working with rotation speed equal to 1150 rpm.



Fig. 2. Investigated object and applied infrared camera

It is necessary to point out that technical state S1, S2 and S3 were very similar and were simulated purposely in order to check whether it was possible to notice a weak change of the technical state on the basis of the considered diagnostic signals. Such a small change in the technical state were also desirable for testing ability of the classifiers recognizing machine technical states difficult to be distinguished.

The thermovision images acquired during the experiment were processed before further analysis. The first operation was selection of interesting areas in the thermograms. One decided to select two Regions Of Interest (ROI3 and ROI4) representing the bearing housings (Fig. 3).

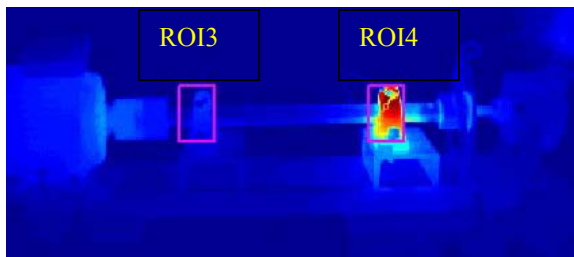


Fig. 3. Thermovision image of the operating laboratory stand, with marked ROIs of the first (left, ROI3) and the second (right, ROI4) bearings

Those ROIs were interesting due to two reasons. Firstly, the most of the machine failures are visible in bearings operation and secondly the construction and shape of both the bearings housing were the same. One expected that changes in the machine technical state affect changes of bearings temperature and should be revealed in the sequence of thermographic images. Taking into account two ROIs presenting a view of the same type of the

bearing housing could be beneficial for the verification of different image features.

In Fig. 4. functions of temperature mean value computed for ROI3 and ROI4 is presented. One can observe that for state S0 heating process of bearing housings is clearly visible on the both plots. In case of ROI3 for states S3 and S5 significant temperature changes are noticeable. Within the boundaries of the ROI4 mean value of temperature along time of observation indicates that rapid temperature change occurs for state S6. In state S4 a significant temperature change is also visible.

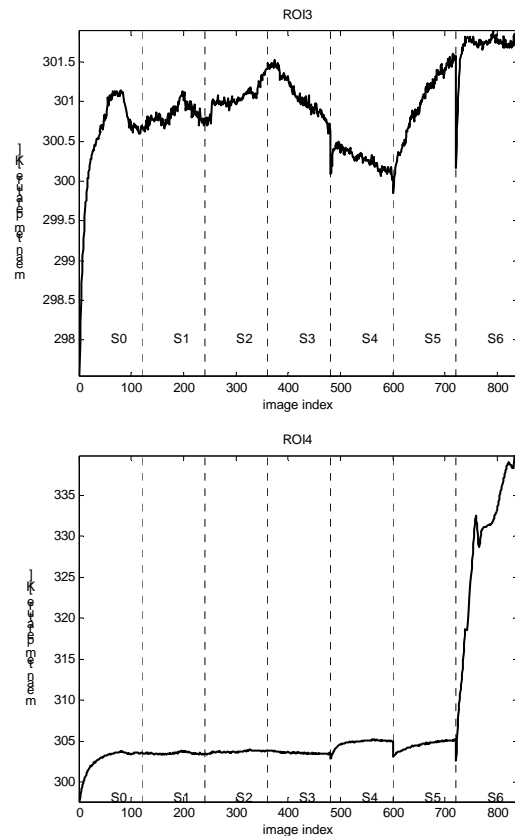


Fig. 4. Course of mean temperature computed over a) ROI3 and b) ROI4

The recorded sequences of thermovision images represented by the selected ROIs was submitted for analysis with use of procedure described earlier.

2.2. Analysis of magnitudegrams and phasegrams

According to proposed procedure of analysis in “micro” time the infrared image sequence for state S1 was selected as reference. For this state reference temperature characteristics over observation time, described by the highest variance was estimated. On the basis of a spectrum of reference temperature characteristics $n=4$ frequency components were identified (Fig. 5). Constant component of the spectrum wasn't considered. Frequency components were identified for both ROI3 and ROI4 and in Fig. 5 exemplary plots of magnitude and phase spectrum for ROI3 is presented. For frequency

values of selected components for each state magnitudegrams and phasegrams were selected for further analysis.

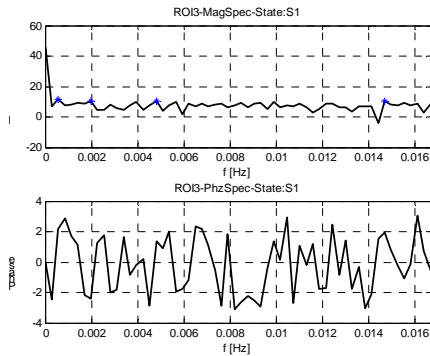


Fig. 5. Exemplary plot of magnitude and phase spectrum with selected 4 highest frequency components

In figure 6a exemplary magnitudegrams and phasegrams of state S4 are showed. Qualitative analysis of presented images is rather difficult due to high level of noise especially for images corresponding to higher frequency components. Image of magnitude corresponding to first frequency component allow identifying shape of the bearings housing. Images of phase are characterized of high level of noise. Visual analysis of the magnitudegrams and phasegrams allowed us to assumed that the most informative for further analysis are images corresponding to the first significant frequency component.

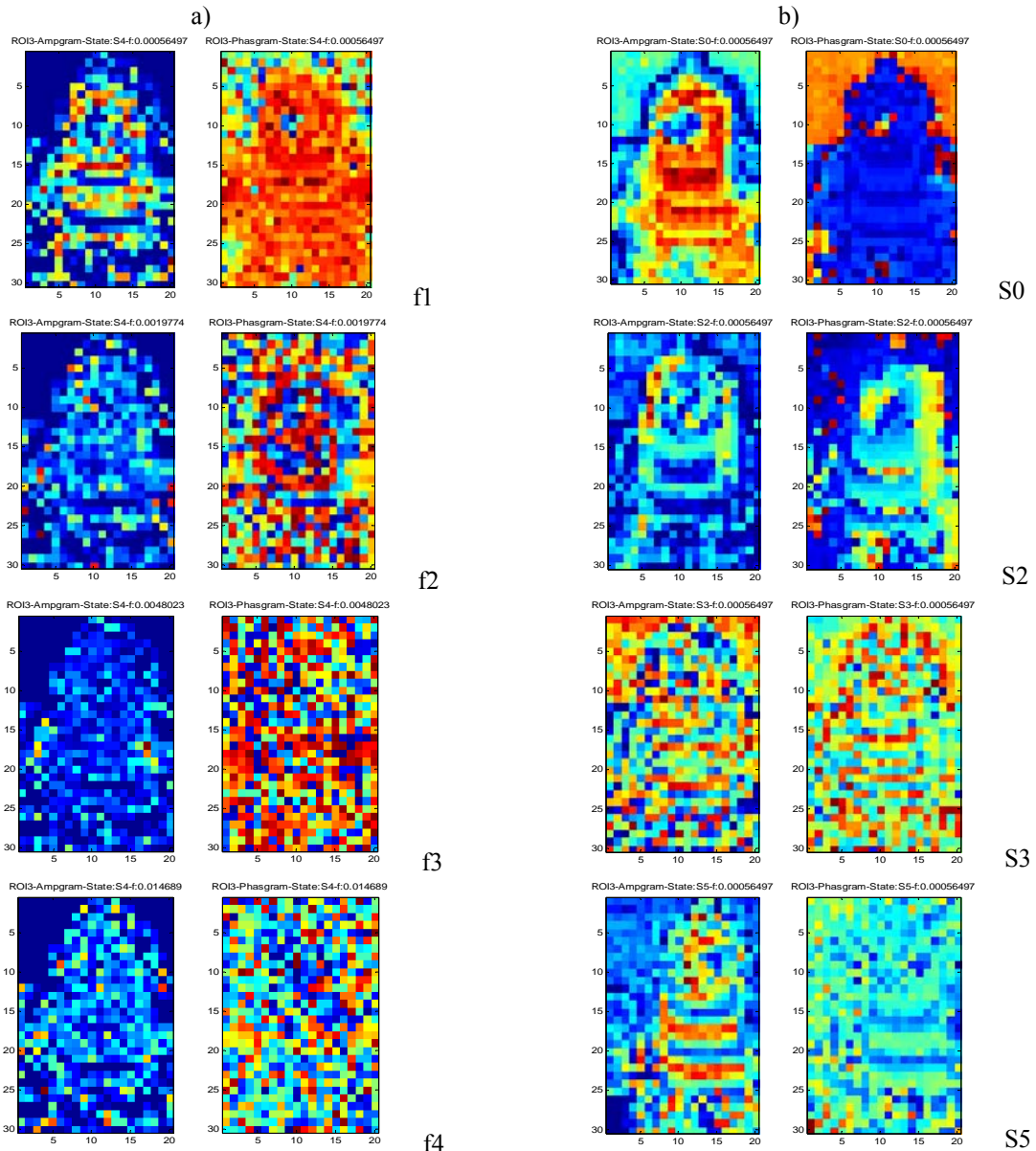


Fig. 6. Magnitudegrams and phasegrams calculated over ROI3 for a) different frequencies and b) different technical states

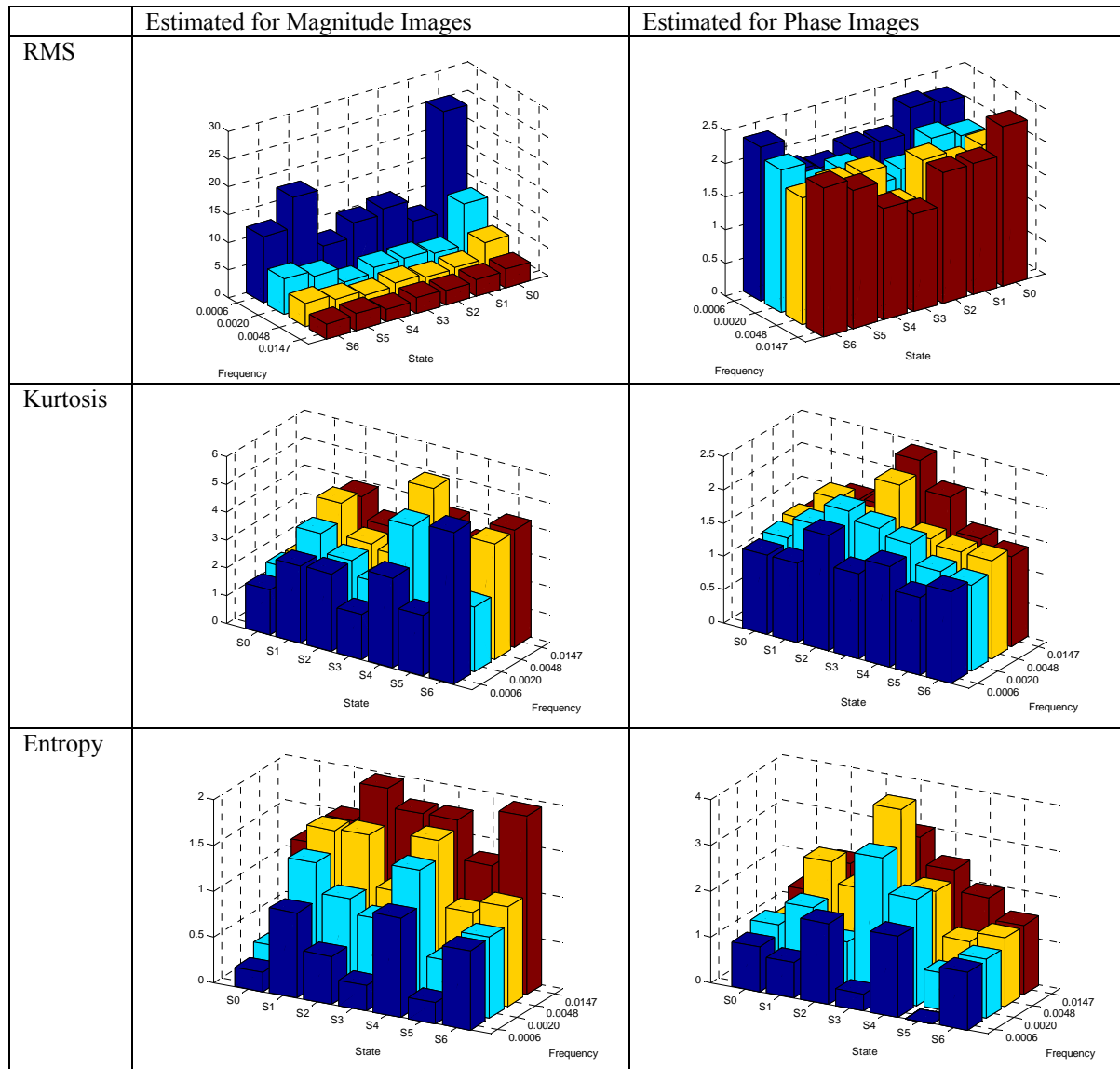


Fig. 7. Exemplary plots of different feature values for magnitudograms and phasegrams represented by ROI3

3. CONCLUSIONS

On the basis of the conducted research it was found that application of Fourier analysis to sequence of infrared images in “micro” time allow us identify changes in the machine technical state. One can state that images of magnitude and phase corresponding to first frequency component are significant and their analysis with use of commonly know statistics allow us to recognize change of technical state manifested by rapid increase or decrease of temperature on observed area of the machine. One can assume that features of magnitudograms and phasegrams could classify machine technical state. In order to confirm this assumption further research are necessary to perform.

REFERENCES

- [1] Cholewa W., Kaźmierczak J.: *Data Processing and Reasoning in Technical Diagnostics*, Wydawnictwo Naukowo_Techniczne, Warszawa, Poland, 1995.
- [2] Fidali M., Jamrozik W.: *Search for optimal estimators of thermogram Fourier images*. In “Recent Developments In Artificial Intelligence Methods”. Edt. Burczyński T., Cholewa W., Moczulski W. AI-METH Series, Gliwice 2009, p. 103-112.
- [3] Fidali M.: *An idea of continuous thermographic monitoring of machinery*. Proceedings of 9th International Conference on Qualitative InfraRed Thermography QIRT 2008, July 2-5, Kraków, Poland, 2008.
- [4] Fidali M.: *Zastosowanie transformaty Fouriera obrazów termograficznych do oceny zmian stanu technicznego maszyny*. Diagnostyka procesów i systemów, Korbicz J., Patan K.,

- Kowal M. (ed.). Akademia Oficyna Wydawnicza EXIT, Warszawa 2007, 181-188.
- [5] R. A. Thomas, *The thermography monitoring handbook*. Machine & systems condition monitoring series, Oxford, UK: Coxmoor Pub., 1999.
- [6] S. M. Nixon and S. Aguado, *Feature Extraction and Image Processing*. Newnes, 2002.
- [7] X. P. V. Maldague, *Theory and Practice of Infrared Technology for Nondestructive Testing*. Wiley, 2001.



Marek FIDALI, PhD, assistant professor at Department of Fundamentals of Machinery Design. Main area of research: technical diagnostics, thermovision, modal analysis, signal and image processing.

MODE SHAPES SUBTRACTION AND WAVELET ANALYSIS FOR DAMAGE DETECTION

Aleksandra ZIAJA, Krzysztof MENDROK

AGH University of Science and Technology, Department of Robotics and Mechatronics,
al. Mickiewicza 30, 30-059 Krakow, Poland, e-mail: mendrok@agh.edu.pl

Summary

One of the modal parameters that indicate damage in a structure are mode shapes. They can be used both for detection and localization of damage, since their shape is locally disturbed by the potential damage. Their another advantage, comparing with natural frequencies or damping factors, is fact that they are less sensitive to environmental factors like ambient temperature changes. The problem is that for small damages the changes in shape of mode are difficult to be detected. To improve this detectability authors decided to subtract the mode shapes of the damage structure from analogous mode shape of the structure in reference state. Additionally to even more improve the sensitivity of the method and allow for some automation of damage detection, the wavelet analysis was introduced.

Keywords: mode shapes, wavelet transform, damage detection.

ODEJMOWANIE POSTACI DRGAŃ WŁASNYCH I ANALIZA FALKOWA DO WYKRYWANIA USZKODZEŃ

Streszczenie

Jednym z parametrów modalnych, które pozwalają na wykrycie uszkodzenia w obiekcie są postaci drgań własnych. Mogą być one stosowane zarówno do wykrywania jak i lokalizacji uszkodzenia, ponieważ są tylko lokalnie zaburzane przez potencjalne uszkodzenie. Ich kolejną przewagą w odniesieniu do częstości drgań własnych czy współczynników tłumienia modalnego jest ich znacznie mniejsza wrażliwość na czynniki środowiskowe takie jak zmiana temperatury otoczenia. Problemem natomiast jest fakt, że dla małych uszkodzeń zmiany są niewielkie i dlatego trudne do wykrycia. Aby poprawić tę wykrywalność autorzy zdecydowali się na odejmowanie postaci drgań własnych układu uszkodzonego od analogicznej postaci układu w stanie referencyjnym. Dodatkowo aby ułatwić interpretację wyników i pozwolić na pewnego rodzaju automatyzację działania metody zastosowano analizę falkową.

Słowa kluczowe: postaci drgań własnych, transformata falkowa, wykrywanie uszkodzeń.

1. INTRODUCTION

The most commonly met division of damage detection methods based on low-frequency vibration measurements is classification using the model type and the type of parameters applied for diagnostics. This division can roughly be presented as:

- methods based on modal models,
- methods based on non-parametric models,
- methods based on regressive parametric models,
- other methods.

The most convenient model, which can be applied in the damage detection, is a modal model, i.e. a set of natural frequencies, modal damping coefficients and modal vectors describing the dynamics of the tested object. The modal model is relatively easy to identify and, by means of operational modal analysis, may be identified only from response data; it is, therefore, very useful in diagnostics. The modal parameter perturbation (natural frequency, modal damping) is the simplest

application of the modal model for damage detection. The results can be obtained from output-only data by means of operational modal analysis. In some cases it enables damage detection, but the detection strongly depends on object geometry, material and the nature of the damage itself. This technique does not provide information about the location of the damage, but the biggest disadvantage of the method is probably the fact that its effectiveness is dependent on environmental conditions. There is a serious problem distinguishing between the changes in parameters resulting from damage and those caused by environmental changes e.g. temperature or humidity. The changes in ambient temperature for civil engineering objects (bridges, viaducts, masts, tall buildings) may reach even tens of degrees in a relatively short period of time. It results in further changes in stiffness and finally in modal parameter variation. This effect is multiplied when the object is unevenly heated – e.g. when one side is exposed to the sun and the other is

kept at a constant temperature due to its proximity to water. The influence of humidity variations is similar – concrete elements absorb moisture and this leads to increases in their mass and variations in modal parameters. Naturally, there are methods which enable the influence of environmental changes on the diagnostic procedure accuracy to be eliminated. In most applications, a lookup table is prepared in which modal parameters identified for different ambient temperatures and values of humidity are gathered together. Such a table is unique and independently prepared for every object as a result of a set of experiments. A more sophisticated method of eliminating the influence of weather conditions on the monitoring system's efficiency is application of an environmental filter [1]. It is generally an autoregressive model with a moving average (ARMA) identified from a set of experimental data. When environmental changes are eliminated in this way, any modification of the object (e.g. lining another asphalt layer on a bridge deck) causes the necessity to repeat the entire set of measurements, to update the lookup table or the environmental filter. There is however another modal parameter that allows not only for damage detection but also for location and what is also very important is much less sensitive for environmental changes [2]. These modal parameters are mode shapes.

2. OVERVIEW OF THE DAMAGE DETECTION METHODS BASED ON MODE SHAPES

Among methods based on changes in mode shapes, a few basic ones can be emphasised:

- tests of correlations between mode shapes in undamaged and current state (MAC or CoMAC),
- analysis of mode shapes curvature,
- analysis of mode shapes deformation energy.

The MAC (Modal Assurance Criterion) coefficient is defined as a scalar product of two modal vectors [3], from which the first is identified for an undamaged system, and the second is a mode shape for the object with damage. If the MAC coefficient is less than one, there is a change in the vibration mode. The MAC coefficient may be calculated both for one coordinate and for a certain area. It was applied to damage detection in the work [4]. For one selected coordinate, it is called *CoMAC* (*Coordinate MAC*). Designating it can additionally define in which area the damage is located. In practice, however, the method is not very sensitive and does not allow damage to be detected in the initial phases of development.

A development of these methods is the analysis of changes in mode shape together with changes in the mode participation factor. This method was described in the paper [5]. The authors divided the analytical model into sub-systems and analysed changes in higher mode shape in successive sub-systems. This method allows the localisation of

damage, because higher mode shapes are changed only for sub-systems containing damage.

A slightly different use of mode shapes for damage detection was proposed by Ettöuney [6]. He calculated the stiffness matrix or compliance matrix on the basis of knowledge of the modal model of undamaged and damaged objects. Changes in the calculated matrices indicated the presence of damage and its location.

In the place of modal vectors, a change in the curvature defined as the derivative or the second derivative of a modal vector are often analysed. This is more sensitive to changes than the mode itself. In particular, this concerns damage to objects which changes mode shapes locally. This method suffers from a relatively large error in cases where the number of measurement points is not sufficiently large to designate the following derivative of vibration modes with suitable accuracy. The derivative is calculated in points by linear approximation passing through the successive points or also through polynomial approximation of the deformation curve and derivative designation analytically. This second method is considerably less sensitive to measurement errors, however, it flattens the shape of modes, which may be a cause of damage being undetected. The effectiveness of applying these methods also includes the localisation of damage.

The first example of the application of mode shape curvature to NDT is the work of Maeck and DeRoeck from 1999 [7]. This method uses dependencies between the beam's bending stiffness and the bending moment divided by a suitable curve, being a second derivative of beam deformation. Changes in the stiffness matrix calculated on the basis of this dependency enable the detection of damage. This method was verified by the authors with the use of data from research conducted on the Z24 bridge in Switzerland.

The next application of modal curvature is the method described in the article [8]. The authors calculated the damage index as a relation of the modal curvature calculated for the damaged object to the analogical curvature of the undamaged object raised to a square. The curvature was counted as a second mode shape derivative. In the work, particular emphasis was placed on the influence of measurement errors on the accuracy of method. They showed that the higher mode shape derivatives are more sensitive to the presence of damage, but also cause multiplications of measurement noise and, due to this, their usefulness is doubtful. In their next publications [9], the same authors proposed a solution to the problem of increasing significance of measurement noise during analysis of changes in curvature. They presented another way of mode shape analysis, which had a high level of sensitivity to damage and low one to measurement error. As a symptom of damage, they proposed a change in the mode shape slope raised to a square. This slope was counted as the first mode shape derivative.

The damage index method from the work [9] was extended by Kim and others [10]. The novelty is based on the application of the method for objects where reference data (without damage) was not available. The authors showed a way to calculate the modal curvature of the object before damage on the basis of data coming only from measurements on the damaged object. In this method it was necessary to use the updated finite element model.

The most precise method based on modal vectors is presented in the work [11]. This method consists of comparing the deformation energy of vibration modes in systems without damage and systems with damage. In the described method a finite element model of the construction can be considered as a system without damage. In order to designate the SER_{ij} energy coefficient, the i -th vibration mode for the j -th element, one should possess the following data: mode shape ϕ_i , natural frequency ω_i , the global stiffness matrix of the finite element model K , as well as the stiffness matrix for the j -th finite element k_j :

$$SER_{ij} = \frac{\phi_i^T k_j \phi_i}{\phi_i^T K \phi_i} = \frac{\phi_i^T k_j \phi_i}{\omega_i^2} \quad (1)$$

The coefficient β_{ij} is named by the authors as a damage coefficient and is designated with the dependency:

$$\beta_{ij} = SER^u_{ij} - SER^d_{ij} \quad (2)$$

where: the index d represents data for constructions with damage, and u represents data for constructions without damage.

As simulation and experimental tests showed, this method is sensitive even to small stiffness changes in the construction (about 5%).

A similar approach can be found in the work [12]. The authors also calculated the damage indicator on the basis of the deformation energy of mode shapes. However, in this case, it was defined a little differently:

$$f_{ij} = \int_{a_{j-1}}^{a_j} \left(\frac{d^2 \varphi_i}{dx^2} \right)^2 dx / \int_0^L \left(\frac{d^2 \varphi_i}{dx^2} \right)^2 dx \quad (3)$$

where: i – mode shape number,
 j – element number,
 L – length of section on which the mode shape curvature is calculated,
 φ – mode shape,
 x – position on the section L ,
 a – integration limit.

The damage indicator was calculated as a relation of the sums f_{ij} along all mode shapes for the

damaged object to analogical sums of the undamaged object.

Carrasco et al. [13] also applied mode shape deformation energy for damage detection and localisation. Their approach consists of dividing the tested object into sub-systems and the calculation of deformation energy separately for each sub-system. Changes in deformation energy in successive sub-systems allowed the authors to locate damage. Additionally, the authors showed that there is a close dependency between the size of the damage and the size of the change.

The mode shape deformation energy for damage detection and localisation was also applied by Choi and Stubbs [14]. Their work concerned damage detection in a two-dimensional element with the use of classic plate theory. As an example, they applied a finite element model to a rectangular plate.

A completely different approach for damage localisation on the basis of mode shapes was presented by Rucka and Wilde [15]. They analysed the mode shape of beam-like and plate-like objects in search of cracks. The tool which was used for this aim was the wavelet transform. The discovered discontinuities, where the geometry of the object was known, were the symptom of damage. This method requires very dense networks of measurement points. Its application to the mode shapes obtained through laser vibrometer measurements are presented in the work [16]. The main advantage of the approach is the fact, that it is a baseline free method. The disadvantages are: relatively small sensitivity to small sized damages and difficulties in unique interpretation of the obtained results.

3. FORMULATION OF THE METHOD

Generally the mode shapes are used for damage localization due to the fact that damage, in most cases, only disturbs the mode shapes locally. Unfortunately for the small sized damages the effect is hardly visible in the mode shapes (the change of mode shapes is very small). In many fields of application to show the small changes between two quantities their difference is presented. That was the main idea behind the proposed method. Instead of analyzing the mode shapes itself it is better to take into account their difference. One can find in the literature the example of mode shapes derivatives subtraction in order to better detect and localize damage [17]. To illustrate above statement in Figure 1 there are presented: 1st mode shape of the undamaged system, 1st mode shape of the damaged system and difference of these two modes. It is clearly visible that for such a small damage the mode shapes are almost identical and only their difference gives potential for damage localization.

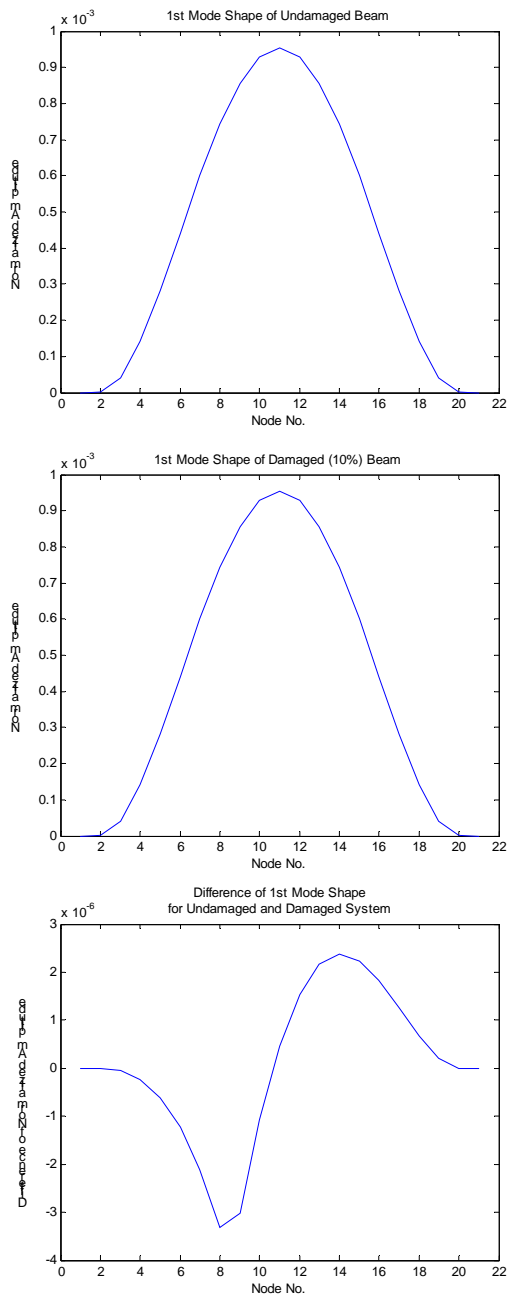


Fig. 1. Example of difference between mass normalized mode shapes for an undamaged structure and a structure with 10 % crack

The idea of the method proposed by authors can be summarized in two steps. In the first step the mode shapes of the structure in current stage are subtracted from the reference counterpart to emphasize eventual changes. As it is shown in Figure 1 the localization of damage based purely on mode shapes difference can be sometimes misleading. In the presented example there are maxima of the characteristic around Node 8 (where the crack was simulated) and 15. So simple amplitude analysis would give false results. One needs to look for discontinuities in the analyzed curve. The very good tool to do that is the wavelet transform. That is why in the next step for better

results interpretation and some procedure automation the wavelet analysis is used in similar manner as in the work [15]. The scheme of diagnostic procedure based on proposed approach is presented in Figure 2.

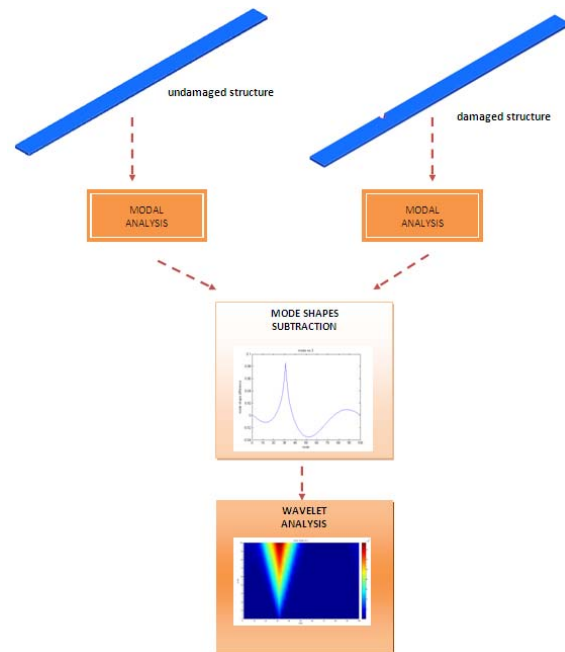


Fig. 2. The scheme of diagnostic procedure

Proposed approach can be characterized by following advantages: it is sensitive even for relatively small damages and provides the possibility for better results interpretation, even automatic crack detection, by usage of wavelet analysis. In opposite to that one can state the following cons: the method is no longer baseline free, and the computational cost is a little bit bigger.

4. SIMULATION VERIFICATION

For the purpose of simulation verification of the described procedure, the following model was developed. This was a steel supported beam of length 10 m with the cross-section dimensions 0.6 x 0.1 m and consisted of 600 plate elements (quad4), with the size of each element 0.1 x 0.1 m. Such a dense mesh was used to allow for different sensor distribution testing. Next, the eigenvalue problem was solved for the model without damage to obtain its modal model parameters. As damage, a beam crack was modeled as node disconnectivity. The depth of the crack amounted to 10% of the entire beam cross-section area. Location of the crack was exactly 3 m from the right-hand end of the beam. For damaged model, the eigenvalue problem was also solved. Having both damaged and undamaged model results, the authors localized damage with the use of a different number of sensors (nodes). In Figure 3 the model is presented together with the damaged area designation.

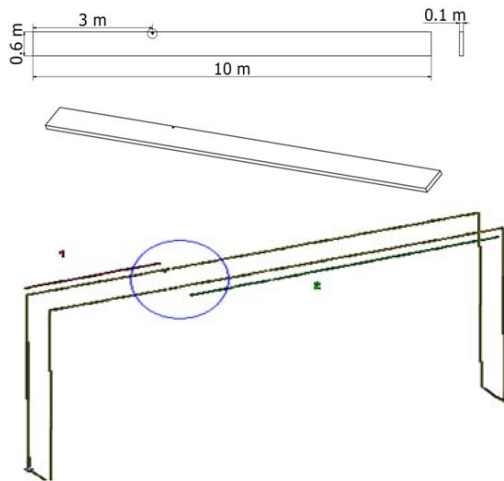


Fig. 3. Model prepared for the simulation verification

The preliminary investigation was focused on the selection of the wavelet that detects the discontinuity in shapes of the mode. The wide literature studies [18, 19, 20, 21, 22] allowed for preliminary selection of 4 types of wavelets:

- Gaussian wavelet of order 4,
- Mexican Hat wavelet,
- Complex Continues Gaussian wavelet of order 4,
- Daubechies wavelet of order 4.

In Figure 4 the results of damage localization with use of different wavelets are shown.

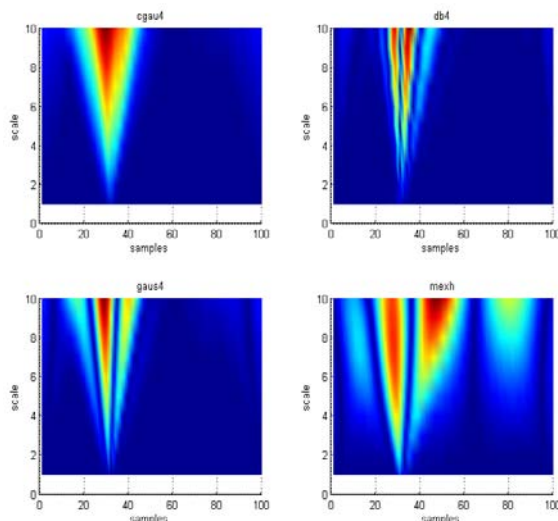


Fig. 4. damage localization with use of different wavelets

Although in case of low modes the Gaussian wavelet of order 4 and Mexican Hat wavelet gave good result, the Complex Continues Gaussian wavelet of order 4 was selected as it was able to detect discontinuities in the biggest number of mode differences and provided only one peak that points to a singularity in shape of mode.

In the next step the wavelet analysis was performed on the damaged mode shapes directly to prove that modes subtraction is necessary. In this work the Continuous Complex Gaussian wavelet with 4 and 6 vanishing moments was used. The type of wavelet was selected empirically. Result of this analysis is presented in Figure 4.

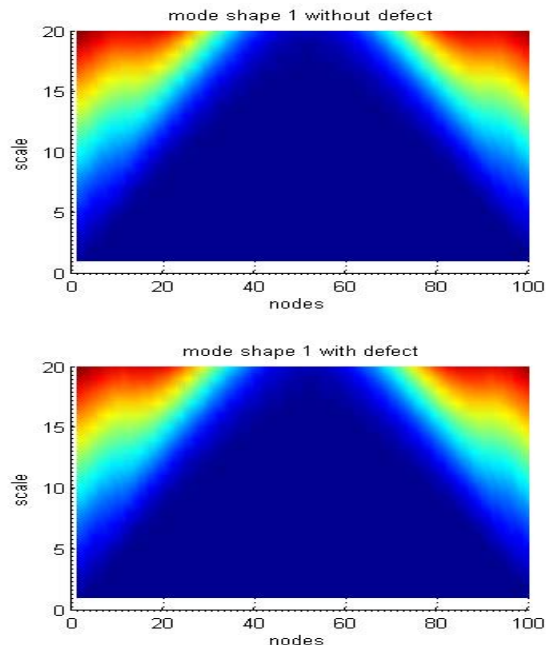


Fig. 4. Wavelet transform of the 1st mode shape of the undamaged and damaged system

The results show that in case of so small crack (10%) the detection of the damage directly from the mode shapes analysis with use of wavelet transform is impossible.

Next the procedure formulated in the section 3 was launched for crack detection and localization. The results example is presented in Figure 5.

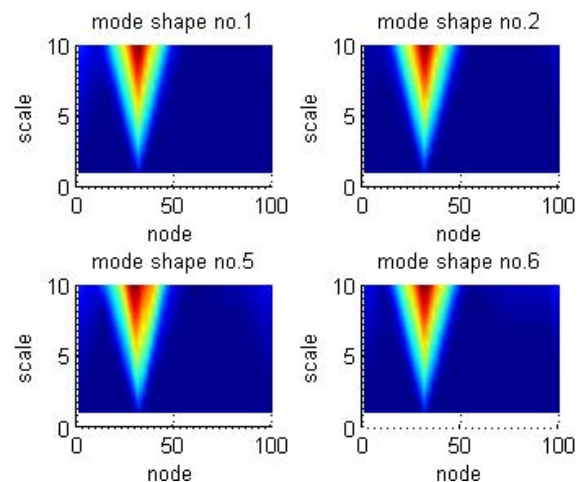


Fig. 5. Results of damage detection and localization

As it can be seen, the method easily detected changes in system's modes and pointed the damage

location. The positions of the detected crack in function of mode shape number are gathered together in Table 1.

Table 1. Crack localization accuracy

MS No.	Recognized crack position [m]	Relative error [%]
1	3.11	3.7
2	3.19	6.3
3	3.11	3.7
4	No detection	-
5	3.06	2
6	3.19	6.3
7	No detection	-
8	3.11	3.7
9	No detection	-
10	3.19	6.3

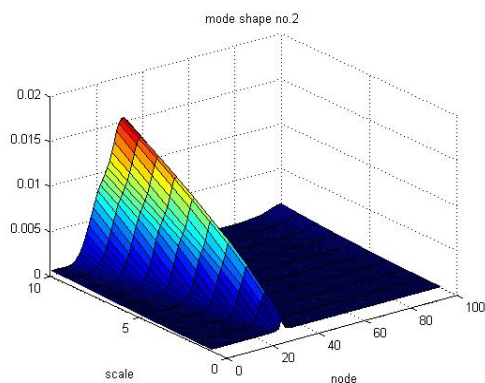
For the 100 sensors (nodes) uniformly spaced along the beam length used in the analysis the localization error was no bigger than 6.5 %. What is also important the analysis of scalograms is very unique and easy for some automation. For example in this case it is enough to look for maxima in the scalograms. The lack of detection for mode shapes no. 4, 7 and 9 results from the fact that in these mode shapes all the movement is in the tangent direction, while only the normal direction responses were taken to the analyses.

5. ANALYSIS OF THE METHOD ACCURACY

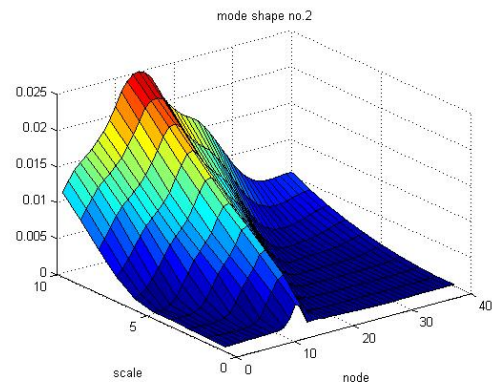
In the last step, the authors analyzed the relation between the number of sensors used for damage localization and the localization accuracy. Having both damaged and undamaged model results, the authors localized damage with the use of a different number of sensors (nodes) and their configurations. The following scenarios were tested:

- consecutively 10, 20, 40 and 100 sensors placed evenly along the length of the beam.

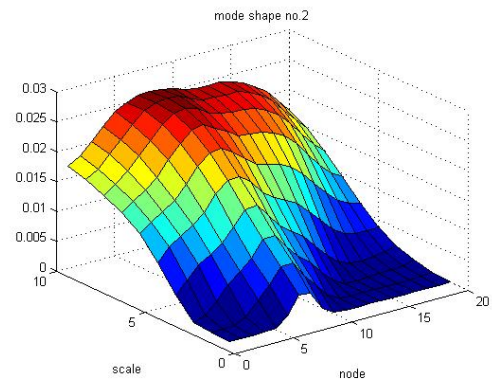
The results for the second mode with use of 100, 40, 20 and 10 sensors are consecutively shown in Figure 6.



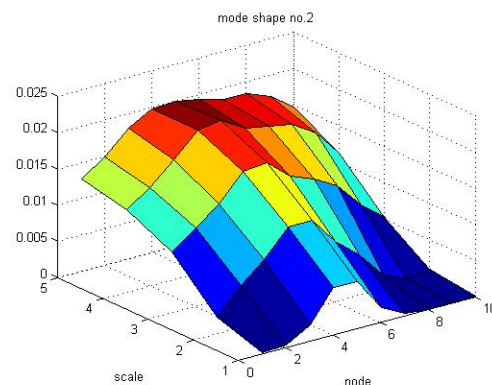
a)



b)



c)



d)

Fig. 6. Wavelet transform modulus of mode shapes difference for 2nd mode; (a) 100 sensors, (b) 40 sensors, (c) 20 sensors, (d) 10 sensors

In Table 2 the results of crack localization in function of sensors (nodes) number are presented.

Table 2. Crack localization accuracy in function of sensors number

No. of sensors	Recognized crack position [m]	Relative error [%]
100	3.145	4.8
40	3.45	15
20	3.94	31.6
10	4.71	57.1

In case of 40, 20 and 10 sensors (nodes) the wavelet of order 6 was used and additionally in case of 10 sensors the scale range was reduced to 1:5.

It was observed that detection of the crack was not possible only for case with 10 sensors for modes higher than 3. What is more, it was seen that the peak of the wavelet transform modulus becomes wider as the scale increases and for higher modes made it impossible to localize the damage properly. From the results of 40 sensors the modes up to 10th was taken into consideration. The localization of the crack was identified as 3.45 m (15.1% relative error). In case of 20 measurement points the wavelet analysis is able detect crack at 3.5-4 m, but in case of mode higher than 3 the localization of crack can be done only according to values corresponding to scale from 1 to 5.

5. CONCLUSIONS

The presented investigations can be summarized by the following conclusions:

- the wavelet transform applied to mode shape difference instead of directly to mode shape of damaged structure provides better results,
- for analysis of mode shape differences the wavelet with at least 2 vanishing moments needs to be used, for wider sensor distribution the order of the wavelet should be increased,
- the best type of wavelet for these applications is the Complex Continues Gaussian wavelet,
- proposed method was able to detect 10 % crack for low mode using only 10 sensors,
- the crack localization relative error for 100 sensors was no bigger than 6.5 %,
- The accuracy of the results drops significantly with the smaller number of sensors used,
- The localization error is mainly produced by mode shape subtraction, as it is visible that the coordinate of the singularity in the signal is shifted in respect to damage localization.

REFERENCES

- [1] Peeters B., Maeck J., De Roeck. G.: "Dynamic Monitoring of the Z24-Bridge: Separating Temperature Effects from Damage," In Proceedings of the European COST F3 Conference on System Identification and Structural Health Monitoring, pp. 377-386, Madrid, Spain, 2000,
- [2] Mendrok K., Uhl T.: "The application of modal filters for damage detection", Smart Structures and Systems, Vol. 6, No. 2, pp. 115-134, 2010
- [3] Uhl T.: „Komputerowo wspomagana identyfikacja modeli konstrukcji mechanicznych”, WNT Warszawa, 1997,
- [4] Natke H.G., Cempel C.: "Model-Aided Diagnosis Based on Symptoms", Structural Damage Assessment Using Advanced Signal Processing Procedures, Proceedings of DAMAS '97, University of Sheffield, UK, pp. 363-375, 1997,
- [5] Ahmadian H., Mottershead J.E., Friswell M.I.: "Substructure Modes for Damage Detection," Structural Damage Assessment Using Advanced Signal Processing Procedures, Proceedings of DAMAS '97, University of Sheffield, UK, pp. 257-268, 1997,
- [6] Ettouney M., Daddazio R., Hapij A., Aly A.: "Health Monitoring of Complex Structures", Smart Structures and Materials 1999: Industrial and Commercial Applications of Smart Structures Technologies, Proceedings of SPIE, vol. 3,326, pp. 368-379, 1998,
- [7] Maeck J., De Roeck G.: "Damage Detection on a Prestressed Concrete Bridge and RC Beams Using Dynamic System Identification", Damage Assessment of Structures, Proceedings of DAMAS 99, Dublin, Ireland, pp. 320-327, 1999,
- [8] Ho Y.K., Ewins D.J.: "Numerical Evaluation of the Damage Index", Structural Health Monitoring 2000, Stanford University, Palo Alto, California, pp. 995-1011, 1999,
- [9] Ho Y.K., Ewins D.J.: "On the Structural Damage Identification with Mode Shapes", European COST F3 Conference on System Identification and Structural Health Monitoring, Madrid, Spain, pp. 677-686, 2000,
- [10] Kim J., Ryu Y., Lee B., Stubbs N.: "Smart Baseline Model for Nondestructive Evaluation of Highway Bridges", Smart Systems for Bridges, Structures and Highways, Proceedings of SPIE, vol. 3043, pp. 217-226, 1997
- [11] Zhang L., Quiong W., Link M.: "A Structural Damage Identification Approach Based on Element Modal Strain Energy", Proceedings of ISMA23, Noise and Vibration Engineering, Leuven, Belgium, 1998,
- [12] Worden K., Manson G., Wardle R., Staszewski W., Allman D.: "Experimental Validation of Two Structural Health Monitoring Methods," Structural Health Monitoring 2000, Stanford University, Palo Alto, California, pp. 784-799, 1999,
- [13] Carrasco C., Osegueda R., Ferregut C., Grygier M.: "Localization and Quantification of Damage in a Space Truss Model Using Modal Strain Energy," Smart Systems for Bridges, Structures, and Highways, Proceedings of SPIE, vol. 3043, pp. 181-192, 1997,
- [14] Choi S. Stubbs N.: "Nondestructive Damage Detection Algorithms for 2D Plates", Smart Systems for Bridges, Structures, and Highways, Proceedings of SPIE, vol. 3043, pp. 193-204, 1997,
- [15] Rucka M., Wilde K.: "Application of continuous wavelet transform in vibration based damage detection method for beams and plates", Journal of Sound and Vibration, vol. 297, pp. 536-550, 2006,

- [16] Krawczuk M, Mieloszyk M., Palacz M., Ostachowicz W.: „*Damage Detection of Riveted Structures by Laser Measurements*”, Proceedings of the Fourth European Workshop Structural Health Monitoring 2008, Uhl T., Holnicki-Szulc J., Ostachowicz W. Eds., DES{em tech} Publications, Inc., Lancaster, Pennsylvania, USA, pp. 915-920, 2008,
- [17] Guan H., Karbhari V. M.: „*Improved damage detection method based on Element Modal Strain Damage Index using sparse measurement*”, Journal of Sound and Vibration, vol. 309, pp. 465-494, 2008,
- [18] Jacob P.J., Desforges M.J., Ball A.D.: „*Analysis of Suitable Wavelet Coefficients for Identification of the Simulated Failure of Composite Materials.*” Structural Damage Assessment Using Advanced Signal Processing Procedures, Proceedings of DAMAS '97, University of Sheffield, UK, pp. 31-40, 1997,
- [19] Naldi G., Venini P.: „*Postprocessing Singular Solutions by the Wavelet Transform.*” Structural Damage Assessment Using Advanced Signal Processing Procedures, Proceedings of DAMAS '97, University of Sheffield, UK, pp. 109-120, 1997,
- [20] Biemans C., Staszewski W.J., Boller C., Tomlinson G.R.: „*Crack Detection in Metallic Structures Using Piezoceramic Sensors.*” Damage Assessment of Structures, Proceedings of DAMAS 99, Dublin, Ireland, pp. 112-121, 1999,
- [21] Staszewski W.J., Biemans C., Boller C., Tomlinson G.R.: „*Impact Damage Detection in Composite Structures-Recent Advances.*” Structural Health Monitoring 2000, Stanford University, Palo Alto, California, pp. 754-763, 1999,
- [22] Staszewski W.J.: „*Structural and Mechanical Damage Detection Using Wavelets*”, The Shock and Vibration Digest, vol. 30, no. 6, pp. 457-472. 1998,



Aleksandra ZIAJA

Is a 2nd degree student in the Department of Robotics and Mechatronics of the AGH University of Science and Technology. Her main interests are related to signal analysis and vibration based machine diagnostic.



PhD. Eng. Krzysztof MENDROK

Is a senior researcher in the Department of Robotics and Mechatronics of the AGH University of Science and Technology. He is interested in development and application of various structural health monitoring algorithms. He mainly deals with low frequency vibration based methods for damage detection and inverse dynamic problem for operational load identification.

OVERALL FACTORY AVERAGE SPECTRUM: GLOBAL VIBRATION INDEX FOR DIAGNOSIS AND PROGNOSIS OF LARGE SETS OF ROTATING MACHINERY

Diego GALAR, Aditya PARIDA, Håkan SCHUNESSON

Division of Operation and Maintenance Engineering,
Luleå University of Technology, Luleå, Sweden

Summary

Spectral analysis of rotating machinery requires studying the signals received from each machine, which converts hundreds of spectra to analyze, especially in big plants, where one can find a large number of similar machines. The maintenance departments require few indicators properly hierarchied with the appropriate information necessary for each organizational level, without exceeding the type and amount of information required at the higher levels. It is therefore, necessary for an indicator to show the current vibratory condition of the entire plant, where trends can be easily understood by people, who are not expert in detailed vibration analysis of spectra. The trend shown by the indicator should assess the success of the implementation of CBM and other maintenance programs in the plant, and these parameters should be easily displayable. Therefore, maintenance managers need this kind of indicators and scorecards to measure through simple methods for the success of their departments for achieving contribution to the company goals.

Key words: vibration, speed, acceleration, predictive maintenance, CBM, data collector, indicator.

INTRODUCTION

In general, the Predictive Maintenance (PdM) contributes in principle to detect the onset of a future failure, as well as provides the tools necessary to analyze the cause of the problem that is being developed. The final result will specify the proper timing to efficiently and effectively perform the necessary corrections to solve the problem identified.

PdM Program consists of three essential stages. detection, identification and correction Detection is the first step in the PdM, and is based on the evolution of one or more parameters selected properly according to their sensitivity to the changes in the condition of the equipment tested. Identification is the process after the problem has been detected; we must therefore, proceed to determine the cause of it, i.e. to identify which element or elements of the machine is or are the cause of the increase in the levels of vibration, in comparison to the accepted references that show a normal condition of mechanical equipment. This article will be presenting a methodology for obtaining such a reference in a dynamic way and adapted to the real condition of the entire plant, where the machine is working. Of course, knowing the cause of the problem and the location of it, allows the maintenance department to organize and implement efficient and effective work for eliminating the problem and their causes.

It is extremely important that identification of likely failure may be found even in its early developmental stage that will allow the maintenance

team to perform intervention at the right time. As shown in figure 1, avoiding unnecessary losses and minimizing costs is possible through the intervention. However the decision to perform interventions are based on different thresholds from standards, based on experience or manufacture's recommendations; that is why many interventions are unnecessary as a result of false alarms due to wrong benchmarking points.

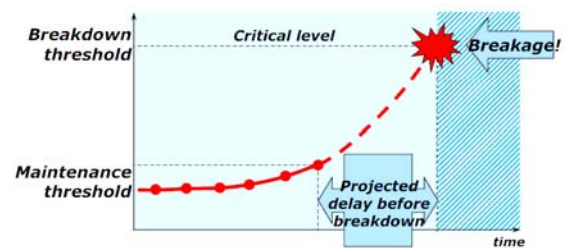


Fig. 1. Analysis of time history for significant parameters

On the other hand, a too optimistic threshold can cause a breakdown before detection. That is the main reason why these thresholds are usually very conservative.

1. INTUITIVE APPROACH

Over the years, either by direct contact or the use of subjective nature of any device, machine operators have used auditory verification techniques, which are "too subjective" to detect specific problems but effective to identify if the behaviour of machines is normal or no.

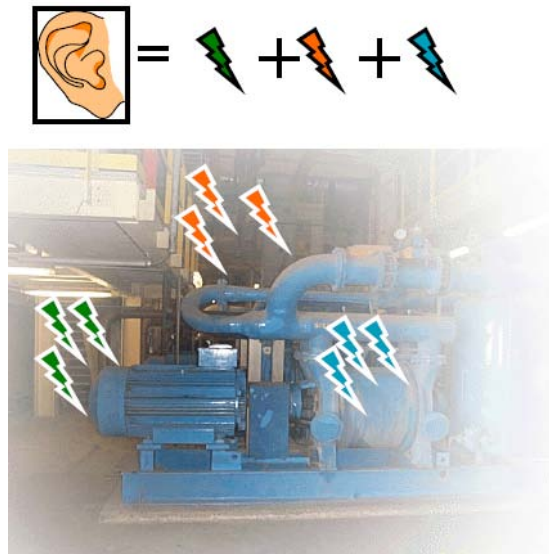


Fig. 2. Auditive perception of real condition of machinery

As a result of forces that occur between elements of a machinery and vibration generated by them, the outer surface of each of the pieces that make up the machine will be of varying shape and position. This causes changes in air pressure that generally surrounds the equipment. This pressure wave propagates in the air affects objects near the source of vibration.

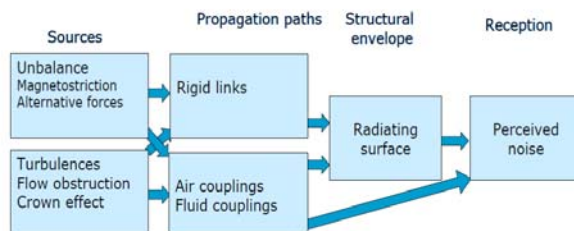


Fig. 3. Intuitive approach of vibration producing noise

One of these objects could be the tympanic membrane of the human ear, through which the rest of the system of the ear, the brain produces the sensation of sound. See Figure 2. In this way, the measurement of sound produced by a machine is the measure of vibrations caused by it. Measuring vibration by sound has the advantage that at the same time, measuring the vibration of all the items of machinery. But, it has one big disadvantage, like; in industrial production, often the sound surrounding comparable or superior to that from the machine needs to be analyzed.

Hence, traditionally, and unconsciously, the vibrations have been used as an indicator of the technical condition of machinery. Nowadays the measurement of vibrations to detect and identify failures and developed or early period of development and have real information about condition of machinery; which is world wide used

and commonly accepted as best technique in rotating machinery.

The vibrations can be observed in time or frequency. In the measurement of the level of vibration, it is necessary to define the physical magnitude to be quantified to describe the vibration; and it can be used for displacement, velocity or acceleration, [1]. We will work from now on the frequency spectrum, because we can run the identification phase of the problem. As magnitude of vibration enlarges, use of speed to be widely used in the analysis for severity of rotating machinery.

In this paper, a methodology for obtaining a parameter of global machine condition is proposed. It provides information similar to that which would have an expert operator with his ear to hear the machine running. Moreover, this parameter will be generalized to obtain what would be a "hearing" simultaneous of all rotating machinery in the factory.

2. GLOBAL VIBRATION SPECTRUM

The use of levels of vibration produced by rotating machines, to determine the technical state of the latter, has a myriad of applications in the industrialized world, because for over three decades effectiveness and utility the information provided by the records of vibration have been proven.

All elements that compose machinery have some features depending on the design and operating speed. Some of these features are the characteristic frequencies, where this component vibrates if it is excited. This implies that, before attempting to identify problems in a machine, based on information supplied by the vibrations it is necessary to determine the frequency of diagnosis of all elements that can vibrate. These frequencies are those which are expected to obtain information on the spectrum of vibrations during the measurements that are made in properly selected points with the selected measurement tools. In this way, it will be necessary to find within the spectral records the frequencies of diagnoses that were previously identified during the casuistic analysis of the machine and observe the evolution of these frequencies.

In general, the forces between the contact elements in a machine during its operation, determine the life period of them. However, what is measured is not the magnitude of these forces, but the vibrations in the machinery. Unfortunately, identical condition of machines doesn't mean identical levels of vibration and this is a common mistake in the traditional vibration analysis creating lots of false alarms. If you change the mechanical fastening or the bench of a machine or two; they differ only in their base plate, the amplitude of the dynamic force may be the same on both machines, but not the vibrations measured in selected points.

2.1. Process for vibration diagnostics

The key for predictive maintenance is to monitor the evolution of the frequencies characteristic associated to all identified components using periodic measurements [4]; See Figure 4.



Fig. 4. Monitoring of frequencies band

This monitoring is not easy, if one takes into account the dynamic behaviour of machines characterized by the fact that:

1. Different temporary records can produce similar spectra.
2. For some frequencies, their corresponding amplitudes can be acceptable. However the same amplitude may be unacceptable for other frequencies within the same spectrum.
3. Several problems can be shown into the same frequency. For example, the unbalances, the deflection of a shaft, or the misalignment producing similar effects in the same frequency. Also, it can happen that a machine shows a frequency caused by any of the above mentioned problems. But, if this vibration is transferred from another machine connected in some way, then we can not trust in some vibration records, if we are not sure of the vibration source.
4. The analysis of a problem at a given frequency in many cases, dependent on the presence of one or more frequencies associated with it.

It is therefore extremely important to have spectra of a machine in different frequency ranges, even if it is possible to apply the technique of ZOOM in different frequency bands, necessary for the analysis of complex machines, [5]. Two stages of work are required: First one is called detection, which requires defining the reference spectrum, which is obviously a spectrum corresponding to vibrations recorded in the same point, where vibration usually is measured in machine, but this was obtained when it was estimated that the machine had a normal mechanical condition. Against this spectrum, by comparing the further measurements, we can detect if frequencies associated with machine components have increased to non-permissible levels, because it may indicate that it is developing a fault.

The second stage includes the identification of the problem. Previous results are the basis for this stage in order to find out where it is located; and what is the problem that has produced excessive levels of vibration. In general, the frequency measured is not deceived, but it can be analyzed incorrectly, measured inappropriately or incorrectly interpreted; due to which; the amplitudes can be overestimated or underestimated. Most of the severity charts included in vibration standards were designed for vibration levels caused by unbalances, [6]. However, for many years these charts have been used and currently are still in use in some cases. In addition, the efforts are always to have the maximum measurements; with each machine having ten or twenty measuring points, generating alarm in the most severe vibration points which do not always mean the most serious problem to be located there. This sort of arrangements produces a large number of false alarms in monitored processes, as discussed above. The consequence of this policy is that no attention is paid to machines with lower levels, but whose prognostics are worse with imminent failures, and there are more failures, even though their levels of vibration have not reached high values according to ISO standards. Galar [11] proposed OFVL (Overall factory Vibration Level) as a global indicator of the general state of large sets of rotating machinery. The use of this indicator instead of the most severe vibration point solves the false alarm problem.

2.2. Need for spectral benchmarks

OFVL provide useful information of the real severity of the machine. In fact, it is a good benchmark for prognosis. However, this reference doesn't provide any information about the causes of the potential failure and the methodologies to avoid it. That is why; diagnosis dynamic benchmark is needed not only to know the severity of the condition of each machine, but the evolution of different potential damages as imbalance, misalignment and so on.

For this purpose, averaging of real spectra becomes the best technique to create a vibration template for diagnosis. Averaging technique is widely used in the analysis of vibration. This is used when performing the operation, to ensure repeatability of the same, so that the collector performs several measurements and averaging. This methodology has a clear utility to prevent that a slip of the sensor causes an abnormal beating producing a false alarm. The average measures in a single machine can raise the quality of this measurement. However, we can and we must average the vibratory state of different machines, to have a benchmark, i.e. a template which provides complete information about the different problems that are being developed in the plant. So, the technician can analyze vibration spectra with his knowledge and

expertise. Besides, he can use a benchmark produced by the current condition of the whole factory or area, as can be seen in figure below. This will reduce the hundreds and hundreds of spectra obtained to an average spectrum, which would give the vibration state of the plant as a whole, as well as you keep your knowledge in the calculation method and data collection without wasting of knowledge associated to specific people in the company. Clearly, this average should be weighted according to those parameters that make it more important or more critical than other machines. This weighted averaging method is proposed using a new parameter, the normalized averaged spectrum. Comparisons of individual spectra measured in each machine with this template will show the difference between the machine and the rest of equipments in the plant regarding the vibration conditions and possibility of failure appearance.

As a general guide, the strategy is generally used to relate the spectra measured with the reference spectrum. In other words, it is believed that the best indicator of the mechanical condition of the machine is given by the changes experienced by the vibration levels with respect to the reference spectra of the machine itself, as can be seen in Figure 5.

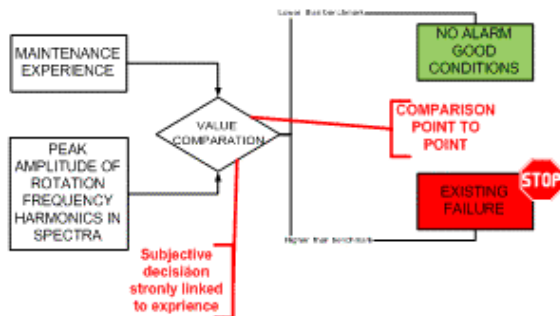


Fig. 5. Traditional method of measurement comparison based on maintenance worker's knowledge

Obtaining the reference spectrum is complex. We can use in new installations, the spectrum after the installation and start-up of machinery, but be sure that the machine is not in a period of infant mortality, where the spectra can be more alarming to the operation at maturity. This may be interesting to consider a spectrum of burn-in period, with eliminated child period of infant mortality, as suggested by the MIL-STD-2074 [7], to test reliability. Machinery that has a running time, unpredictable spectrum is considered. Even, after an overhaul, total reset of the machine may have natural frequencies of the plant or machinery coming, and some of defective parts.

2.3. Average of measured spectra

Suppose that $v(t)$ is a signal velocity of vibration at the time limited by an interval between 0 and T. Fourier transformation of this segment is expressed as follows:

$$V(f) = \int_0^T v(t)e^{-j2\pi ft} dt \quad (1)$$

The segment $v(t)$ is limited between 0 and T, just as its Fourier transform is limited between -F and F. In practice, the sampled segment of finite length and the spectrum can be limited using a low pass filter. With these restrictions, it is only necessary to describe $v(t)$, a finite number of samples of the signal itself in time or its spectrum $V(f)$. Thus, if the $V(f)$ spectrum is sampled at intervals of frequencies equal to the so-called Nyquist interval, $1/T$, within the $-F$ to F , the number of samples required will be:

$$N = \frac{2F}{\frac{1}{T}} = 2FT \quad (2)$$

Hence, we can see that the tool is interesting for analysis in the frequency domain of our signal, DFT (Discrete Fourier Transform), which provides a discrete spectrum, which is easy to be processed. No information is lost, if we use the minimum resolution defined by Nyquist sampling frequency in the discretization process. This discrete spectrum will be as follows, [2]:

$$V(k) = \frac{1}{N} \sum_{n=0}^{N-1} v(n)e^{-j\frac{2\pi kn}{N}}$$

$$v(n) = \sum_{k=0}^{N-1} V(k)e^{-j\frac{2\pi kn}{N}} \quad (3)$$

$$n = 0, 1, \dots, N-1$$

$$k = 0, 1, \dots, N-1$$

With $v(n)$, the sampled vibratory signal, $V(k)$ the discrete spectrum, is obtained by DFT and; N is the number of discrete samples of a segment of the vibratory signal. This set of N discrete samples is often called segment. In the case of vibration processing, signals are real and discrete spectrum $V(k)$ is complex. . When, we do the DFT, using N as a power of two, better known as FFT (Fast Fourier Transform), it saves us time to process a very high, especially in portable collectors, which makes this FFT widely used for its simplicity throughout the vibration analysis, [3].

It is therefore proposed to use the spectrum-weighted average, which is normalized to the frequency of rotation, projecting the vibration

spectrum on that template. The average normalized expression of the spectrum would be allocated as follows:

$$V_{media}(k) = \frac{\sum_{i=1}^n v_i \left(\frac{1}{N} \sum_{n=1}^{N-1} v(n)_i e^{-j \frac{2\pi kn}{N}} \right)}{\sum_{i=1}^n v_i} = \frac{\sum_{i=1}^n v_i V(k)_i}{\sum_{i=1}^n v_i}$$

$$n = 0, 1, \dots, N-1$$

$$k = 0, 1, \dots, N-1$$

$v(n)_i$ is the time segment of vibration measured on the collector at point i and $V(k)$ is the fast Fourier transform of this segment.

Where, v_i is the speed associated to the point i . $v(n)_i$, at point i , where n is the total number of measured points on the machine in question: Horizontal, vertical and axial, not the housings of the bearings. N is the number of sampling points of the signal temporal result of sampling with the Nyquist frequency, as a minimum. Under the DFT (Discrete Fourier Transform), therefore, $V_{media}(k)$, must have these items for as little and not to lose information in the transformed. We'll therefore like to get an averaged spectrum as analyzed by the machine.

2.4. Importance of normalization and interpolation

Thus, we must normalize the spectrum in the frequency axis by the rotational speed, i.e. get the value of 1x frequency, the frequency of rotation, 2x etc. In this process, normalization will be necessary to interpolate a number of samples to achieve this shift in frequency that allows the matching frequency of rotation.

Be $V_1(k)$ FFT be of N samples with the frequency of rotation f_1

And; $V_2(k)$ FFT be of N samples with the frequency of rotation f_2

Obviously, in the standardization process, we will lose slight information of one of the spectra, to keep the number of samples N invariable. In this case, we can use two methods of work: Normalize the frequency higher, and therefore, interpolation, or normalized to the lower frequency and therefore sub sample with the loss of additional information. If you opt for the interpolation, we need to calculate the ratio of the higher frequency, compared with the lowest coming to interpolate a number of samples in the spectrum according to their relationship. Normally, the difference in the frequency of rotation is between machines that rotate at 1000 RPM and

machines that rotate at 1500 RPM, (Karassik, 2001). In this case, the interpolation ratio of 1.5 is quite small, so that the methods of linear interpolation or cubic splines provide good results. When there is rotating machinery, such as; steam turbines that rotate at 4000 RPM or 4500, it is preferable for those machines, sub-sample at a frequency lower, which as mentioned is usually 1000 or 1500 RPM. The process of interpolation from 1000 RPM to 4000 RPM in all the machinery that is normalizing with respect to the frequency of rotation of the turbine would introduce too much distortion in the system.

Once interpolated spectrum, it should be noted that, it will increase in length of N samples to $N \frac{f_2}{f_1}$ samples, increasing the frequency usually represented 1 KHz to $\frac{f_2}{f_1}$ KHz, so the last step in

this process of normalization will cut this spectrum obtained in the N sample, assuming that little loss of information at high frequencies. In the case of machines of different speeds (reducing or pulleys), help us to harmonics in the frequency of rotation and match them properly and are averaged. Similarly, the number of points, i.e. the spectral resolution of the DFT must be the same for all. This confirms that; analysis, which takes in more points in DFT for gear machines, must match the number of DFT points made in all spectra; otherwise, it will be impossible vectors resulting weighted average. With these assumptions, the resulting weighted average spectrum, which will call OFAS (Overall Factory Average Spectrum) respond to the following expression:

$$OFAS(k) = \frac{\sum_{i=0}^n P_i V_i(k)}{\sum_{i=0}^n P_i} \quad (5)$$

Where, V_i is the average of the vibration machine i , as calculated above, P_i is the power installed in the machine i and n the number of machines included in the search for the global average spectrum of vibration. What we get is; therefore, an average spectrum, normalized to the frequency of rotation for the entire area of analysis that we are contemplating.

9. OFAS LIKE CBM TOOL

OFAS utilities are basically two, clearly differentiated: Firstly the OFAS is a standard template on which the current state of vibration of a machine at a particular time is projected. The condition of dynamic template, changing with time, is interesting to study. It may examine the deviations of vibration of the machine studied, with regard to

general conditions at that particular time, and not with respect to static conditions, which are often not reproducible. Obviously, we need different templates in function of the age of machinery, because the vibration signature and the interpretation of this signature are changing during that time.

Secondly, we can obtain the trend of global problems that are manifested as harmonics rotation speed or highly localized in certain frequency bands, such as; imbalance, misalignment, clearances, hydraulic problems or problems of lubrication.

3.1. OFAS as standard reference template

The templates used in the early stages of operating the machine, often do not coincide with the pattern repeated after ten years of operation, because the signature of each machine gives it a hallmark, which is not a symptom of malfunction, but the result the configuration of the installation itself. In rotating machinery, it is important to take into account the dynamic nature of these projection templates, i.e., the signature of the machine changes over time and is influenced by factors, such as; repairs, the machinery that surrounds it, or the conditions of operation.

In this way, we can get different OFAS periodically measured as a result of data collection, which will mutate over time. We can calculate the OFAS for a particular type of equipment in the plant, for a given area or for the entire plant.

The OFAS, is an averaged variable, so the reliability of it depends on the items listed. Therefore, OFAS calculated using large rotating machinery which provides more reliable results. In Figure 8, we can see that the OFAS of a machine is calculated, i.e. by calculating the average spectrum of the measuring points. In this case, a motor coupled to a pump with the following control points: 1H, 1V, 1A, 2H, 2V, 3H, 3V, 4H, 4V, 4A.

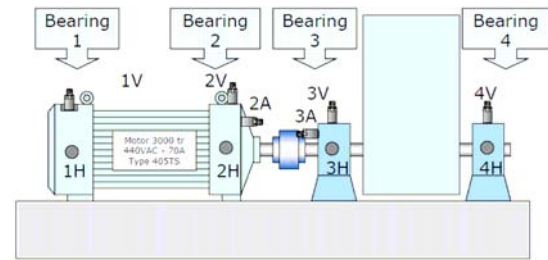


Fig. 6. Measurement points in a motor-pump

The OFAS of the machine will therefore be calculated using the following expression, because there is only one element driving (with a given power) and the motor and pump rotating at a single speed, as you can see in Figure 6.

$$OFAS(k) = \frac{V_{1H}(k) + V_{1V}(k) + V_{1A}(k) + V_{2H}(k) + V_{2V}(k)}{10} + \frac{V_{3H}(k) + V_{3V}(k) + V_{4H}(k) + V_{4V}(k) + V_{4A}(k)}{10} \quad (6)$$

The other spectrum is the OFAS for all the pump rooms, where the machines are located as you can see in Figure 7 and OFAS of the whole rooms can be calculated simultaneously with the OFAS of our pump in order to do further comparisons.



Fig. 7. Pump room where the machine is located

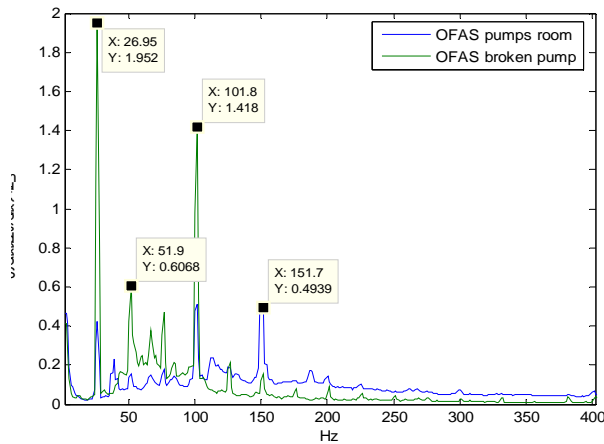


Fig. 8. OFAS of a pumps room versus OFAS of a broken pump

We can see that, the OFAS of our machine, compared with the overall plant OFAS, presents some important variations. In this case, the peaks of the 1x and 4x of our pump are several orders of magnitude higher than the average plant spectrum. So, we have a machine with a major breakdown; an imbalance in the rotor and the development of important clearances. Detailed analysis of spectra of this machine will give more information and can define the problem; the speed of OFAS machine in comparison with respect to global OFAS is obvious. This comparison is an additional advantage, as it not only perceives the existence of a fault; but, we also see the divergence with the rest of the plant, which eliminates the possibility of a crash on all machines.

In Figure 9, we can see another pump in the room with respect to global OFAS.

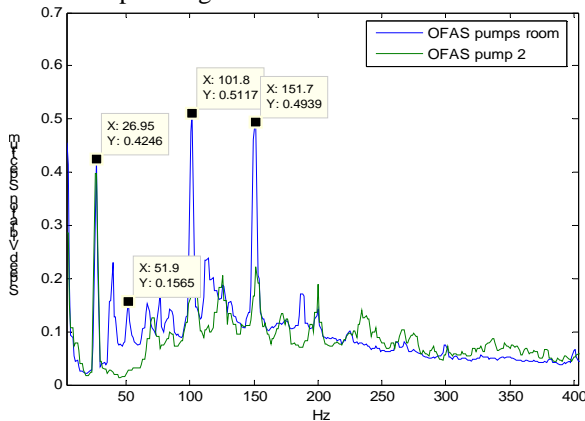


Fig. 9. OFAS of a pumps room versus OFAS of non broken pump

None of the peak stresses are above the global OFAS; so, this pump is below the signature characteristic of the vibration in the room at the time of measurement. It is therefore, a pump that is in normal use and below the levels of vibration of the machines that surround it.

3.2. OFAS as generalized fault diagnosis in factory

The second utility OFAS is the analysis of trends for the detection of pathologies generalized to the entire plant. Through this standardized and averaged spectrum, we can view the status of certain pathologies associated with harmonics of the frequency of rotation. It is important to note that, it is not going to get the information for immediate intervention, but the trend of a fault and its propagation. In Figure 10, we can observe the OFAS for the pump room; which we studied previously. The peaks at 1x, 4x y 6x those remain high, despite the extent of the averaging effect softer, which may be indicative of several failures A progression upward with peak at 1x, may indicate excessive or unbalanced rotors defective benches in most cases. Peak 4x and 6x show us housings with early bearing clearances and hydraulic problems. The trend of these peaks and the averaged OFAS will tell us if a problem persists and increases or on the contrary is circumstantial.

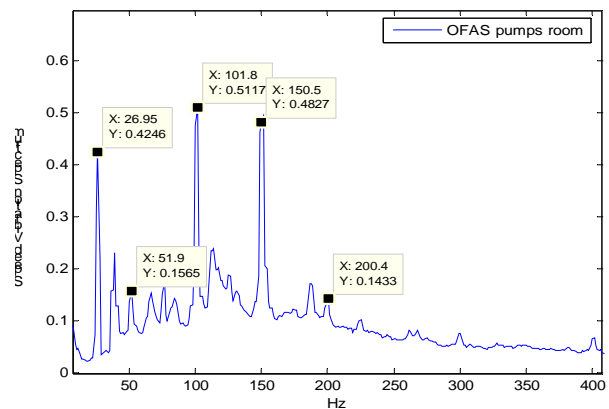


Fig. 10. OFAS of a pumps room

Specifically, we can visualize in the OFAS, the development of pathologies associated with multiples and fractions of the frequency of rotation, whose cumulative effect on the OFAS will indicate the severity of the problem. The OFAS, therefore, has some disadvantages, such as; non-occurrence of errors associated with absolute frequencies. For example, the failure of benches with soft foot is shown in 100Hz, which is delocalised and blurred in the standardization process. Therefore, it disappears from our field of observation. The average and frequency displacement became the 100 Hz peak invisible.

The other disadvantage is the coincidence of several types of failure in a single frequency, [9]. Can the typical peak at 1x, which if high, could raise pronounced imbalances or faulty benches? To this end, we compare the OFAS with some of the critical points of the machines, as supports of the pumps, to identify and segregate the source of the vibration. Despite the comments above with respect to the

frequency of failure, i.e., the overlap of some diseases on the same frequencies, we can differentiate a number of interesting bands that will allow us to analyze the overall trend of problems at the plant. In the case of centrifugal pumps installed in sufficient number, normalized and averaged spectrum shows some data depending on whether the problems associated with the frequency of rotation and its harmonics. Flow problems, poor lubrication or poor design of the impellers and pipes of the plant will produce peaks in the reference frequencies. When these problems are restricted to a single machine, the effect of averaging, minimize alarm considerably. Similarly, excessive peaks 1x indicate general imbalance or hydraulic imbalance, pathology more common in the global plant. Similarly, frequency of 5x to 20x will give us a general state of the bearings, or at lower frequencies, we can see the general state of the housings of the bearings. Therefore, we need to identify problems associated with harmonics in the frequency of rotation, which in the spectrum to the same standard, have a cumulative impact on the OFAS. [10] describes some pathologies of rotating machinery, associated to harmonics or sub harmonics to be observable in OFAS.

Imbalance: The OFAS reflects a sharp peak at 1x on plants with high levels of imbalance or benches in a poor state.

Misalignment: The hallmark of the misalignment is the generation of the three harmonics in the frequency of rotation. If the frequencies 1x, 2x and 3x are present in OFAS, we must align the plant. In fact, most of the plants are lined up all the rotating machines at once with a given time period, or when there are symptoms of misalignment on the operation.

Bearing clearances with respect to the shaft: The OFAS provide this information in a quality parameter in the installation of the bearings by the maintenance team.

Bearing clearances with respect to housing: If there are clearly four harmonics of the frequency of rotation, then, it is very likely that the bearing is "loose" with regard to their accommodation.

Failures in gears: OFAS will have a reduced peak gear, but be abundant in number; it indicates a very poor state of gear machines in the plant.

Vibrations caused by oil whirlwinds: OFAS peak of 0.4x to 0.5X to assess the quality of lubrication programme of the plant within the PM programme.

Bearings Defects: Many experts also agree in saying that the ruling is imminent in the bearing; when the highest peaks generated by it, decreasing in frequency to around 20X harmonic. Therefore, we see in our OFAS a band bearing terminal state to be monitored.

4. CONCLUSIONS

The development of indicators for maintenance requires scorecards tailored to the personnel who will use them in making decisions. Implementations of CBM and specifically the analysis of vibrations get detailed analysis of the state machinery; but, specific data are not exported to higher levels of the organization. Maintenance managers with hundreds of rotating machinery in-charge need a small set of indicators that presents trends appropriate to analyze at a glance the general state of health of the machinery of the plant. The OFAS is an appropriate scorecard for technicians and maintenance engineers and even the other managers and director of the department. It is therefore, a leading indicator of interest, which also provides references to determine the deviations from it. Once the hierarchical level of this indicator is established, it should highlight the two major advantages in implementation. On the one hand, we obtain the reference template on which to project our spectra. This template, in contrast to what the manufacturer tells us, will be dynamic and will change depending on operating hours and repairs incurred. It will be the signature of our own facility, a unique and irreproducible one, whose evolution is very interesting to evaluate the overall condition of the machines. Moreover, the evolution of OFAS shows the progress of some diseases. Therefore, it should be reflected by high peaks at 1x, 2x, 3x etc.... depending on the severity and repetition of some fault in the machinery. This is interesting, because, there are diseases such as misalignment, clearances or inadequate lubrication often repeated in a large number of machines, so that the appearance of these peaks in OFAS is a symptom of its existence. Therefore, the evolution of some peaks will be strongly correlated with the lubrication programme, annual alignment of the plant during maintenance stop, the general state of the structures and benches as well as the expertise of the maintenance team in assembling and handling bearings, shafts and housings.

5. BIBLIOGRAPHY AND REFERENCES

- 1 Girdhar P.2004. *Practical Machinery Vibration Analysis and Predictive Maintenance*. Oxford: Elsevier.
- 2 Palomino E. 1997. *La Medición Y El Análisis De Vibraciones En El Diagnóstico De Máquinas Rotatorias*. Cuba: CEIM - Innovación y Mantenimiento.
- 3 Oram-Brigham E. 1988. *The Fast Fourier Transform and its applications*. UK: Prentice Hall.
- 4 Bloch H. & Geitner F. 1999 *Machinery Failure Analysis and Troubleshooting. Practical Machinery Management for Process Plants*. Volume 2,3rd Edition Elsevier.

- 5 Mobley, R. 1999. *Vibration fundamentals*. USA:Butterworth–Heinemann.
- 6 Kumaraswamy. S. & Rakesh. J. 2002. *Standardization of Absolute Vibration Level and Damage Factors for Machinery Health Monitoring*. Proceedings of VETOMAC-2, 16-18 December,2002.
- 7 MIL-STD-2074 1978. *Failure Classification For Reliability Testing*. Washington: USA Department Of Defense.
- 8 Karassik, Igor J.; Messina, Joseph P.; Cooper, Paul; Heald, Charles C. 2001. *Pump Handbook* (3rd Edition). McGraw-Hill.
- 9 Reeves C. W. 1998. *The Vibration Monitoring Handbook*. USA: Coxmoor Publishing Co
- 10 Marscher W. 2004. *The Relationship of Vibration to Problems in Centrifugal Pumps*. *Chemical engineering*. New York: Mc Graw-Hill.
- 11 Galar D. 2010. *Overall Factory Vibration Level: The need for global indicators in CBM*. DIAGNOSTYKA' 2(54)/ 2010.

DECORRELATION OF INDICES FOR A SINGLE NUMBER ASSESSMENT OF THE ACOUSTIC QUALITY OF SACRAL OBJECTS

Krzysztof KOSAŁA

AGH University of Science and Technology, Department of Mechanics and Vibroacoustics
Al. Mickiewicza 30, 30-059 Kraków, Poland, e-mail: kosala@agh.edu.pl

Summary

A new approach for solving the problem of a single number index formula by creating the index from mutually-correlated indices by means of decorrelation of the Index Observation Matrix (IOM) was shown. The orthogonal singular vectors obtained from SVD were used in order to build a single number index. Application of the proposed formula for a local single number index of selected acoustic parameters of the interiors of six Roman Catholic churches was shown. Decorrelation of the indices for a single number assessment of the acoustic quality of sacral objects will be applied for complex global acoustic assessment of such interiors' index method, which is currently being improved.

Keywords: Singular Value Decomposition (SVD), decorrelation, index method of assessment

DEKORELACJA WSKAŹNIKÓW W JEDNOLICZBOWEJ OCENIE JAKOŚCI AKUSTYCZNEJ OBIEKTÓW SAKRALNYCH

Streszczenie

Pokazane w artykule nowe podejście do rozwiązania problemu opracowania wskaźnika jednoczłobowego, polega na utworzeniu tego wskaźnika ze wskaźników skorelowanych ze sobą, na drodze dekorelacji wskaźnikowej macierzy obserwacji. Do konstrukcji wskaźnika jednoczłobowego wykorzystano, uzyskane z rozkładu SVD, ortogonalne wektory szczególnie. Weryfikację zaproponowanego wzoru na jednoczłobowy lokalny wskaźnik wybranych parametrów akustycznych obiektów sakralnych pokazano na sześciu rzeczywistych kościołach rzymskokatolickich. Dekorelacja wskaźników w jednoczłobowej ocenie jakości akustycznej obiektów sakralnych będzie wykorzystana do kompleksowej globalnej oceny jakości akustycznej obiektów sakralnych - metody wskaźnikowej, która jest w dalszym ciągu udoskonalana.

Słowa kluczowe: rozkład względem wartości szczególnych, dekorelacja, wskaźnikowa metoda oceny.

1. INTRODUCTION

The state of object quality can be diagnosed by means of assessment indices. There are many acoustic parameters in interior acoustics, which are used to assess the acoustic quality of investigated objects. The measured values of those parameters and the comparison of their values to preferred ones are the basis of the assessment.

Long-term scientific research performed at the Department of Mechanics and Vibroacoustics has been carried out in order to elaborate a complex method of acoustic quality assessment of public buildings, such as sacral objects [3].

An index method for the acoustic quality of sacral objects proposed by Engel and Kosała in 2007 in [4] was based on the designed partial indices of assessment. The partial indices calculated from some relation are used in the assessment of particular acoustic properties of the object. An approximate assessment is conducted by means of single number

global index. The index method is still being improved by using the Singular Value Decomposition (SVD) technique [9, 7].

An acoustic assessment by means of the index method (described in [5]) has one main drawback because certain information included in the correlated indices is duplicated. The application of singular vectors, obtained from SVD, is proposed to solve this problem. At the beginning, correlation research between partial indices is needed. When the partial index is not correlated (or weakly correlated) with the other ones, it can be used for the global assessment. However, a single local index of selected acoustic parameters, on the basis of strong correlated indices, should be created. A local index, as a single number, will be the next component of global assessment.

A single number index is obtained, by using the SVD technique, in two ways. One of them, which is shown in [8], is based on a single number index, and contains a new set of perfectly mutually-correlated

indices, which is obtained from the Index Observation Matrix (IOM).

The next proposition for creating a local index is a solution based on the decorrelation of mutually-correlated indices, which is described in the article. A local index is based on uncorrelated singular vectors, which are obtained from the decomposition of the IOM by means the SVD technique.

2. DECORRELATION OF INDICES USING THE SVD TECHNIQUE

The IOM (Index Observation Matrix) was obtained from the values of mutually-correlated partial indices, which are described in [8]. The columns of the IOM are formed using the consecutive partial indices. The rows of the IOM are the sacral objects listed in Table 1 in [8].

The next step is decomposition of the IOM by the Singular Value Decomposition in, for example, Matlab environment.

The SVD is a calculation technique, which is commonly used in linear numerical algebra [6,10] and has applications in many fields of science such as diagnostics [1] and vibroacoustics [2],[4].

Due to the Singular Value Decomposition theory, three other matrices are obtained from the matrix $IOM \in R^{m \times n}$

$$IOM = U \cdot \Sigma \cdot V^T \quad (1)$$

where: U – orthonormal matrix $m \times n$, Σ - diagonal matrix $n \times n$, V – orthonormal matrix $n \times n$.

Equation (1) can be expressed in the following way:

$$\begin{bmatrix} IOM \end{bmatrix} = \begin{bmatrix} U \end{bmatrix} \begin{bmatrix} \Sigma \end{bmatrix} \begin{bmatrix} V^T \end{bmatrix} \quad (2)$$

where: Σ - singular values of the matrix IOM , U – left singular vectors of the IOM - u_i , V^T - right singular vectors of the IOM - v_i .

Σ is the diagonal matrix:

$$\sigma_{ij} = \begin{cases} \sigma_i > 0 & \text{for } i = 1 \dots n \\ \sigma_i = 0 & \text{for } i > n \end{cases} \quad (3)$$

Diagonal elements fulfill the condition:

$$\sigma_1 \geq \sigma_2 \geq \dots \geq \sigma_n \quad (4)$$

Decorrelation of mutually-correlated variables, such as indices - the components of the IOM, can be obtained by SVD. A new set of the left and right singular vectors in the matrices U and V^T suitably, are obtained. All the singular vectors in the matrix U are orthogonal to each other, as such they are entirely uncorrelated. The singular vectors of the matrix V^T have the same properties. Such properties were used to create a single number index of assessment, which contains a new set of the indices uncorrelated to each other.

It is proposed to construct the matrix with uncorrelated indices

$$B = u_1 v_1 + u_2 v_2 + \dots + u_n v_n \quad (5)$$

where: $u_i \div u_n$ – singular vectors of the matrix U , obtained from SVD of the IOM,

$v_i \div v_n$ – singular vectors of the matrix V^T , obtained from SVD of the IOM.

The matrix B is the sum of the products of orthogonal singular vectors. The columns of the matrix B create a new set of uncorrelated indices.

A single number index of assessment is calculated from the matrix B , according to the formula

$$W_{WPAj}^{uncor} = \sum_{i=1}^n b_{ji} \quad (6)$$

where: W_{WPAj}^{uncor} – a single number index to assess selected acoustic parameters of the j -th object, corresponding to the j -th row of the matrix B , b_{ji} – an uncorrelated partial index, corresponding to the j -th object (j -th row) of the matrix B and the i -th column of the matrix B .

A single number index W_{WPA}^{uncor} is the sum of the products of the singular vectors, corresponding respectively to the approximation rank from 1 to n , without taking into account the common components, such as approximations – the singular values $\sigma_1, \dots, \sigma_n$. It is proposed to use only such orthogonal (uncorrelated) singular values for assessment.

3. USE OF DECORRELATION OF INDICES IN ASSESSING THE ACOUSTIC QUALITY OF SACRAL OBJECTS

A graph with an IOM was shown in Fig. 1. The matrix was created on the basis of three mutually-correlated partial indices: the reverberation index – W_p , the music sound index W_M and the speech intelligibility index W_Z . The indices' computation procedures, applied to six sacral objects, were shown in [8]. The values of the coefficients of linear correlation between the partial indices are higher than 0.93 [8].

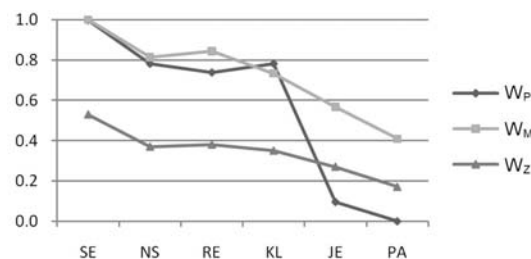


Fig. 1. Content of the Index Observation Matrix - IOM

The singular vectors and singular values were obtained by applying the Singular Value Decomposition to the IOM. The singular vectors were used for building the matrix B (Formula (5)).

Content of the matrix B with the uncorrelated indices as well as the singular vectors and the singular values, obtained from Singular Value Decomposition of the matrix B are shown in the Fig.2-5.

The singular values $\sigma_1=\sigma_2=\sigma_3=1$ (approximately) and graphs in Fig. 4. determine a lack of correlation between the columns of the matrix B. This is also determined by the condition number $\text{cond}(B)=1$.

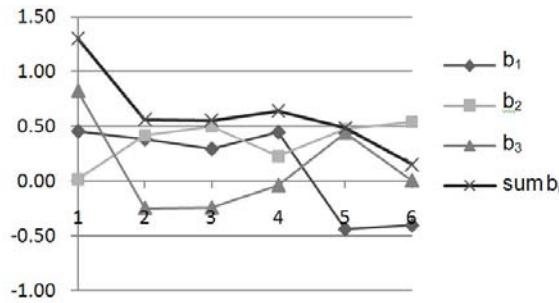


Fig. 2. Content of the matrix B with the uncorrelated indices

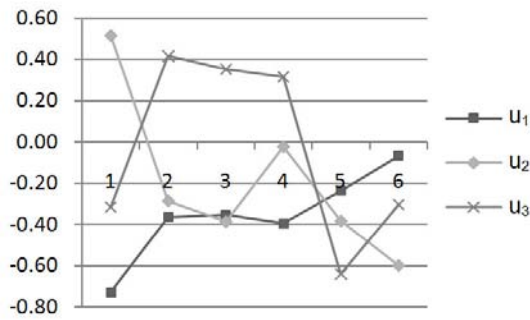


Fig. 3. Left singular vectors

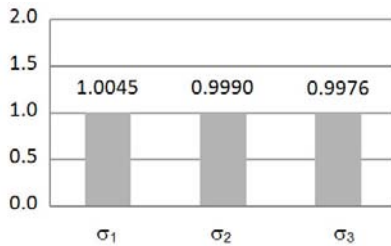


Fig. 4. Singular values

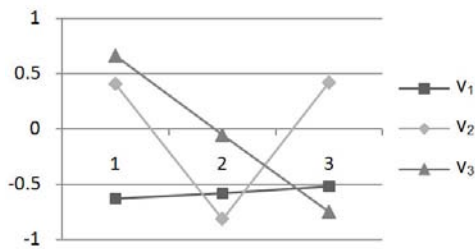


Fig. 5. Right singular vectors

The values of the index W_{WPA}^{uncor} within the range 0.15 to 1.3 from the formula (6) have been obtained. The maximum value of the index exceeded the

assumed ones, equal to 1, therefore normalization in the shape of a transforming quotient was applied. All values of the indices W_{WPA}^{uncor} were divided by its maximum value. The result before (index W_{WPA}^{uncor})

and after (index W_{WPA}^{uncor*}) normalization are shown in Fig. 6.

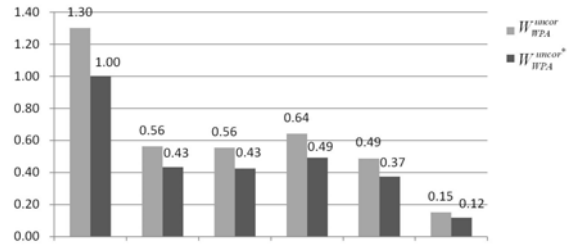


Fig. 6. The values of single number indices W_{WPA}^{uncor} and W_{WPA}^{uncor*}

The uncorrelated indices, which are written in the matrix B from the correlated partial indices – the components of the Index Observation Matrix, were obtained. They were obtained from the sum of the products of left and right singular vectors. However, the first index of the IOM - W_P and corresponding index b_1 of the matrix B, are correlated. The value of the coefficient of linear correlation between them is very strong and equals: 0.9820. Therefore, the proposed method, to obtain a single number index (the local index), which is complex and contains additional uncorrelated indices, seems to be proper.

According to Fig. 3, the best acoustic properties appear in the church of St. Sebastian in Strzelce Wielkie ($W_{WPA}^{uncor*}=1$), whereas acoustically the worst is a modern one, built on a circular lay-out: St. John Kanty's Church in Bochnia ($W_{WPA}^{uncor*}=0.1$). The assessment of those two objects is consistent with the subjective opinions of the churchgoers as well as with assessment by using the index method, proposed in 2007 [5].

4. CONCLUSIONS

A new approach to the problem of a single number assessment of the acoustic quality of a sacral object, where a few mutually-correlated indices have been used, was shown in the paper. So far, a single number global assessment by means of correlated and uncorrelated indices has had one main drawback because certain information included in correlated indices was duplicated. A separation of correlated and uncorrelated indices was proposed. A local single number index of selected acoustic parameters from correlated indices was created. A single number index consists of the uncorrelated single vectors obtained from Index Observation Matrix

decomposition. The proposed formula was applied to assess the real Roman-Catholic churches. The values of the index within the range 0.1 - for an object, which is acoustically bad, to 1 – for an object which has good acoustic properties, have been obtained. The assessment of those two objects is consistent with the subjective opinions of the churchgoers.

More accurate subjective assessment of investigated objects will be the next stage of research and then more precise verification of obtained results will be conducted. The convolution functions for speech and music signals with impulse responses of the investigated churches will be used for subjective research.

The approach of the decorrelation of correlated indices, which was shown in the paper, together with different uncorrelated indices, will be used to create the global index of acoustic assessment of sacral objects.

Further investigation will be based on application of a single number assessment to other types of public building or different technical objects.

ACKNOWLEDGEMENT

The paper has been performed within the statutory works of the Department of Mechanics and Vibroacoustics of AGH – 2010-2013, No. 3: “Prediction and experimental research of the new structures in acoustical adaptation of buildings”.

REFERENCES

- [1] CEMPEL Cz.: *Reduction of Data Set in Machines Diagnostics*, *Zagadnienia Eksploatacji Maszyn*, 4(44), 1980, p. 571-585.
- [2] ENGEL Z., ENGEL J.: *Application of Singular Value Decomposition in Analysis of Vibroacoustic processes*. Proceedings of XXXIV Ogólnopolskie Sympozjum „Diagnostyka Maszyn”, Węgierska Górka, 2007, p. 17-24.
- [3] ENGEL Z., ENGEL J., KOSAŁA K., SADOWSKI J.: *The Bases of Acoustics of Sacral Objects*, Kraków-Radom, ITE, 2007.
- [4] ENGEL Z., ENGEL J., KOSAŁA K.: *Vibroacoustic processes: sources, research, analysis*. Kraków, Faculty of Mechanical Engineering and Robotics AGH, 2009.
- [5] ENGEL Z., KOSAŁA K.: *Index Method of the Acoustic Quality Assessment of Sacral Buildings*, *Archives of Acoustics*, 32, 3, 2007, p. 3-22.
- [6] KIELBASIŃSKI A., SCHWETLICK H.: *Linear Numerical Algebra*. Warszawa, WNT, 1992.
- [7] KOSAŁA K.: *Calculation Models for Acoustic Analysis of Sacral Objects*. *Archives of Acoustics*, 34, 1, 2009, str. 3-11.

- [8] KOSAŁA K.: *Full Correlation of Indices for a Single Number Assessment of the Acoustic Quality of Sacral Objects*, Proceedings of Wibrotech 2010, Warszawa-Sękocin Stary, 29-30.11.2010, Warszawa, PW, 2010.
- [9] KOSAŁA K.: *The Possibilities of Application of Singular Value Decomposition in Acoustical Properties Analysis of Sacral Objects*. Proceedings of Wibrotech 2007, Warszawa-Jachranka, 29-30th November 2007, p. 159-168.
- [10] LANCZOS C.: *Linear Differential Operators*. Van Nostad, London, 1961.



PhD. Eng. **Krzysztof KOSAŁA** is a researcher at Department of Mechanics and Vibroacoustics of AGH University of Science and Technology, Kraków, Poland. Research interests: acoustic of the sacral objects, methods of assessing acoustic quality of the objects, environment

protection from the noise.

A CONCEPT OF DEFECT IDENTIFICATION WITH USE OF TEXTURE ANALYSIS METHODS¹

Anna BZYMEK

Department of Fundamentals of Machinery Design, Silesian University of Technology
44-100 Gliwice, ul. Konarskiego 18a, tel. (32) 237 10 63, fax (32) 237 13 60,
anna.bzymek@polsl.pl

Summary

One of fast developing methods for non destructive testing (NDT) is machine vision. The application of vision systems and image analysis and recognition procedures to variety of problems such as quality control of different products, surface quality estimation and defect identification is very popular nowadays. In the paper short review of applications of vision systems in diagnostics was presented, problem of texture in the images was described, some methods of textured image analysis was enumerated. Finally, the concept of defect identification with the use of image analysis techniques was presented. The purpose was to choose the methods of analysis and recognition which make possible to detect anomalies without the necessity of defect database and texture database creation. Two methods of texture analysis – GLCM and SVD were elaborated and results of algorithm operation were presented. Research were elaborated in Department of Fundamentals of Machinery Design of Silesian University of Technology within the framework of N504403735/32889 project.

Keywords: texture, image analysis, defect detection and localization.

KONCEPCJA DETEKCJI DEFEKTÓW POWIERZCHNI Z ZASTOSOWANEM METOD ANALIZY OBRAZÓW

Streszczenie

Jedną z bardzo szybko rozwijających się gałęzi badań nieniszczących jest wizja maszynowa. Metoda ta bazuje na technikach przetwarzania, analizy i rozpoznawania obrazów. Znajduje ona szerokie zastosowanie w systemach kontroli jakości m.in. do oceny stanu powierzchni oraz detekcji i identyfikacji defektów. W artykule przedstawiono krótki opis systemów wizyjnych oraz przegląd ich zastosowań w diagnostyce maszyn. Przedstawiony został również problem, związany z analizą obrazów, jakim jest występowanie tekstury na obserwowanych powierzchniach. W artykule opisane zostały wybrane metody analizy obrazów reprezentujących teksturę oraz przedstawiono koncepcję detekcji i lokalizacji defektów na takich obrazach. Badania zostały przeprowadzone w Katedrze Podstaw Konstrukcji Maszyn w ramach projektu N504403735/32889.

Słowa kluczowe: tekstura, analiza obrazów, detekcja i lokalizacja defektów.

1. INTRODUCTION

One of fast developing methods for non destructive testing (NDT) is machine vision. The application of vision systems and image analysis and recognition procedures to variety of problems such as quality control of different products, surface quality estimation and defect identification is very popular nowadays. The vision systems used in industrial applications allow reducing human factor influence in production procedures such as tiredness,

subjective evaluation, working speed, particularly in quality control processes. In case of machine vision conditions of image acquisition and images analysis and recognition methods applied in the system play the leading role. An images acquired with use of vision systems usually are two-dimensional representations of three-dimensional objects. Depending of type of a camera and band within which objects are being observed, one can obtain: regular images (photos), thermograms, ultrasonic images or X-ray images. Moreover, depending on

¹ Scientific work financed from resources assigned to science in the years 2008-2011 as a research project

the applied optics an object in the image can be represented in macro-, micro- or nano- scale.

One of properties of the observed objects that is represented and visible in the images is a texture. This property can be understood in two ways as a property of the object or property of the area in the image representing the object. Problems concerning the way of perception of textures done by human beings and by machines have been described in numerous publications [17],[18],[19],[28]. It is understood and well described that the texture can cause great difficulties in image processing and analysis. Taking into account the image analysis the texture is described as a distribution of brightness of pixels visible in the image (when a type of the image is constrained to monochromatic image) [10], [15], or the distribution of the colours (when taking into account images in RGB or in another colour format) [11],[26]. In the paper the first case was taken into account and all analyzed textures were monochromatic or colour images were changed to monochromatic before processing.

The subject of the paper deals with the problem of localization and identification of anomalies in the textured image, where an "anomaly" is supposed to be a "defect" of the surface represented in the analyzed image. A very important aspect of the presented approach is to detect the area of the image that differ from the rest of the image. It is usually performed with use of appropriate image analysis and recognition methods. Such region that differs from the neighbourhood is taken into account in further, more detailed analysis. The localized anomaly, after its analysis, at the following stages of operation of the algorithm could be identified as a defect. An essential assumption of the concept of detection, localization and identification of anomalies on surfaces of various technical objects was a fact that the algorithm should work without the support neither of the database of images representing defective textured surfaces nor database of the textures nor defects.

In the article, first of all some problems concerning setting up the vision system were mentioned, next, types of texture were described. Some methods of its analysis were cited and two of them – that had been used in algorithm, were described. Finally a concept of localization and identification of the anomalies on various textured surfaces was described and some initial results were presented.

2. VISION IN DIAGNOSTIC

In technical diagnostics such modern method as machine vision is applied more often and often. With the application of the vision systems in diagnostics some essential groups of problems can be solved. There are problems connected with particular elements of the vision system such as: lightning, cameras, position of cameras and illumination in relation to an object being observed.

Types of cameras and lightning have to be well suited to the task and they strongly depend on the problem to be solved. Nowadays, the choice of equipment for the vision system is practically unlimited therefore all problems and tasks have to be well thought over before setting up the system.

Concerning the hardware - cameras, it is possible to choose among cameras with the areascan or linescan matrices, slow cameras or fast cameras, where the acquisition speed begins from several frames/second up to several hundred or even thousand frames/second. Moreover, it is possible to choose between cameras with low or very high resolution.

Concerning the illumination, there is also a large assortment available. It is possible to choose a different type (IR, UV, visible) and colour of the light, representing different phenomena of illumination (diffused, focused, collimated). Another problem concerns the position of the lighting towards camera and object being observed. It is possible to apply frontlight, backlight, in various combinations: dark field and bright field. Depending of the lighting position different details could be distinguished from the observed object so they are better visible in the acquired image and thanks to that image processing and analysis methods applied at the further stage of algorithm could be less complicated and their application could be faster. In Fig.1 the influence of the position of the illuminator and difference in the acquired images was presented.

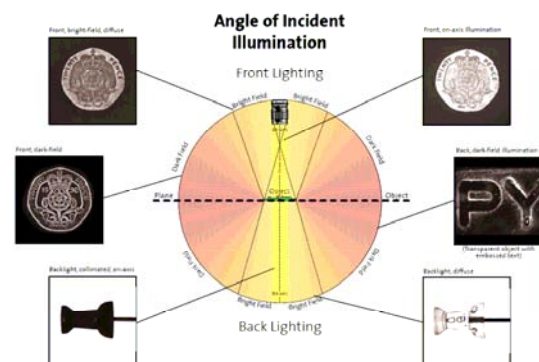


Fig1. Influence of the position and a type of illumination on the details visible in the acquired images [42]

The application of the machine vision in technical diagnostics is strongly connected not only with the well suited hardware but also to image processing and image analysis techniques that are indispensable. In the literature one can find number of methods of image processing and analysis. The usage of particular methods depends on a defined task and kind of a problem to be solved. Moreover, the type of the image (colour or monochromatic) influences the selection of the image analysis methods. In the domain of image analysis that has been developing from the early 60's, one can distinguish a group of methods

dedicated to the analysis of images representing various types of images: natural images e.g. in geographic research [3],[38], images acquired during medical examinations such as x-ray or ultrasonic [1],[29],[32] and images of technical objects. In technical/ industrial applications vision systems are widely employed [4] and technical objects are observed in macro-, micro- and nano- scales [12], [40]. Images characteristic for all these domains could be processed and analyzed with use of numerous methods.

As it was mentioned in the introduction, one of very important properties of objects representation is a texture. The texture in the image may be helpful or on the contrary, can cause the image analysis difficult depending of a purpose of the image processing. The texture and problems connected with its presence at the surface were described in the following paragraphs of the paper.

3. TYPES OF TEXTURES REPRESENTED IN THE IMAGES

In the image analysis domain a texture is treated as a property of the image representing observed object. The texture is a property which is well understood by a human, but it causes problems when has to be recognized by means of machine vision methods. In the paper a term “texture” is understood as a property of an observed object represented in the image whereas the image can contain a part of the observed object or the whole object. It has to be underlined that texture could be described in 2D or 3D. In case of 2D the texture could be understood as a pattern or group of patterns on a flat surface, whereas in 3D case the texture means coarseness or smoothes of the surface.

In the paper textures are understood as a “pattern on the flat surface”, even if in reality the surface is visible in 3D. As it was mentioned, the texture is described as a distribution of brightness of pixels visible in the image (when a type of the image is constrained to monochromatic image), or the distribution of the colours (when taking into account images in RGB or in another colour format).

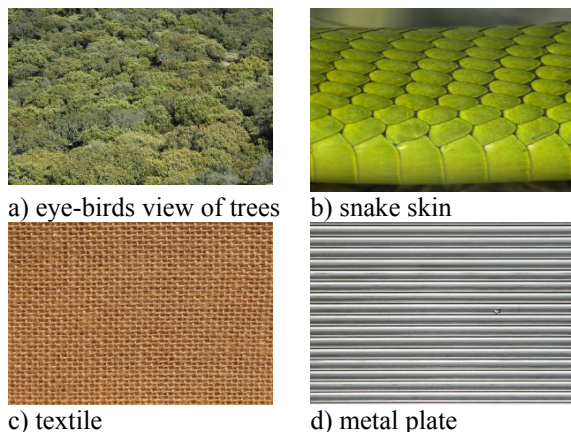


Fig. 2. Examples of natural and manufactured textures [41]

In the paper all analyzed textures were monochromatic or were changed to monochromatic before processing. All the images used in the paper were downloaded from a texture database for computer games [<http://www.cgtextures.com/>].

The photos used, are photos of real objects, made in natural environment. The purpose of the author, at this initial stage of the research was to apply these photos as a testing set for elaborated procedures. In the further research images acquired in laboratory conditions will be processed and influence of appropriate selection and configuration of vision system elements such us cameras and illumination will be taken into account and examined.

Textures could be divided into two groups: for the sake of their origin – one can distinguish natural textures (Fig. 2a, 2b) or human manufactured textures (Fig 2c, 2d), for the sake of the distribution of the pattern – one can distinguish textures: regular, random and oriented. Examples were presented in Fig 3. [41]

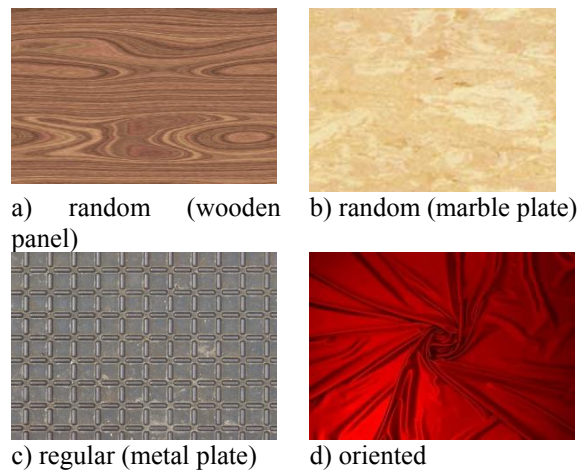


Fig. 3. Examples of three types of manufactured textures [41]

As it was mentioned above the presence of the texture in the analyzed image sometimes could be helpful, but more often is a source of analysis faults and misunderstandings of the image. Problems concerned with the texture analysis were divided into four groups and processing of textured images was related to four main aspects concerned with texture analysis and recognition [22],[27]. The first consists in texture classification – that means identification of a surface type through analyzing its texture. The second is texture segmentation – the division of the image into regions of different textures. The third problem is to find out whether the textured surface contains defects which is defined as texture defect identification. The paper deals with this aspect of texture analysis. The fourth problem concerned with the texture is defined as “shape from texture” and is understood as the estimation of the shape (in 3D) of the observed object on the basis of changes of 2D texture in the analyzed image. Another very important problem related to texture processing and analysis is that the texture is scale

and resolution sensitive. The same object observed from different distances looks differently. Similar situation is when the textured surface is observed with high and low resolution cameras. When working with the texture analysis, these factors have to be taken into account [27], [34].

4. TEXTURE ANALYSIS METHODS

The texture analysis methods can be divided into four groups. There is a lot of examples of applications of the various methods from every group in the literature. Below only some groups and selected methods have been enumerated. These groups are [10], [22],[39]:

- statistical,
 - histogram analysis [7],[24],
 - Gray Level Co-occurrence Matrix (GLCM) [15], [32],
 - Singular Value Decomposition (SVD) [20], [36]
 - Principal Component Analysis (PCA) [5], [35],
 - Local Binary Pattern (LBP) [21],[25],
- structural,
 - morphological methods [2] [9],
 - primitive measurement [15], [33]
- model based,
 - random fields models [10],
 - fractal models [29],
- filter based,
 - spatial domain filtering,
 - frequency analysis [31],[37],
 - joint spatial/frequency analysis [6],[16].

In the presented research, two selected methods from the first group have been applied, and some exemplary results have been presented in the further part of the paper. Therefore these two methods GLCM and SVD have been shortly explained below.

4.1. Gray Level Co-occurrence Matrix (GLCM)

Gray Level Co-occurrence Matrix method is called the second order histogram and is one of the most well-known and widely used methods in texture analysis. The GLCM is a new matrix created from the matrix of a digital image where gray levels were reduced to n . The GLCM is $n \times n$ matrix that contains the information concerning pairwise relations between pixel intensities for a particular distance d , and orientation q . These two parameters determine the position of the second investigated pixel in relation to a reference pixel. Distance d is counted in pixels, and orientation, described in degrees that equals usually to the range from 0° to 135° , determines direction in that the investigated pixel is placed. In [13] one can find precise information how to create GLCM. For every created GLCM the estimation of statistical features is possible. In [14] Haralick proposed the estimation of 14 features for GLCM created with the use of $d=1$

but in each direction what was time-consuming. On the basis of the research made afterwards it was established that five of the features were relevant (eq.1), so that features that were usually estimated were constrained:

$$\begin{aligned} \text{Energy} &= \sum_i \sum_j N_d^2(i, j), \\ \text{Entropy} &= - \sum_i \sum_j N_d(i, j) \log_2 N_d(i, j), \\ \text{Contrast} &= \sum_i \sum_j (i - j)^2 N_d(i, j), \\ \text{Homogeneity} &= \sum_i \sum_j \frac{N_d(i, j)}{1 + |i - j|}, \\ \text{Correlation} &= \frac{\sum_i \sum_j (i - \mu_i)(j - \mu_j) N_d(i, j)}{\sigma_i \sigma_j}, \end{aligned} \quad (1)$$

where μ_i, μ_j were means and σ_i, σ_j were standard deviations of the row and column sums $N_d(i)$ and $N_d(j)$ defined by:

$$\begin{aligned} N_d(i) &= \sum_j N_d(i, j) \\ N_d(j) &= \sum_i N_d(i, j) \end{aligned} \quad (2)$$

Enumerated features of GLCM (1) were estimated and used in further investigations.

4.2. Singular Value Decomposition (SVD)

The Singular Value Decomposition method is a statistical well known method of matrix decomposition into several component matrices that contain useful information and properties of the original matrix. Image analysis SVD is usually applied to compression and reconstruction of images, image restoration, and texture analysis [20], [36]. This method is based on statements from linear algebra:

For every complex matrix \mathbf{A} of dimensions $m \times n$, there are such unitary complex matrices \mathbf{U} and \mathbf{V} , that

$$\mathbf{U}^* \mathbf{A} \mathbf{V} = \mathbf{\Sigma} = \text{diag}(\sigma_1, \dots, \sigma_l), \text{ where } \begin{aligned} l &= \min(m, n), \text{ and when} \\ r &= \text{rank}(\mathbf{A}) \end{aligned} \quad (3)$$

$$\sigma_1 \geq \sigma_2 \geq \dots \geq \sigma_r > 0, \quad \sigma_{r+1} = \dots = \sigma_l = 0$$

Numbers $\sigma_1, \dots, \sigma_r$ are unequivocally determined in \mathbf{A} and they are called singular values of matrix \mathbf{A} . So the matrix $\mathbf{\Sigma}$ is:

$$\mathbf{\Sigma} = \begin{bmatrix} \mathbf{S} & \mathbf{0} \\ \mathbf{0} & \mathbf{0} \end{bmatrix} \in \mathbb{R}^{m,n}, \quad \mathbf{S} = \text{diag}(\sigma_1, \dots, \sigma_r) \quad (4)$$

When solving equation (1) with regard to \mathbf{A} , one gets an equation (3)

$$\mathbf{A} = \mathbf{U} \mathbf{\Sigma} \mathbf{V}^* \quad (5)$$

In order to detect anomalies on the textured surface with the use of SVD, the original image had to be divided into k subregions of the $n \times n$ dimension

each. For every subregion SVD was calculated and than the matrix Σ was taken into account. The first singular value of S is σ_1 and was treated as a new value of the whole subregion. The values in subregions differ when the anomaly appears. As a result of such approach a new map representing the original image is obtained. In the map the regions where in the original image anomalies appear differ from the regions without anomalies.

In this method, the essential problem is to find an appropriate value of n . This value determines the dimension of subregions ($n \times n$) and is important for detection of the anomaly. If the size of the region is too big, anomalies could be omitted or not detected, or, in case when n is too small, there is too many subregions, so the calculations might be very time consuming.

These two methods GLCM and SVD were used at two different stages of the algorithm elaborated on the basis of a concept presented in the next paragraph. They were used in order to detect texture presence and to localize an anomaly in the analyzed images.

5. BACKGROUND OF THE CONCEPT

The idea of undertaken research was to elaborate and test algorithm that allow anomaly detection, localization and defect identification on the various surfaces of technical objects with the use of image analysis and recognition techniques. The most important assumption of the concept was the fact that defects should be found on the textured surfaces. The purpose was to choose the methods of analysis and recognition which make possible to detect anomalies without the necessity of defect database and texture database creation. This assumption was made on the basis of a fact that it is hard to specify the localization, type, size and number of defects that appear on different textured surfaces during different production processes and these factors could make impossible to build an appropriate database. In the paper an "anomaly" is understood as an area in the image that is supposed to be a "defect" of the real surface. Therefore a very important aspect of the presented approach was to detect the area of the image being analyzed that differs from the rest of the image. Such region that differs from the neighbourhood was taken into account in further, more detailed analysis. The anomaly, after its analysis, at the following stages of the algorithm could be identified as the defect. The concept of the way of achieving this aim was presented in the next paragraph. Moreover, in the presented concept, identification of presence of one of three types of texture was scheduled.

5.1. Concept of defect detection, localization and identification

The algorithm was divided into three main parts. They were presented in Fig. 4. More detailed

scheme of the algorithm was presented in Fig. 5. Three main blocks were named from their functionalities. The first block represents texture type determination, where the GLCM method was used. The second part stands for the main part of the whole algorithm that is anomaly detection, localization and analysis. At the stage of localization of an anomaly the SVD method was used, and on the basis of its results a region of interest (ROI) with the anomaly was distinguished. Further analysis was made only for distinguished ROI region.

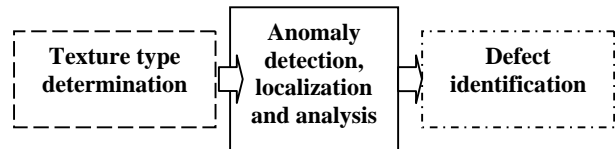


Fig. 4. General schema of the concept

The third block stands for defect identification which means the estimation whether the anomaly found in the image should be treated as a defect. In the next paragraph two first parts of the algorithm have been described more precisely and some results have been presented. The third part of the algorithm has not been described in details and results obtained by means of this part of the algorithm have not been presented. There are currently being elaborated.

5.2. Operation of the algorithm and the first results

The scheme of the concept of the algorithm was presented in (Fig. 5). In the image every general block was divided into more detailed parts where three main steps were visible.

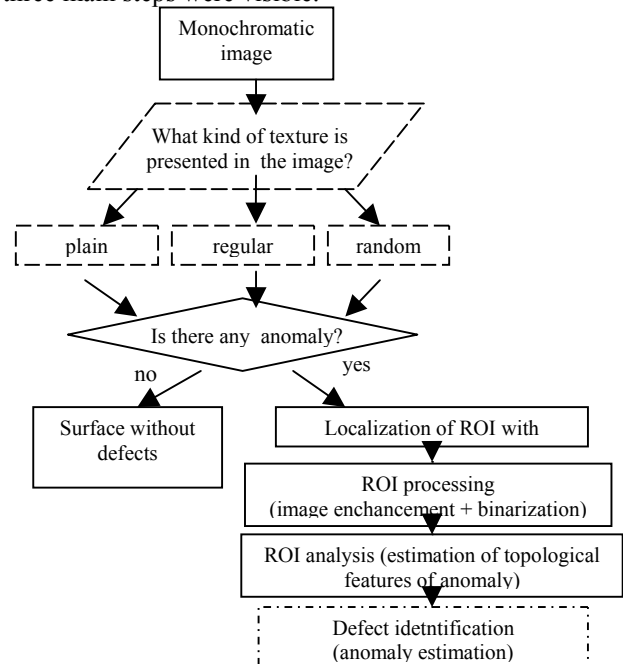


Fig.5. Scheme of the elaborated concept

The first stage of the algorithm consists in texture type determination. It is possible to distinguish regular and random textures from plain surfaces at this stage of the algorithm. Texture type identification procedures operate on the basis of GLCM method that investigates the distribution of intensity level of pixels in the image. According to the method, new gray levels co-occurrence matrices were created and five statistical features (equations 1) were estimated. Afterwards, the chosen statistic feature values were plotted. On the basis of the plots it was possible to identify if the texture in the image was plain, random or regular. When changes of the statistical values were random – the texture was treated as random as well. If changes of the chart were minimal, or did not appear, one can state that the texture is plain. If the changes of the plot were regular (periodical), one could state that the surface represented in the image was also regular. This estimation was based on the visual survey of the plots. It is planned in further research to elaborate other methods that can help to find automatically regularities in these textures.

The example presented below concerns the application of GLCM to three kinds of textures. In Fig. 6. there are plots of *contrast* estimated for the gray level co-occurrence matrices created for the original matrix investigated in two directions: horizontal, q is equal to 0° (column 3) and vertical q is equal to 90° (column 4), for the distance d equal to 1 (pixel). All the examples were obtained for the images transformed to monochromatic and scaled to 128 gray levels. It is clearly visible that for images representing surfaces with regular texture, plots of the statistical feature (contrast) in these two directions, are regular (1st and 2nd row in Fig. 6). What is interesting in the case of the first texture (1st row) it is possible to observe a trend in the plots which represents the orientation of the texture in the image.

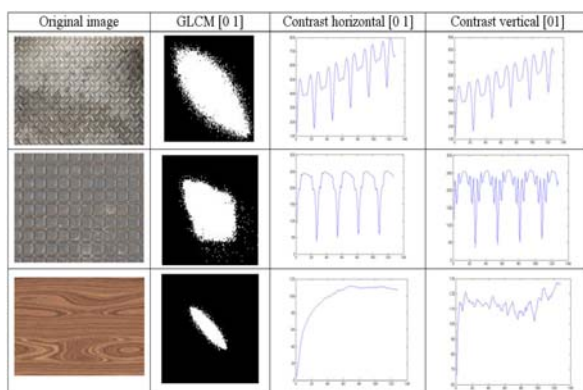


Fig. 6. Texture type determination

The second stage of the algorithm consists in localization of the region of interest with a defective part of the textured image. At this stage, size and spatial localization of the ROI in the image is estimated and saved. The searching for the anomalies is based on the SVD method. As a result

of the application of this method the ROI with the anomaly found is marked, and distinguished. An example of the operation of SVD method in order to localize and distinguish the ROI with an anomaly was presented in Fig.7. In further processing only the ROI with anomaly was taken into account.

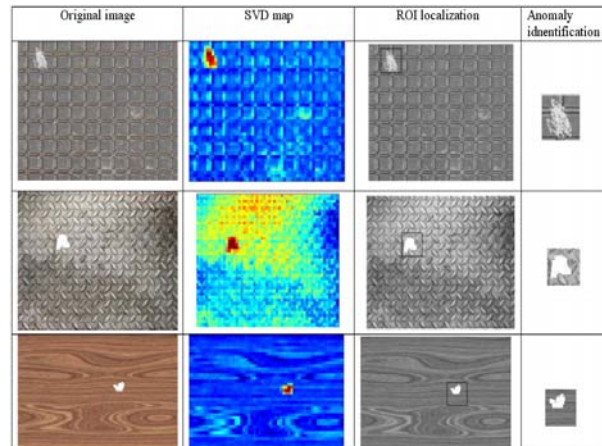


Fig. 7. Localization of an anomaly

The following stage of the algorithm consisted in ROI enhancement and binarization. At this stage of the algorithm, the ROI was binarized – with one threshold set experimentally on the basis of results from the experiments. The threshold was established in advance. As a result, binary image with extracted and well visible anomaly was obtained. Such the image was an input for the next step in the algorithm - ROI analysis. At this stage for the distinguished anomaly (the object in the image), some topological (geometrical) features were estimated. As the result a vector of the values of chosen features was created.

Features which values were estimated were e.g.: area, perimeter, diameter, Feret diameter, moments of inertia of the object and other factors connected with the shape and localization of the object. These features are estimated with the use of LV functions. It is possible to distinguish up to 81 different features. Some of them are correlated, therefore only representative features have to be chosen [8]. Investigations concerning usefulness of the representative features for different anomalies are being currently conducted. Thanks to topological analysis, it is possible to estimate the size and shape of the anomaly.

6. CONCLUSIONS

On the basis of the initial research on the described concept of defect detection and identification, one can state that it is possible to use image analysis methods to distinguish regions with the anomalies even on the textured surfaces. With use of statistical methods of matrix analysis the anomalies could be detected and localized without the necessity of the database containing images of textures and textures with anomalies.

The first step of the algorithm can be treated as a possibility because taking into account the main purpose of the algorithm – anomaly detection and texture type determination seem to be not necessary. Simultaneously, it is thought that it can be helpful for choosing a texture method analysis, since some methods are dedicated for a particular type of textures.

In the paper the last step of the algorithm that consists in defect identification has been only mentioned, since it is currently being elaborated. Such identification could be made with use of classification or clustering procedures on the basis of a vector of relevant features. The method of anomalies identification will be chosen dependently on the available information of expected defects.

On the basis of literature review, one can state that the method that requires only a minimal training stage using a few normal samples, named “novelty detection” [23], [30] can be also attractive in defect identification problem. This approach is a subject of the further research of the author.

BIBLIOGRAPHY

- [1] Abeyratne, U., Petropulu, A., and Conant, E. (1997). *Higher order versus second order statistics in ultrasound imagedeconvolution*. IEEE Transactions on Ultrasonics, Ferroelectrics and Frequency Control, 44(6):1409–1416.
- [2] Aparicio Fernandes, J., Campos Neves, J., and Couto, C. (1999). *Defect detection and localization in textiles using co-occurrence matrices and morphological operators*. Proceedings of M2VIP'99, Turkey.
- [3] Błaszczuk, M. and Drzewiecki, W. (2006). *Wstępna ocena możliwości wykorzystania obrazów satelitarnych aster w monitorowaniu lodowców svalbard glaciern*. Archiwum Fotogrametrii, Kartografii i Teledetekcji, 16:29–39.
- [4] Batchelor, B. and Whelan, P. (2002). *Intelligent Vision Systems for Industry*. Bruce G. Batchelor, Paul F. Whelan 2002. eBook.
- [5] Bharati, M. and MacGregor, J. *Texture analysis of images using principal component analysis*, <http://citeseerx.ist.psu.edu/viewdoc/download?doi=10.1.1.128.2779&rep=rep1&type=pdf>
- [6] Bodnarova, A., Bennamoun, M., and Latham, S. (2002). *Optimal gabor filters for textile flaw detection*. Pattern Recognition, 35(12):2973–2991.
- [7] Broadhurst, R. (2005). *Statistical estimation of histogram variation for texture classification*.
- [8] Bzymek, A. and Timofiejczuk, A. (2009). *Estimation of welding process stability based on image analysis and recognition*. Diagnostyka, 4(52)/2009.
- [9] Chetverikov, D. and Hanbury, A. (2002). *Finding defects in texture using regularity and local orientation*. Pattern Recognition, 35(10):2165 – 2180.
- [10] Davies, E. R. (2005). *Machine Vision: Theory and Practicalities*. Morgan Kaufmann, San Francisco, 3rd edition. Imprint of Elsevier.
- [11] Drimbarean, A. and Whelan, P. (2000). *Colour texture analysis: A comparative study*. Pattern Recognition Letters, 22:1161–1167.
- [12] Gadelmawla, E. S. (2004). *A vision system for surface roughness characterization using the gray level co-occurrence matrix*. NDT e International, 37(7):577–588.
- [13] Hall-Beyer, M. (2007). *Glm texture: Tutorial*. <http://www.fp.ucalgary.ca/mhallbey/transposimg.htm>.
- [14] Haralick, R.M., a. S. K. (1973). *Textural features for image classification*. IEEE transactions on systems, man, and cybernetics, (NO.6).
- [15] Haralick, R. M. (1979). *Statistical and structural approaches to texture*. IEEE, 67(5).
- [16] Jain, A. K. and Farrokhnia, F. (1990). *Unsupervised texture segmentation using gabor filters*. IEEE.
- [17] Julesz, B. (1962). *Visual pattern discrimination*. IRE Transaction on Information Theory, pages 84–92.
- [18] Julesz, B. (1986). *Texton gradients: The texton theory revisited*. Journal Biological Cybernetics, 54(4-5):245–251.
- [19] Landy, M. and Graham, N. (2004). *Visual perception of texture*. In The Visual Neurosciences, pages 1106–1118. MIT Press.
- [20] Lu, C.-J. and Tsai, D.-M. (2005). *Automatic defect inspection for lcds using singular value decomposition*. In The International Journal of Advanced Manufacturing Technology, volume 25, pages 53–61. Springer London.
- [21] Maenpaa, T., Turtinen, M., and M, P. (2003). *Realtime surface inspection by texture*. Real-Time Imaging, Vol.9(5):pp. 289–296(8).
- [22] Materka, A. and Strzelecki, M. (1998). *Texture analysis methods – a review*, Technical report, Technical Institute of Electronics, University of Lodz, Brussels. COST B11.
- [23] Monadjemi, A. (2004). *Towards efficient texture classification and abnormality detection*. PhD thesis, University of Bristol.
- [24] Ng, H.-F. (2006). *Automatic thresholding for defect detection*. Pattern Recogn. Lett., 27(14):1644–1649.
- [25] Ojala, T., Pietikainen, M., and Maenpaa, T. (2002). *Multiresolution gray-scale and rotation invariant texture classification with local binary pattern*. IEEE Transactions on Pattern Analysis and Machine Intelligence, 24(7):971–987.
- [26] Palm, C. (2004). *Color texture classification by integrative cooccurrence matrices*. Pattern Recognition, 37:965–976.
- [27] Petrou, M. and Sevilla, P. (2006). *Image Processing: Dealing with Texture*. Wiley.

- [28] Pratt, W. (2001). *Digital Image Processing*. Wiley and Sons Inc.
- [29] Rangayyan, R. (2005). *Biomedical Image Analysis*. The Biomedical Engineering. CRC Press, USA. edited by M. R. Neumann.
- [30] Singh, S. and Markou, M. (2004). An approach to novelty detection applied to the classification of image regions. *Knowledge and Data Engineering, IEEE Transactions on*, 16(4):396–407.
- [31] Song, K., Petrou, M., and Kittler, J. (1995). *Texture crack detection*. 8(1):63–75.
- [32]. Strzelecki, M. and Materka, A. (1999). *Ilościowa analiza tekstur obrazów tomograficznych rezonansu magnetycznego*. *Zeszyty Naukowe Elektronika*, vol. 4:115–124. European Project Cost B11:Quantitation Of Magnetic Resonance Image Texture.
- [33] Sznaiier, M. and Camps, O. (2005). *A Hankel operator approach to texture modelling*. In Proceedings of the 4th International Workshop on Texture Analysis and Synthesis, pages 125–130.
<http://robustsystems.ee.psu.edu/papers/Hankeltecture05.pdf>.
- [34] Tessier, C. (2004). *Detection de type de sol par analyse de texture pour le guidage de vehicules*. Report sur R2M Projet Cemagref.
- [35] Tomczak, ., Mosorov, V., Sankowski, D., and Nowakowski, J. (2007). *Image defect detection methods for visual inspection system*. In Proceedings, Polyanna, Ukraine. CADSM.
- [36] Tomczak, ., Mozorov, V., and Kaczorowski, D. (2006). *Nowa metoda detekcji defektów tekstury w automatycznej inspekcji wizyjnej*. *Automatyka*, 9(3).
- [37] Tsai, D.-M. and Hsieh, C. Y. (1999). *Automated surface inspection for directional textures*. *Image and Vision Computing*, 18(1):49 – 62.
- [38] Tymków, P. and Borkowski, A. (2006). *Wykorzystanie danych lotniczego skaningu laserowego do klasyfikacji pokrycia terenu dla modelowania hydrodynamicznego*. *Archiwum Fotogrametrii, Kartografii i Teledetekcji*, 16:537–546.
- [39] Xie, X. (2008). *A review of recent advances in surface defect detection using texture analysis techniques*. *Electronic Letters on Computer Vision and Image Analysis*, 7(3):1–22.
- [40] Zawada-Tomkiewicz, A. (2007). *Analiza obrazu powierzchni obrabianej do celów estymacji parametrów tej powierzchni*. *Acta Mechanica et Automatica*, 1(2):79–84.
- [41] <http://www.cgtextures.com>
- [42] <http://www.firstsightvision.com>



Anna BZYMEK is PhD. student in the Department of Fundamentals of Machinery Design. Main area of her research are: vision systems in diagnostics, machine vision, image processing, analysis and recognition, signal processing.

VIBROTHERMOGRAPHY - MEASUREMENT SYSTEM DEVELOPMENT AND TESTING

Łukasz PIECZONKA, Mariusz SZWEDO, Tadeusz UHL

Akademia Górniczo-Hutnicza w Krakowie, Katedra Robotyki i Mechatroniki
Al. Mickiewicza 30, +48 12 634 35 05, lpiecz@agh.edu.pl

Summary

The paper investigates practical aspects of vibrothermographic testing. Vibrothermography is a nondestructive testing method that monitors heat produced by damage under vibration and/or ultrasonic excitation in order to evaluate the structural health. Detailed description of a prototype measurement system, that has been developed, is given together with the description of preliminary tests on a composite specimen. The parameters that influence the efficiency of damage detection in vibrothermography have been investigated in more detail. Presentation and discussion of the results is given in the paper.

Keywords: SHM, NDT, vibrothermography, damage detection.

WIBROTHERMOGRAFIA - ROZWÓJ I TESTOWANIE SYSTEMU POMIAROWEGO

Streszczenie

Artykuł omawia praktyczne aspekty pomiarów metodą wibrotermografii. Rozważana metoda pomiarowa bazuje na pomiarze temperatury generowanej w miejscach występowania uszkodzeń w strukturze pod wpływem wymuszenia drganiowego i/lub ultradźwiękowego. Artykuł zawiera szczegółowy opis prototypowego stanowiska badawczego oraz wstępnych testów przeprowadzonych na płycie kompozytowej. Ponadto przeprowadzono analizę wpływu niektórych parametrów pomiarowych na wydajność wykrywania uszkodzeń omawianą metodą. Wyniki badań oraz ich analiza przedstawione są w niniejszym artykule.

Słowa kluczowe: SHM, NDT, wibrotermografia, detekcja uszkodzeń.

1. INTRODUCTION

Structural Health Monitoring plays an increasing role in contemporary engineering [1-3]. This fact can be attributed to several factors. Firstly, the critical failures resulting in loss of life that are discussed by the mass media motivate the regulatory agencies to demand some form of structural health monitoring of the infrastructure. Secondly, the aging infrastructure that, especially in European conditions, operates beyond its designed life period needs to be monitored in order to avoid fatal damages and to reduce maintenance costs. Other important factors include the increased availability of affordable measurement equipment and damage detection techniques that provide the means for implementation of SHM procedures in industrial applications. In recent years a number of different damage detection methods have been developed [1-3]. The success of these methods often depends on three major factors, namely: (1) on the simplicity of interpretation of the result that they provide, (2) on the necessity to use the baseline reference data (measured in undamaged state), (3) on the cost and complexity of their implementation. A group of methods particularly advantageous in all three aspects is infrared thermography [4-5]. This family of NDT techniques is based on temperature

measurements to reveal structural damage. Infrared thermography can be divided into two categories: passive methods and active methods. Of special interest in the group of active methods, due to its efficiency, is vibrothermography that is considered in this paper.

2. THEORETICAL BACKGROUND OF THE METHOD

Vibrothermography, also known as thermosonics, sonic IR or ultrasonic thermography is a special deployment of active thermography that uses mechanical vibration excitation [4-6]. Excitation signal can be applied in various forms. The most popular being the ultrasound burst thermography, lock-in thermography and continuous thermography [5-6]. In ultrasound burst thermography, as shown in Fig. 1, a burst ultrasonic signal is applied on the transducer to induce stress waves in a test structure. Periodic stress waves propagating in a structure cause frictional sliding at discontinuities (e.g. delaminations, fatigue cracks) and therefore the conversion of mechanical energy into thermal energy generating heat. Thus, the heat source in vibrothermography, unlike in other thermographic techniques, is the discontinuity itself, which makes the identification of defects simpler.

Heat generated at discontinuities propagates to the surface where temperature change is measured by a sensitive infrared camera. Typical infrared cameras that are used for this type of tests measure electromagnetic radiation in the Medium Wavelength Infrared (MWIR) spectrum, i.e. from 2.5 to 5 μm . Diagnostic information is evaluated from the acquired data by means of customized image processing algorithms. Theoretical considerations regarding the nature of energy dissipation mechanisms and heat propagation are outside of the scope of this paper and an interested reader can find more information in [4-7].

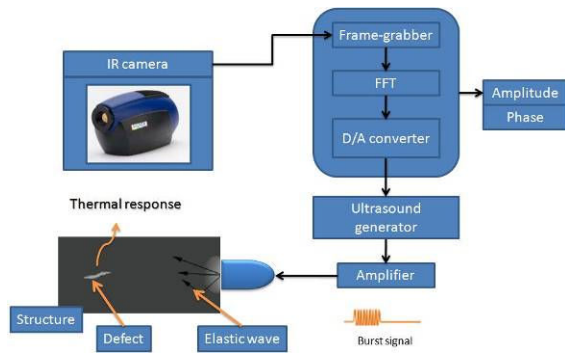


Fig. 1. Ultrasound burst thermography

The excitation is typically applied using an ultrasonic device as depicted in Fig. 2. that comprises three elements: (1) converter - a bolt clamped Langevin type transducer that allows for a high power and narrowband frequency operation; (2) booster - a metal piece (typically aluminum or titanium alloy) that is used to clamp the entire ultrasonic assembly and to amplify vibration amplitude; (3) sonotrode - an element that comes into contact with inspected structure and further amplifies vibration amplitude. When designing such ultrasonic device it is important to remember that specific natural frequencies of these elements have to be perfectly matched for proper operation.

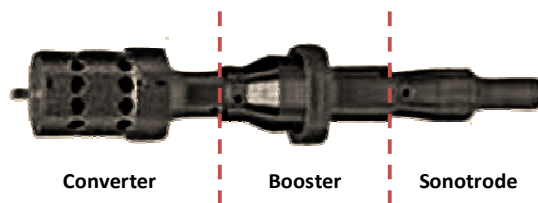


Fig. 2. Ultrasonic assembly

Vibrothermography is a wide area noncontact measurement technique. The component to be tested does not have to be dismantled from the structure and accessibility from only one side is sufficient. Additional advantages of the method include short measurement time, easy interpretation of the detection results. Under ultrasonic excitation damaged areas become heat sources which improves the contrast of obtained thermal images. The drawbacks of the method include the inability to

detect voids in the material which do not dissipate ultrasonic energy and a potential risk of damaging sample's surface (e.g. paint or varnish coating) under the sonotrode if the power of ultrasonic converter is set too high for a particular test sample.

3. DESCRIPTION OF THE MEASUREMENT SYSTEM

A prototype system for vibrothermographic testing has been developed at AGH-UST within the scope of the research project acronym MONIT [8].

The system consists of four main components:

- High sensitivity infrared camera;
- Ultrasonic signal generator and amplifier;
- Ultrasonic excitation assembly;
- Mobile computer for image acquisition and control of infrared camera and signal generator.

The system has been developed in two variants as shown in Fig. 3. Both variants share the four abovementioned basic components but differ in the design of the bearing structure. The first variant, depicted Fig. 3a, is a stationary system designed for laboratory use. The bearing structure is composed of a light aluminum frame, pneumatic press system and fixture for the ultrasonic excitation assembly. The second variant, depicted in Fig. 3b, is a mobile system for field measurements. The bearing structure in this case has been reduced to a fixture for the ultrasonic excitation assembly with an ergonomic hand grip for easy operation.

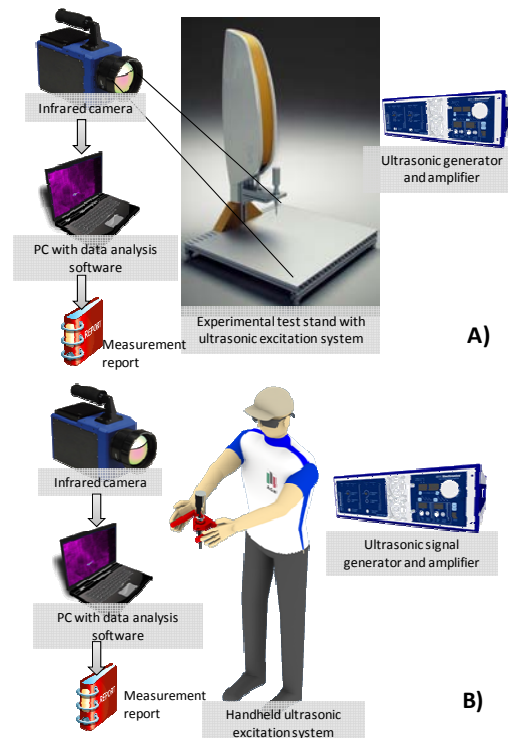


Fig. 3. Developed measurement system. Stationary version (A) and mobile version (B)

The main parameters of the constituent components of the measurement system are briefly

summarized below. The parameters have been initially specified after an extensive literature study and preliminary numerical and experimental investigations.

Infrared camera that has been chosen for the system is a cooled detector MWIR camera. The main parameters of this camera are summarized in Table 1.

Table 1. Characteristic parameters of the infrared camera

Sensor type	InSb
Sensor resolution	320x256
Spectral range	2.5 - 5 μ m
Frame rate	Up to 380Hz
NETD	<25mK
Interface	USB / CameraLink

Ultrasonic signal generator and amplifier has been designed in close cooperation with a local electronic systems manufacturer, to meet the specific needs of vibrothermographic measurements. High voltage and high power output were required for proper operation of the ultrasonic excitation system. Signal generator had to be equipped with a frequency tuning circuit to match the working resonant frequency of the transducer assembly. Moreover appropriate trigger outputs had to be designed to allow for seamless operation with the infrared camera. Trigger outputs were also necessary for lock-in measurement configurations. All parameters of the signal generator and amplifier are controllable from the software layer. The main parameters of the prototype design are summarized in Table 2.

Table 2. Parameters of the designed ultrasonic generator and amplifier

Frequency range	20 - 50 [kHz]
Output power	1.5 [kW]
Trigger output	TTL
Control interface	USB (Matlab, C/C++ library, dedicated application)
Output signal options	Continuous, Burst, Modulated

Considered design of the **ultrasonic excitation assembly** allows for high power narrowband frequency operation. Because of changing wavelengths of the elastic waves and changing maximum output power possible at different frequencies it has been decided that two ultrasonic assemblies should be used. Assemblies with central working frequencies of 20kHz and 35kHz have been prepared. Both assemblies can be used in stationary and mobile versions of the measurement system and are powered by the designed signal generator and amplifier. The choice of the assembly to be used depends on the characteristics of the test structure, mainly on its material, overall dimensions and mass.

Software framework for processing the acquired infrared images has been also prepared. Developed software procedures allow to acquire, enhance and post process infrared image sequences in order to obtain valuable diagnostic information. Additionally, software tools that allow setting up measurement parameters have been prepared. It is possible to control the parameters of the signal generator and amplifier as well as the parameters of the infrared camera.

The main software modules that have been implemented include the following:

- Thermographic image acquisition from infrared camera;
- Pre- and post- processing of thermal images (filtering, image transformations, advanced spectral processing);
- Image analysis (point, line and area statistical operations);
- Signal generator control;
- Reports generations (thermal images, processing and analyzing results, comments, system configurations and parameters could be reported).

Stationary configuration of the test system allows to control the contact pressure between the sonotrode and a test piece. It is also possible to measure the dynamic force during operation of the ultrasonic assembly. This unique feature allows to collect measurement data that can be subsequently used to perform a virtual test and validate a numerical model.

4. EXPERIMENTAL TESTING

Experimental testing of the developed prototype has been performed in order to find optimal ranges of operational parameters. Multiple tests have been performed on different test specimens using both stationary and mobile versions of the developed system. Hardware platform and software procedures had to be verified on laboratory test specimens with known damage parameters, before the procedures could be applied for damage detection in real working conditions.

The following main parameters of the system have been tested:

- Dependence of the temperature gain on damaged area on the power of ultrasonic converter;
- Dependence of the temperature gain on damaged area due to changes in contact pressure between the sonotrode and the specimen;
- Dependence of the temperature gain on damaged area on the type of coupling material.

Design of Experiments (DOE) has been performed in order to find the most suitable configurations of measurement parameters. Box-Behnken design has been prepared for three parameters of the measurement system, namely: the power of ultrasonic converter, contact pressure between the sonotrode and the test specimen,

excitation time. Box-Behnken design has been chosen for this preliminary study because it provides good exploration of the parameter space and at the same time is very economical in terms of the number of sampling points [9].

Composite plate made of carbon epoxy prepreg 950-GF3-5H-1000 has been used as a test case (see Fig. 4). The plate has been damaged in a with low velocity impact event. The result was a matrix and fiber cracking in the vicinity of the impact location.

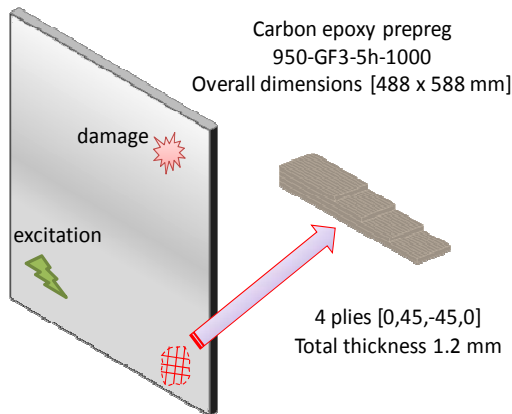


Fig. 4. Analyzed test specimen

Field of view of the infrared camera was set to the upper left corner of the plate where the defect was located. The plate was excited in a lower left corner i.e. on the diagonal from damage. Excitation location was outside of the field of view.

Sample thermal image of the damaged area of the plate, acquired during vibrothermographic test is shown in Fig. 5. Star shaped marker indicates the location for which the subsequent comparisons have been performed. Image processing and analysis techniques as implemented in the developed software framework have been used for subsequent analyses. Implemented thermal images processing can be used to estimate sizes and localizations defects in tested component. Advanced processing of image data could be used for further diagnostics and monitoring algorithms and application [7].

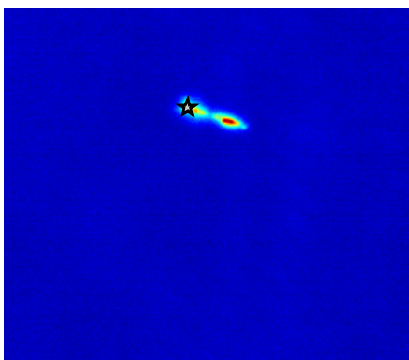


Fig. 5. Thermal image of damaged area

According to the prepared DOE plan, experimentation has been performed on the test specimen. Performance metric that has been

considered was a maximum gain in temperature for a chosen point on damaged area (marked with a star in Fig. 5). The quality of vibrothermographic test is dependent on the amount of heat generated at structural defects. The more vibration energy is dissipated on defects the better is the contrast of the thermal image. Thus evaluation of damage parameters is easier.

All experiments in the DOE plan have been performed according to the same measurement plan composed of four main steps:

1. Stabilization of the temperature of the test piece to a reference ambient temperature (21°C);
2. Synchronized start of the ultrasonic excitation and data acquisition with IR camera;
3. Acquisition of thermal images for 10 seconds;
4. Post-processing of the acquired image sequence.

Influence analysis has been performed on the results obtained from experimentation in order to identify the most important factors responsible for thermal response. First order effects have been computed for the three process parameters. Results are shown in Fig. 6. It can be seen that the most important factor is the contact pressure between the sonotrode and the test piece. This parameter is representative for the transfer of ultrasonic energy generated by the converter to the test specimen. Measurement time and power of the ultrasonic converter also influence the amount of energy dissipated by damage. The longer is the measurement time the more energy is transferred into the test specimen and thus better thermal response. Clearly enough the power generated by the ultrasonic converter also influences thermal response. The most important observation that has been made is the fact that the coupling between the ultrasonic assembly and the test piece is the most influential measurement parameter.

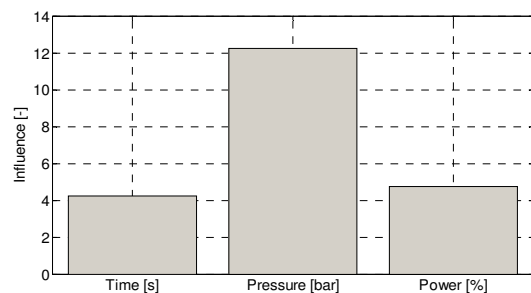


Fig. 6. Influence analysis of measurement parameters

According to literature survey, coupling between the ultrasonic assembly and the test specimen is indeed one of the most important measurement parameters [10]. Certain configurations of coupling pads and coupling pressure can produce an effect described as 'acoustic chaos' [11]. This effect allows to obtain broadband excitation of the structure with use of narrowband ultrasonic converter typically used in vibrothermographic measurements.

Additional experimental tests have been performed to analyze the influence of the pressure between the sonotrode and the plate. As previously stationary version of the system has been used to perform measurements. Different pressure applied to the pneumatic press system produced different contact force between the sonotrode tip and a surface of a test piece. Force in the range from 0.01 to 2.76 kN has been considered in fourteen increments. It is important not to apply force that could destroy the surface of the test specimen. Applied thrust force should not exceed the blocking force of the piezoceramic stack inside the ultrasonic converter. This is important especially for low power operation.

Differences in thermal responses obtained for measured configurations can be seen in Fig. 7. Temperature evolution on damaged area (marked with a star in Fig. 5) shows significant differences between measured configurations.

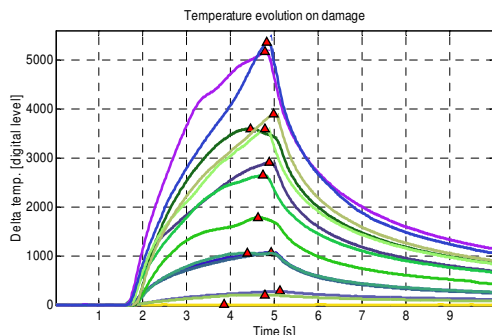


Fig. 7. Temperature evolution on damage for different interface forces

Fig. 8 presents maximal temperature gain measured in considered point. It can be seen that the pressure between the sonotrode and the test specimen is directly proportional to the measured thermal response.

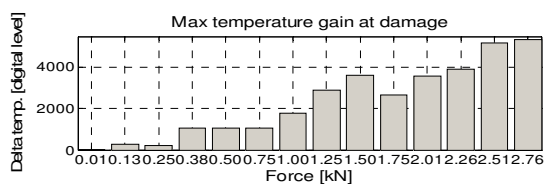


Fig. 8. Maximum temperature gain on damage for different interface forces

Additional tests have been performed to check the influence of the power applied to the ultrasonic converter on the measured thermal response. The initial assumption was that the energy delivered to the ultrasonic converter is directly proportional to the vibration energy delivered to the test specimen and hence to the energy dissipated at structural defect. Power ranging from 20% to 80% of the maximum power that the ultrasonic converter could provide have been tested. Maximum available power output has not been used as it could damage the

surface the composite plate. As expected, it is clearly visible in Fig. 9 that with an increasing power of the ultrasonic transducer thermal response is also increasing.

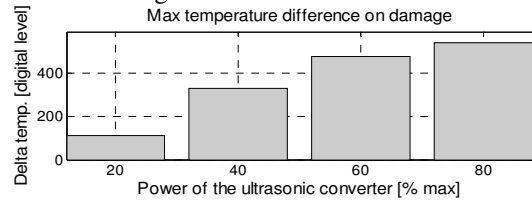


Fig. 9. Maximum temperature gain on damage for different power levels of ultrasonic converter

As the last step in the analysis of the prototype measurement system different coupling pads have been tested. Coupling pad is applied between the sonotrode and the surface of tested object in order to improve impedance match between the two and to protect the surface of the test specimen. Based on a literature study four materials typically used for as coupling have been tested, namely: rubber, felt, woven fabric and paper. The same measurement parameters have been used in each case. Differences in the obtained thermal responses are depicted in Fig. 10. It can be seen that the type of coupling influences measured thermal response. More detailed study has to be, however, performed in order to verify the influence of coupling material in connection with the applied contact pressure and ultrasonic power.

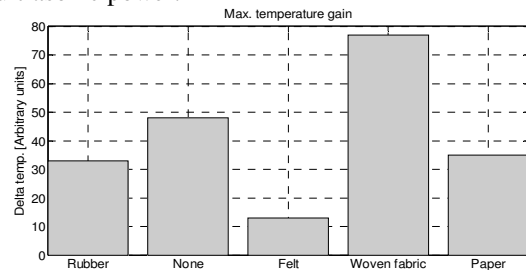


Fig. 10. Differences in thermal response for different coupling materials

5. CONCLUSIONS

Designed prototype measurement system for vibrothermographic testing has been verified to be fully functional. Preliminary testing has been performed on a composite specimen in order to analyze measurement parameters that have the largest influence on measurement results. Contact pressure between the sonotrode and the test specimen has been identified as one of the most important measurement parameters apart from the power of ultrasonic converter, measurement time and coupling material that is used. Further experimentation is necessary to identify the effects of different coupling materials in more detail and ultimately to identify optimal measurement parameters for given structures.

Vibrothermography has a great potential of application in many industrial and research applications, which has been verified experimentally by the authors. The configuration of measurement system is flexible and can be fairly easily adapted to a specific application. Main fields of application of the method, as identified from performed experiments and from literature survey, is the detection of:

- cracks in metallic and composite materials;
- delaminations in composite materials;
- defects in welded joints,
- loose rivets and bolted connections.

The main practical advantages of vibrothermography are:

- nondestructive and noncontact testing procedure;
- short measurement time (typically only few seconds are enough to obtain satisfactory results);
- detection, localization and size of the defect can be evaluated from thermal image processing;
- ease of interpretation of the results.

6. ACKNOWLEDGMENTS

The work on vibrothermography was financed from the research project MONIT - „Monitoring of Technical State of Construction and Evaluation of its Lifespan” (no. POIG.01.01.02-00-013/08-00) made in the scope of the European Union Operational Programme - Innovative Economy 2007-2013

7. BIBLIOGRAPHY

- [1] Balageas D., Fritzen C. P., Guemes A., (Ed.): *Structural Health Monitoring*, ISTE, London, Newport Beach, 2006.
- [2] Staszewski W., Boller C., Tomlinson G., (Ed.): *Health Monitoring of Aerospace structures, Smart sensors and signal processing*, Wiley & Sons, Chichester, 2003.
- [3] Inman D. J, Farrar C. R., Lopes V., Valder S., (Ed.): *Damage Prognosis for aerospace, civil and mechanical systems*, Wiley & Sons, Chichester, 2005.
- [4] Maladague X. P. V: *Theory and practice of infrared technology for nondestructive testing*, Wiley, & Sons, New York, 2001.
- [5] Pieczonka L., Szwedo M., Uhl T.: *Thermographical damage detection techniques*, *Pomiary Automatyka Kontrola PAK*, vol. 55(9), pp. 699–702, 2009.
- [6] Busse G.: *From photothermal radiometry to lock-in thermography methods*, *Journal of Physics: Conference Series*, vol. 214, 2010.
- [7] H. Madura (red.): *Practical problems in thermovision*. Agenda Wydawnicza PAK, Warszawa, 2004 (in Polish).

- [8] MONIT - „Monitoring of Technical State of Construction and Evaluation of its Lifespan”, <http://www.monit.pw.edu.pl>, 2011.
- [9] Myers R. H., Montgomery D. C.: *Response Surface Methodology: Process and Product Optimization Using Designed Experiments*, John Wiley & Sons. 1995.
- [10] Shepard S. M., Ahmed T., and Lhota J. R.: *Experimental considerations in vibrothermography*, *Proceedings of SPIE*, vol. 5405, pp. 332-335, 2004.
- [11] Han X.: *Acoustic chaos for enhanced detectability of cracks by sonic infrared imaging*, *Journal of Applied Physics*, vol. 95(7), 2004.



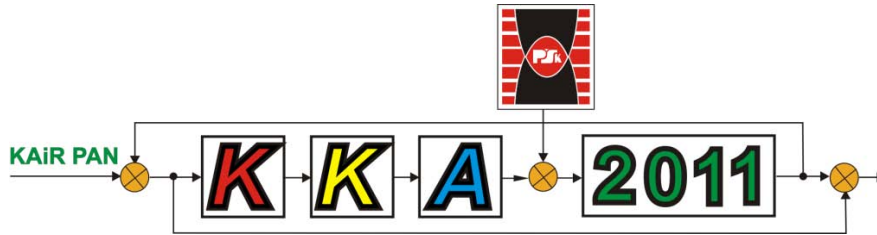
Prof. Tadeusz UHL is the head of the Department of Robotics and Mechatronics at AGH-UST. His scientific interests include structural dynamics in particular modal analysis, active vibration reduction, control systems and Structural Health Monitoring. He is the author of 15 books and over a hundred research papers concerning those problems.



Mariusz Szwedo PhD is a researcher at the Department of Robotics and Mechatronics at AGH-UST. His scientific interests include image processing and analysis techniques, machine vision and its application in robotics, mechatronics and control systems.



Łukasz Pieczonka PhD is a postdoctoral researcher at the Department of Robotics and Mechatronics at AGH-UST. His scientific interests include structural dynamics, uncertainty quantification, verification and validation and structural health management.



**XVII KRAJOWA KONFERENCJA AUTOMATYKI
KKA'2011
19-22.06.2011 KIELCE – CEDZYNA**

W dniach 19-22.06.2011 r. w Politechnice Świętokrzyskiej w Kielcach oraz malowniczo położonym ORW "Echo" w Cedzynie odbyła się XVII Krajowa Konferencja Automatyki KKA'2011. Organizatorem konferencji był Komitet Automatyki i Robotyki Polskiej Akademii Nauk (KAiR PAN), natomiast realizację tegorocznej konferencji powierzono Politechnice Świętokrzyskiej w Kielcach. Komitet programowy konferencji stanowili profesorowie członkowie KAiR PAN oraz pracownicy Wydziału Mechatroniki i Budowy Maszyn (WMiBM) oraz Wydziału Elektrotechniki, Automatyki i Informatyki (WEAiI) Politechniki Świętokrzyskiej (PŚk.) w Kielcach. Przewodniczącym komitetu programowego był prof. dr hab. inż. Krzysztof Malinowski, przewodniczący KAiR PAN, a przewodniczącym komitetu organizacyjnego był prof. dr hab. inż. Ryszard Dindorf z WMiBM PŚk. Patronat honorowy konferencji objął JM Rektor Politechniki Świętokrzyskiej w Kielcach prof. dr hab. inż. Stanisław Adamczak dr h.c. mult. Patronatem medialnym konferencji KKA'2011 objęło

kilkanaście branżowych czasopism naukowo-technicznych oraz portali internetowych.

Krajowa Konferencja Automatyki organizowana jest co trzy lata. Konferencja stanowi tradycyjne krajowe forum prezentacji wyników oryginalnych prac badawczych i aplikacyjnych w dziedzinie automatyki, techniki systemów i robotyki. Intencją Organizatorów jest integracja instytucji akademickich, ośrodków badawczych i przemysłu.

W tegorocznej XVII Krajowej Konferencji Automatyki KKA'2011 uczestniczyło 115 osób. Wygłoszono 93 referaty. Referaty odbywały się w dziesięciu sekcjach: Identyfikacja i optymalizacja, Systemy pomiarowe, Zastosowania metod sztucznej inteligencji, Teoria sterowania, Układy regulacji, Optymalizacja i sterowanie systemów, Modelowanie, Systemy automatyzacji, Robotyka. Wygłoszono również 6 znaczących naukowych referatów plenarnych. Prof. Tadeusz Kaczorek wygłosił referat na temat: "Dodatknie ciągłodyskretne układy liniowe". Prof. Jerzy Klamka wygłosił referat na temat: "Analiza stanu badań w



zakresie teorii sterowania". Prof. Józef Korbicz wygłosił referat na temat: "Systemy inteligentne w automatyce i diagnostyce procesów". Prof. Piotr Holnicki wygłosił referat na temat: "Modelowanie, optymalizacja i wspomaganie decyzji: model oceny skutków zdrowotnych zanieczyszczenia powietrza w Warszawie - studium przypadku". Prof. Piotr Tatjewski wygłosił referat na temat: "Wybrane układy i systemy automatyki przemysłowej: systemy sterowania, sterowanie zaawansowane, diagnostyka, zarządzanie alarmami". Prof. Edward Jezierski wygłosił referat na temat: "Kształcenie na kierunku automatyka i robotyka w polskich uczelniach technicznych". Obrady odbywały się w nowym Gmachu Auli Głównej Politechniki Świętokrzyskiej w Kielcach oraz w ostatnim dniu trwania konferencji w ORW "Echo" w Cedzynie. W obradach odbywających się w Politechnice Świętokrzyskiej w Kielcach licznie uczestniczyli pracownicy WMiBM i WEAiI oraz doktoranci i studenci kierunków mechanika i budowa maszyn, automatyka i robotyka.

W drugim dniu konferencji KKA'2011 odbyło się uroczyste otwarcie Laboratorium Mechatroniki, Automatyki i Robotyki – Pracowni Automatyki i Robotyki w Centrum Laserowych Technologii Metali oraz Pracowni Mechatroniki w budynku B

Politechniki Świętokrzyskiej w Kielcach, które powstały z funduszy Unii Europejskiej.

Organizatorzy XVII Krajowej Konferencji Automatyki uatrakcyjnili konferencję licznymi imprezami towarzyszącymi. W drugim dniu uczestnicy konferencji zwiedzali ruiny Zamku Królewskiego w Chęcinach oraz Park Etnograficzny w Tokarni. Pracowity dzień zakończono uroczystą kolacją w Zamku Rycerskim w Sobkowie. Uczestników konferencji KKA'2011 gospodarze Sobkowa powitali w iście sarmackim stylu - pokazem burdy szlacheckiej i wystrzałem z armaty. Biesiadę połączono z przejazdami powozami, pływaniem po rzece Nidzie oraz przedstawieniem plenerowym Pan Twardowski.

Trzeciego dnia goście konferencji mogli podziwiać piękno Gór Świętokrzyskich uczestnicząc w wycieczce na Święty Krzyż. Na szczycie Świętego Krzyża (Łysiec, 595 m n.p.m.) zwiedzano Klasztor Misjonarzy Oblatów Maryi Niepokalanej (dawne opactwo benedyktyńskie), Sanktuarium Relikwii Krzyża Świętego oraz przepiękne i okazałe gołoborze. Następnie uczestnicy zwiedzili Galerię Mineralów i Skamieniałości w Św. Katarzynie, gdzie mogli ulec magii blasku i mocy różnych kamieni w tym największej kolekcji krzemienia pasiastego.





płk prof. dr hab. inż. Stanisław NIZIŃSKI
(5.03.1937– 24.07.2011)

WSPOMNIENIE O PROFESORZE STANISŁAWIE NIZIŃSKIM

Prof. Stanisław NIZIŃSKI urodził się 5 marca 1937 r. w miejscowości Wizna, gdzie w 1951 r. ukończył 6 klas szkoły podstawowej. W tym samym roku rozpoczął naukę w Korpusie Kadetów w Warszawie, którą ukończył w 1956. W roku 1956 został przyjęty do Wojskowej Akademii Technicznej. W 1961 uzyskał dyplom mgr inż. mechanika, w specjalności samochody i ciągniki.

Jako absolwent WAT został skierowany do Oficerskiej Szkoły Samochodowej w Pile na stanowisko wykładowcy, gdzie w roku 1967 został starszym wykładowcą.

W 1972 r. podjął stacjonarne studia doktoranckie na Wydziale Mechanicznym w Instytucie Eksploatacji Pojazdów Mechanicznych WAT. Pracę doktorską na temat „Badania akustyczne stanu technicznego tłokowych silników spalinowych” obronił 27 czerwca 1975 r.

Po ukończeniu studiów doktoranckich wrócił do Wyższej Oficerskiej Szkoły Samochodowej w Pile, na stanowisko Kierownika Cyklu Konstrukcji Pojazdów Mechanicznych. W 1981 r. został wyznaczony na stanowisko Szefa Katedry Budowy i Eksploatacji Pojazdów Mechanicznych.

W 1984 r. został mianowany na stanowisko Kierownika Zakładu w Wojskowym Instytucie Techniki Pancernej i Samochodowej w Sulejówku.

Dnia 23 czerwca 1987 r. obronił na Wydziale Maszyn Roboczych i Pojazdów Politechniki Poznańskiej, rozprawę habilitacyjną nt. „Kryterium stanu technicznego w podsystemie obsługiwanego pojazdu mechanicznego”.

Z dniem 1 maja 1993 r. został profesorem nadzwyczajnym w Akademii Rolniczo – Technicznej w Olsztynie (od 1999 roku na Uniwersytecie Warmińsko – Mazurskim), pracując na Wydziale Mechanicznym w Instytucie Maszyn i Urządzeń Rolniczych (później na Wydziale Nauk Technicznych w Katedrze Budowy, Eksploatacji Pojazdów i Maszyn).

W sierpniu 1995 r. odszedł na emeryturę (w stan spoczynku jako pułkownik WP), zaś we wrześniu tego roku zaczął pracę w Wojskowym Instytucie

Techniki Pancernej i Samochodowej na stanowisku profesora nadzwyczajnego.

Tytuł profesora nauk technicznych otrzymał z rąk Prezydenta RP w 2000 roku. W roku 2002 został zatrudniony na stanowisku profesora zwyczajnego Uniwersytetu Warmińsko-Mazurskiego w Olsztynie.

Profesor S. NIZIŃSKI był niezwykle aktywnym członkiem wielu zespołów, towarzystw i organizacji naukowych, takich jak: Polskie Towarzystwo Diagnostyki Technicznej, Sekcja Podstaw Eksploatacji Komitetu Budowy Maszyn PAN, Zespół Diagnostyki Komitetu Budowy Maszyn PAN, Komisja Mechanizacji i Elektryfikacji Rolnictwa Oddział PAN w Lublinie, Sekcja Technicznych Środków Transportu Komitetu Transportu PAN, pełniąc w organizacjach tych różnego rodzaju funkcje.

Działalność naukowa prof. S. NIZIŃSKIEGO była skupiona w obszarze następujących zagadnień:

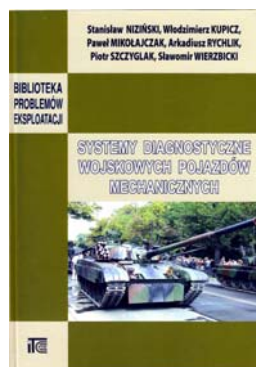
- podstawy teoretyczne i koncepcje budowy modeli systemów sterująco-diagnostycznych;
- diagnostyka pojazdów mechanicznych;
- strategię eksploatacji obiektów technicznych;
- systemy logistyczne w przedsiębiorstwach;
- zarządzanie eksploatacją obiektów technicznych;
- pojazdy inteligentne.

Dorobek naukowy prof. S. NIZIŃSKIEGO jest imponujący, był m.in.: promotorem 7 prac doktorskich, autorem i współautorem ponad 300 prac naukowych, oraz około 30 podręczników i monografii. Do najważniejszych z nich należą: Podstawy diagnostyki pojazdów mechanicznych (1980), Diagnostyka samochodów osobowych i ciężarowych (1999), Eksploatacja obiektów technicznych (2002), Diagnostyka obiektów technicznych (2002), Logistyka ogólna (2011), Systemy diagnostyczne wojskowych pojazdów mechanicznych (2011), Logistyka dla inżynierów (2011). Był kierownikiem kilkudziesięciu prac badawczych oraz autorem licznych recenzji prac naukowych i dorobku naukowego.

Za działalność naukową i organizacyjną prof. S. NIZIŃSKI był wielokrotnie nagradzany i odznaczany różnego rodzaju odznaczeniami m.in.: Złotym Krzyżem Zasługi, Krzyżem Komandorskim Orderu Odrodzenia Polski, Medalem Komisji Edukacji Narodowej, Nagrodą Głównego Inspektora Techniki WP, medalem Immanuela Kanta nadanym przez Uniwersytet Techniczny w Kaliningradzie, medalem im. Prof. Ziembę nadanym Sekcją Podstaw Eksploatacji KBM PAN oraz wielokrotnie nagradzany nagrodami: Komendanta (Rektora) Wyższej Oficerskiej Szkoły Samochodowej w Pile, Rektora ART w Olsztynie oraz Rektora UWM w Olsztynie.

Prof. Stanisław NIZIŃSKI zmarł nagle 24 lipca 2011 roku, do końca będąc człowiekiem pełnym zapału i energii. W naszej pamięci pozostanie jako człowiek niezwykle pracowity, życzliwy i szlachetny.

Opracował: Sławomir WIERZBICKI



Stanisław NIZIŃSKI
Włodzimierz KUPICZ
Paweł MIKOŁAJCZAK
Arkadiusz RYCHLIK
Piotr SZCZYGLAK
Sławomir WIERZBICKI

**Systemy diagnostyczne
wojskowych pojazdów
mechanicznych**

ITE, Radom, 2011

Niniejsza praca jest poświęcona systemom diagnostycznym, których tem są zagadnienia: logistyki, bezpieczeństwa i eksploatacji wojskowych pojazdów mechanicznych.

Rozdział pierwszy pracy poświęcono ogólnemu przeglądowi wojskowych pojazdów mechanicznych, których znajomość budowy i eksploatacji jest podstawą konstrukcji efektywnych: autonomicznych, zewnętrznych i mieszanych systemów diagnostycznych. Omówiono klasyfikacje pojazdów cywilnych i wojskowych.

W rozdziale drugim przedstawiono istotę diagnostyki technicznej pojazdów mechanicznych. Podano niektóre definicje diagnostyki technicznej, także opisano pojęcia podstawowe, takie jak: stan pojazdu, sygnały diagnostyczne, sygnały wejściowe i zakłócenia.

Podstawy budowy systemów diagnostycznych wojskowych pojazdów mechanicznych zawarto w rozdziale trzecim. Przedstawiono pojazd jako system antropotechniczny i dokonano jego analizy diagnostycznej. Pokazano sposoby wyboru elementów pojazdu, które powinny być diagnozowane oraz ustalania zbioru koniecznych, a nieprzypadkowych parametrów diagnostycznych.

W rozdziale czwartym dokonano analizy rozwiązań konstrukcyjnych systemów diagnostycznych pojazdów mechanicznych, a w szczególności rozpatrzono:

- właściwości systemów diagnostycznych,
- system diagnostyczny silników spalinowych o zapłonie iskrowym,
- system diagnostyczny silników o zapłonie samoczynnym.

Przedstawiono także niektóre systemy diagnostyczne wojskowych pojazdów mechanicznych, a w tym: czołgów M1A2 Abrams i Leclerc oraz systemu Finders.

Istotnym elementem tego rozdziału są kierunki doskonalenia systemów diagnostycznych pojazdów mechanicznych, dotyczące w szczególności:

- opracowania pokładowego systemu diagnostycznego (OBD) obejmującego cały pojazd mechaniczny,

- systemów diagnostycznych silników zasilanych wodorem, ogniw paliwowych, pojazdów hybrydowych i z napędem elektrycznym,
- budowy systemów diagnostycznych w aspekcie sterowania bezpieczeństwem pojazdów mechanicznych, w tym pojazdów wojskowych.

W rozdziale piątym książki przedstawiono hierarchiczny model diagnostyczny samochodu Honker oraz modele: kinematyczny i informacyjny jego układu napędowego. Omówiono architekturę systemu diagnostycznego, a w tym strukturę cybernetyczną i komunikacyjną. Dodatkowo opisano główne elementy modelu materialnego systemu diagnostycznego,

a w szczególności: jego budowę i funkcjonowanie, ekrany informacyjne, diagnozowanie i obsługiwanie.

Rozdział szósty książki poświęcono symulatorowi systemu diagnostycznego pojazdu Honker. Podano przykłady rozwiązań konstrukcyjnych symulatorów różnych urządzeń technicznych. Pokazano rolę symulatorów w kształceniu operatorów maszyn. Rozpatrzono etapy budowy modelu symulacyjnego oraz podano opis programu symulacyjnego systemu diagnostycznego pojazdu Honker.

W rozdziale siódmym książki pokazano miejsce systemu diagnostycznego w strukturze wojskowego pojazdu mechanicznego.

Ósmy rozdział pracy omawia istotne zagadnienia dotyczące wpływu systemu diagnostycznego na bezpieczeństwo wojskowych pojazdów mechanicznych, a w tym:

- uszkodzenia jako podstawowe elementy niezawodności i bezpieczeństwa,
- identyfikacja zagrożeń bezpieczeństwa,
- ryzyko jako kryterium bezpieczeństwa,
- algorytm sterowania bezpieczeństwem,
- kształtowanie bezpieczeństwa wojskowych pojazdów mechanicznych jako środków pola walki,
- zarządzanie bezpieczeństwem.

Rozdział dziewiąty opracowania poświęcono identyfikacji związków: logistyki, eksploatacji i diagnostyki jako narzędzi podwyższenia gotowości technicznej wojskowych pojazdów mechanicznych, tym samym gotowości bojowej wojsk. Dokonano tu analizy i oceny procesów eksploatacji niektórych państw NATO. Oddzielne zagadnienie poświęcono analizie i ocenie procesów eksploatacji pojazdów mechanicznych WP, a w tym eksploatacji pojazdów w czasie pokoju i wojny.

Obszar zainteresowania czasopisma to:

- ogólna teoria diagnostyki technicznej
- eksperymentalne badania diagnostyczne procesów i obiektów technicznych;
- modele analityczne, symptomowe, symulacyjne obiektów technicznych;
- algorytmy, metody i urządzenia diagnozowania, prognozowania i genezowania stanów obiektów technicznych;
- metody detekcji, lokalizacji i identyfikacji uszkodzeń obiektów technicznych;
- sztuczna inteligencja w diagnostyce: sieci neuronowe, systemy rozmyte, algorytmy genetyczne, systemy ekspertowe;
- diagnostyka energetyczna systemów technicznych;
- diagnostyka systemów mechatronicznych i antropotechnicznych;
- diagnostyka procesów przemysłowych;
- diagnostyczne systemy utrzymania ruchu maszyn;
- ekonomiczne aspekty zastosowania diagnostyki technicznej;
- analiza i przetwarzanie sygnałów.

Topics discussed in the journal:

- General theory of the technical diagnostics,
- Experimental diagnostic research of processes, objects and systems,
- Analytical, symptom and simulation models of technical objects,
- Algorithms, methods and devices for diagnosing, prognosis and genesis of condition of technical objects,
- Methods for detection, localization and identification of damages of technical objects,
- Artificial intelligence in diagnostics, neural nets, fuzzy systems, genetic algorithms, expert systems,
- Power energy diagnostics of technical systems,
- Diagnostics of mechatronic and antropotechnic systems,
- Diagnostics of industrial processes,
- Diagnostic systems of machine maintenance,
- Economic aspects of technical diagnostics,
- Analysis and signal processing.

Wszystkie opublikowane artykuły uzyskały pozytywne recenzje wykonane przez niezależnych recenzentów.

All the published papers were reviewed positively by the independent reviewers.

Redaktorzy działów:

dr hab. inż. Tomasz BARSZCZ
prof. dr hab. inż. Wojciech CHOLEWA
prof. dr hab. Wojciech MOCZULSKI
prof. dr hab. inż. Stanisław RADKOWSKI
prof. dr hab. inż. Wiesław TRĄMPCZYŃSKI
prof. dr hab. inż. Tadeusz UHL

Recenzenci / Reviewers:

prof. dr hab. inż. Jan ADAMCZYK
prof. dr hab. inż. Wojciech BATKO
prof. dr hab. inż. Zbigniew DĄBROWSKI
dr hab. inż. Jacek DYBAŁA
dr hab. inż. Andrzej GRZĄDZIELA, prof. AMW
dr inż. Marcin JASIŃSKI
dr inż. Tomasz KORBIEL
dr inż. Jędrzej MĄCZAK
prof. dr hab. inż. Stanisław RADKOWSKI
prof. dr hab. inż. Wiesław TRĄMPCZYŃSKI
dr inż. Jacek URBANEK
dr inż. Mirosław WITOŚ

Kopia wszystkich artykułów opublikowanych w tym numerze dostępna jest na stronie www.diagnostyka.net.pl

Druk:

Centrum Graficzne „GRYF”, ul. Pieniężnego 13/2, 10-003 Olsztyn, tel. / fax: 89-527-24-30

Oprawa:

Zakład Poligraficzny, UWM Olsztyn, ul. Heweliusza 3, 10-724 Olsztyn
tel. 89-523-45-06, fax: 89-523-47-37



XXXIX

**Ogólnopolskie Sympozjum
DIAGNOSTYKA MASZYN**

Wisła 05.03. | 10.03.2012 r.

organizatorzy:

Wydział Transportu Politechniki Śląskiej

Polskie Towarzystwo Diagnostyki Technicznej

Zespół Diagnostyki Sekcji Podstaw
Eksploatacji KBM PAN

www.konferencje.polsl.pl/diagmasz

KOMUNIKAT NR 2

Wszystkie opublikowane w czasopiśmie artykuły uzyskały pozytywne recenzje, wykonane przez niezależnych recenzentów.

Redakcja zastrzega sobie prawo korekty nadesłanych artykułów.

Kolejność umieszczenia prac w czasopiśmie zależy od terminu ich nadesłania i otrzymania ostatecznej, pozytywnej recenzji.

Wytyczne do publikowania w DIAGNOSTYCE można znaleźć na stronie internetowej:

<http://www.diagnostyka.net.pl>

Redakcja informuje, że istnieje możliwość zamieszczania w DIAGNOSTYCE ogłoszeń i reklam.

Jednocześnie prosimy czytelników o nadsyłanie uwag i propozycji dotyczących formy i treści naszego czasopisma.

Zachęcamy również wszystkich do czynnego udziału w jego kształtowaniu poprzez nadsyłanie własnych opracowań związanych z problematyką diagnostyki technicznej. Zwracamy się z prośbą o nadsyłanie informacji o wydanych własnych pracach nt. diagnostyki technicznej oraz innych pracach wartych przeczytania, dostępnych zarówno w kraju jak i zagranicą.